

Simulation and Visualization of In- and Outdoor Sound

Vom Fachbereich Informatik
der Technischen Universität Kaiserslautern
zur Erlangung des akademischen Grades
Doktor der Naturwissenschaften
(Dr. rer. nat.)
genehmigte Dissertation von

Frank Michel

Dekan:	Prof. Dr. Karsten Berns
Vorsitzender der Prüfungskommission:	Prof. Dr. Karsten Berns
Erster Berichterstatter:	Prof. Dr. Hans Hagen
Zweiter Berichterstatter:	Prof. Dr. Dianne Hansford

Tag der wissenschaftlichen Aussprache: 30. September 2008

Acknowledgements

I am grateful to have the chance to thank all the people I worked with and which supported me during the work on this dissertation. First of all I would like to thank my doctoral advisor Hans Hagen not only for giving me the chance to be a part of the International Research Training Group *IRTG1131* - "Visualization of Large and Unstructured Data Sets" at the University of Kaiserslautern but also for providing valuable suggestions in work and non work related matters. I would also like to thank my co-advisor Dianne Hansford for support and advice during my visits to Arizona State University.

I would like to thank all my colleagues in the "Computer Graphics and Visualization" group and the IRTG for the intellectual exchange and fruitful discussions, especially Martin Hering-Bertram for the invaluable discussions on the topic and his constructive criticism and Eduard Deines for the excellent collaboration on our common projects which resulted in a great part of this thesis. Special thanks go to Inga Scheler and Mady Gruys which were always there when I needed them and for managing all the organisational things in the background.

Last - but certainly not least - I wish to thank my parents for their unwavering yet unobtrusive support which allowed me to undertake my studies in the first place and gave me the freedom I needed.

Zusammenfassung

Wir sind immerwährend und überall von Geräuschen umgeben, egal ob angenehme Musik in einer Konzerthalle oder störender Lärm von der Straße vor unserer Haustür. Die fundamentalen Eigenschaften beider Arten von Geräusch sind identisch, nämlich die Ausbreitung von Schallwellen ausgehend von einer Schallquelle, aber wir nehmen sie unterschiedlich und zwar abhängig von unserem momentanen Gemütszustand oder ob das Geräusch gewünscht ist oder nicht.

Im Rahmen dieser Dissertation werden anhand von Schallsimulationen und Visualisierungen der Ergebnisse sowohl angenehme Musik als auch störender Lärm untersucht. Obwohl die fundamentalen Eigenschaften beider Arten identisch sind liegt das Interesse doch auf unterschiedlichen Merkmalen. Zum Beispiel ist die Nachhallzeit ein wichtiges Merkmal einer Konzerthalle, wohingegen bei der Betrachtung von Lärm im Endeffekt nur der Schallpegel, zum Beispiel auf dem eigenen Balkon, von Interesse ist.

Diese Unterschiede spiegeln sich ebenso in der Methode der Simulation wieder wie in den Anforderungen an die Visualisierungen. Aus diesem Grund ist diese Dissertation in zwei abgeschlossene Teile aufgesplittet.

Der erste Teil behandelt mit Raumakustik die Simulation und Visualisierung von Schall und akustischen Gütemaßen, wie Deutlichkeit und Klarheitsmaß, in Innenräumen. Zur Simulation werden zwei unterschiedliche Methoden verwendet und verglichen. Zum einen ein geometrisches Verfahren, Phonon Tracing, und zum anderen ein wellenbasiertes, eine Finite Elemente Methode. Die vorgestellten Visualisierungsmethoden geben einen Einblick in die Ausbreitung und Interaktion von Schall in Räumen sowohl aus einem globalen als auch aus einem Zuhörerzentrierten Blickwinkel. Desweiteren wird eine akustische Renderinggleichung präsentiert mit dessen Hilfe Interferenzeffekte visualisiert werden. Außerdem wird eine neue Methode zur Visualisierung von niederfrequentem Schall vorgestellt welche es erlaubt die topologische Struktur von Druckverteilungen zu analysieren.

Der zweite Teil beschäftigt sich mit der Simulation und Visualisierung von Umgebungslärm, insbesondere Verkehrslärm. Das gesetzlich vorgeschriebenen Berechnungsverfahren wird ausführlich diskutiert und ein Ansatz zur Berechnung von Lärmvolumen und eine Erweiterung der Simulation, welche interaktive Lärmbe-

rechnungen ermöglicht, vorgestellt. Zur Darstellung der berechneten Lärmdaten werden diese in eine interaktive dreidimensionale Umgebung eingebettet und verschiedene Techniken zur Visualisierung präsentiert. Durch das hinzufügen erweiterter Information wird die Verständlichkeit der Lärmdaten weiter erhöht und das Nutzungsfeld des Systems erweitert.

Abstract

Sound surrounds us all the time and in every place in our daily life, may it be pleasant music in a concert hall or disturbing noise emanating from a busy street in front of our home. The basic properties are the same for both kinds of sound, namely sound waves propagating from a source, but we perceive it in different ways depending on our current mood or if the sound is wanted or not.

In this thesis both pleasant sound as well as disturbing noise is examined by means of simulating the sound and visualizing the results thereof. However, although the basic properties of music and traffic noise are the same, one is interested in different features. For example, in a concert hall, the reverberation time is an important quality measure, but if noise is considered only the resulting sound level, for example on ones balcony, is of interest.

Such differences are reflected in different methods of simulation and required visualizations, therefore this thesis is divided into two parts.

The first part about room acoustics deals with the simulation and novel visualizations for indoor sound and acoustic quality measures, such as definition (original "Deutlichkeit") and clarity index (original "Klarheitsmaß"). For the simulation two different methods, a geometric (phonon tracing) and a wave based (FEM) approach, are applied and compared. The visualization techniques give insight into the sound behaviour and the acoustic quality of a room from a global as well as a listener based viewpoint. Furthermore, an acoustic rendering equation is presented, which is used to render interference effects for different frequencies. Last but not least a novel visualization approach for low frequency sound is presented, which enables the topological analysis of pressure fields based on room eigenfrequencies.

The second part about environmental noise is concerned with the simulation and visualization of outdoor sound with a focus on traffic noise. The simulation instruction prescribed by national regulations is discussed in detail, and an approach for the computation of noise volumes, as well as an extension to the simulation, allowing interactive noise calculation, are presented. Novel visualization and interaction techniques for the calculated noise data, incorporated in an interactive three dimensional environment, enabling the easy comprehension of noise problems, are presented. Furthermore additional information can be integrated into the frame-

work to enhance the visualization of noise and the usability of the framework for different usages.

Contents

I	Room Acoustics	13
1	Introduction	15
1.1	Motivation	15
1.2	Related work	17
1.2.1	Simulation	17
1.2.2	Visualization	18
1.3	Overview	21
2	Simulation	23
2.1	Phonon tracing	24
2.1.1	Phonon tracing for sound energy	25
2.1.2	Phonon tracing for sound pressure	28
2.1.3	Phonon tracing with scattering	29
2.2	Finite Element Model	30
2.3	Comparison of phonon tracing and FEM results	33
3	Visualization	41
3.1	Visualizing the phonon map	42
3.1.1	Phonon map	42
3.1.2	Phonons on surfaces	45
3.1.3	Phonon propagation	48
3.1.3.1	Particles	48
3.1.3.2	Triangulated wave fronts	50
3.2	Listener based visualizations	55

3.2.1	Listener spheres	55
3.2.2	Surface importance	58
3.2.3	Sound tracing using an acoustic rendering equation	70
3.3	Visualizing low frequency sound	81
3.3.1	Simulation	81
3.3.2	Visualization	82
3.3.3	Results	83
4	Conclusion and future work	91
II	Environmental Noise	93
5	Introduction	95
5.1	Motivation	95
5.2	Open problems	96
5.3	Overview	97
6	Basics	99
6.1	What is noise?	99
6.2	Measurement and computation	100
6.2.1	Definition of sound	100
6.2.2	Noise parameters	100
6.2.3	Noise indicators	103
6.2.4	Noise propagation	103
6.3	Sources	107
6.3.1	Traffic noise	107
6.3.2	Aircraft noise	108
6.3.3	Railway noise	108
6.3.4	Industrial noise	109
6.3.5	Recreational noise	109
6.4	Health effects	110
6.4.1	Noise-induced hearing loss	111

6.4.2	Cardiovascular impact	111
6.4.3	Annoyance	112
6.5	History of noise mapping	112
6.6	Current regulations	114
6.6.1	European Union	114
6.6.2	Germany	115
7	State of the Art	117
7.1	Noise maps	117
7.1.1	Types of noise maps	117
7.1.2	Coloring	119
7.2	Software	119
7.2.1	Commercial tools	121
7.2.2	Research	125
8	Simulation	131
8.1	Calculation method - VBUS	131
8.1.1	Street segments	132
8.1.2	Noise levels	133
8.1.3	Emission level $L_{m,E}$	134
8.1.4	Distance and air absorption D_s	134
8.1.5	Screening D_z	135
8.1.6	Ground and meteorological damping D_{BM}	137
8.1.7	Time of day dependent sound propagation D_{met}	138
8.1.8	First reflections	140
8.1.9	Multi-reflections D_{refl}	141
8.2	Implementation	141
8.2.1	Input data	143
8.2.2	Verification Test-VBUS	144
8.3	Extensions	144
8.3.1	Noise volumes	145
8.3.2	Dynamic rendering	146

9 Visualization	151
9.1 General overview	151
9.2 Noise visualization	154
9.2.1 Information visualization	154
9.2.2 Building exposure	155
9.2.3 Noise maps	156
9.2.3.1 2D maps	156
9.2.3.2 Multilayer 2D maps	157
9.2.4 Noise volumes	158
9.2.4.1 Isosurfaces	158
9.2.4.2 Volume rendering	158
9.3 Results	161
10 Conclusion and future work	163
A Room Acoustics	165
A.1 Wave Equation	165
A.2 Room acoustic parameters	166
References	169
List of Figures	180
List of Tables	187
Curriculum Vitae	191
Publications	193

Part I

Room Acoustics

Chapter 1

Introduction

1.1 Motivation

Room acoustics is a subarea of acoustic science which tries to explain why a room has good or bad acoustic qualities. More precisely it is concerned with the structural properties of a building or room, namely geometry and material properties, and the influence of these properties on the propagation of sound inside the room.

The characteristic feature used when determining the acoustic quality of a room is the impulse response, the response to a unit pulse propagated from a sound source and received by a listener. The impulse response contains the direct sound signal as well as the sound reflected by the room boundaries back to the listener. The acoustic quality of a room is then characterized by the ratio between early and late received sound, time delay of the signal, incident direction of the early sound or the distribution of late reverberations.

Research on room acoustics has been done for many decades. W.C. Sabine, a pioneer in room acoustics, was the first to characterize the acoustics of a room by its reverberation time [CM78]. Since then numerous studies have been done to measure the subjective impression of acoustics with objective metrics [Rei68, Ber04, Thi53, LB61, Yam72, Kür69]. Some of these metrics, which are based on the impulse response of the room and especially on the relation of early to late received sound, are incorporated in the ISO3382 norm [ISO97].

The problem arising when building a new room or refitting an existing one is, that the metrics for measuring the quality of the acoustics differ depending on the proposed usage of the room. For example:

- In a room used mainly for speech, e.g. a lecture room or a theater, comprehensibility of speech plays a crucial role. To achieve a good comprehensibility the amount of direct sound should be high compared to the late reverberations, the delay of early reflections should be low and reach the listener preferably from the speaker direction to enhance clarity and supports localization. In consequence, the amount of late reflections, i.e. the reverberation time, should be low.
- Opposed to speech music desires a good spatial impression, e.g. in a concert hall. This can be achieved by a good balance between direct sound and reflections, where the direct sound should be high enough to perceive the music precisely. Additionally early reflections should be well distributed and strong compared to the total amount of received sound and the reverberation time should be longer than for speech to get a good spatial impression.

As one can see it is nearly impossible to design a room which fits all kinds of usage without reconfiguration. The question now is how to design or remodel a room so that it fits the proposed usage.

Enabled by the fast development of computer technology it is possible to simulate the acoustics of a room, especially not yet existing virtual rooms, instead of doing extensive measurements, which are obviously not possible in virtual rooms. Additionally these complex calculations not only give an impulse response for chosen listener positions but also extensive information on how the sound propagates before reaching the listener. This data can be used to improve the acoustics of a room, existing or planned, in an easy way if presented properly to the designer or engineer. The sheer amount of data prohibits the presentation by simple tables, thus novel techniques for the visualization of these information are needed. This includes the visualization of sound propagation from a global as well as a listener based viewpoint. With a good visualization of room acoustic criteria and the underlying data it is possible to easily identify possibilities to improve a room for a given usage even before it is build.

1.2 Related work

1.2.1 Simulation

Nowadays, many computer-aided algorithms for modeling and simulating acoustics inside enclosures exist. They are mostly based on wave-theoretical or geometric acoustics.

The wave-based acoustics deal with the numerical solution of the wave equation. The numerical methods often used include the Finite Difference Time Domain (FDTD) techniques [Yee66, Bot95, SLH02], the Boundary Element Methods (BEM) [Wu00], and the Finite Element Methods (FEM) [Bra03, Ihl98]. These methods subdivide the domain into small elements such that the differential wave equation can be approximated by functions which can be solved easier. Since the elements must be small compared to the smallest wave length, these methods are restricted to low frequencies only.

However, in room acoustic design and especially in acoustic virtual reality applications mostly methods based on geometrical acoustics are applied. They are related to optical fundamentals, and make use of approaches developed there.

The image source method [AB79, Bor84] models specular sound reflections by inserting new sound sources, which are obtained by mirroring the location of audio source over polygonal surfaces inside the scene. In the ray tracing method [Kro68, Kul84, Vor88] several reflection paths are traced from the sound source to receivers, which are typically represented as spheres to collect the incident sound. The reflections over the surfaces in the scene take place according to Snell's law of specular reflection or diffuse reflections. Usually Lambert's law is used for diffuse reflection calculation, but there exist approaches for modeling scattering more realistically [EAS01, CR05, TLDD07a].

Another widely used technique in acoustic computation is the beam tracing method. Beam tracing overcomes the aliasing problem of classical ray tracing by recursively tracing beams (i.e. a sets of rays) of polygonal [FCE⁺98, FMC99, FTC⁺04], conic [Ama84, MM93, Dal96], triangular [Lew93, Far95], or rectangular (frustum tracing) [LCM07b, LCM07a] cross-sections.

Ray tracing and image source methods both depend on the receiver position. Changing the listener position implies a recalculation of the room impulse response. In contrast, radiosity methods [SZ93, NHA04] are receiver independent. Thereby ideal diffuse reflections, i.e. surfaces reflect sound uniformly in all directions, are assumed. Incorporating also specular reflections, the acoustic rendering equation [SLS07a, SLS07b] was derived for use in room acoustic simulations applying also acoustic BRDFs. Due to the computation complexity, these methods do not seem practical for large environments. Due to the shortcomings of the approaches described above, advanced approaches have been developed e.g. [Vor89, Hei93, Nay93, Lew93, AFST04, WH05]. Mostly, they employ parts of the classical schemes or a combination of them.

Approaches extending geometric algorithms by modeling diffraction effects are proposed in [TFNC01, TSK01, PLS02, LSS02, PL03, CSF05]. Also, methods exist [JK04, TG97, TG98, TLDD07b, TLDD07a] exploiting programmable graphics hardware to accelerate the simulation calculations.

Sonel mapping [KJM04, KJM05b, KJM05a] is a particle based Monte Carlo method for geometric acoustics inspired by photon mapping (an approach for photorealistic rendering in computer graphics [Jen96]). It is a two stage, sound particle based method modeling specular and diffuse reflections, as well as diffraction of the sound wave.

1.2.2 Visualization

As mentioned before it is important to determine the amount and the direction of the received sound energy / pressure in order to judge acoustic quality at a listener position. The visualization of the sound wave behavior inside the room is a helpful tool. It is important, not only for teaching purposes, but also for engineers designing and treating rooms. Visual representation of sound propagation as well as representation of sound received at a listener position can help understanding this complex processes.

The existing acoustic visualization techniques for room acoustics can be classified into two groups. The first group considers the propagation of the sound waves, modeled as rays, inside the room independent of the listener position, whereas the

second group is based on the measured or simulated room impulse response for individual listener positions.

Yokota et. al. [YST02] visualized sound propagation of two-dimensional room sound fields resulting from a wave-based simulation using the FDTD method. They consider different simple shaped rooms which are typical for concert halls. The effects of changing reflection characteristics of the walls as well as the effect of diverse suspended panel arrays were investigated. However, the reflection coefficients are chosen equal for all rooms and frequencies.

Petrausch and Rabenstein [PR05] introduced a program for the simulation and OpenGL based visualization of two-dimensional sound wave propagation in real time. The simulation is performed using a functional transformation method. According to the authors the program supports frequency dependent and independent damping, dispersion, multiple excitations, spatially distributed excitations, as well as flexible boundary conditions.

Tokita and Yamasaki [TY05] visualized particle displacements on a rigid three-dimensional grid in a cube shaped room. The displacements are computed with a wave-based numerical simulation. The visual results are presented at several time steps using VRML97¹. In his PhD thesis Lokki [Lok02] presented a visualization using the image-source method. The image-sources and the edge-sources (sources of the corners of room objects) of different order are depicted as boxes. Furthermore, the impulse response for each pixel is calculated and plotted for a single time step resulting in a representation of wave fronts emitting from each of those virtual sources.

The image source method has been extended in order to simulate edge diffraction. In [PL03] Pulkki and Lokki present an approach visualizing this phenomenon. First order edge image-sources are displayed as cylinders. The radii and color of these cylinders vary depending on the pressure magnitude. The cylinders are connected to a degenerated curve representing first-order edge diffractions. Each of the first-order diffraction sources produce a curve diffraction on another edge. For all first-order edge-sources diffracts on a given edge the result is a large number of image-sources arranged on a planar surface. The authors rendered the surfaces color coded depending on the pressure magnitude. A blue-white-red color scheme is used to depict

¹<http://www.web3d.org>

negative and positive polarity of the wave. The authors restricted the visualization to first- and second-order diffraction.

Funkhouser et. al. [FCE⁺98] visualized source points, receiver points, pyramidal beams and reverberation paths in order to understand and evaluate their acoustic modeling method. Lauterbach et. al. [LCM07b] showed the sound propagation resulting from their approach using frustum tracing. Khoury et. al. [KFW98] represented the sound pressure levels inside the room by means of color maps. Additionally, the authors analyzed the precedence effect (or "law of the first wave front") by using isosurfaces. Lokki and Nenonen [LN06] utilized cave equipment for immersive visualization of trace paths and particle paths propagating inside closed rooms.

Sound wave fronts of different frequencies arrive at the listener position from different directions at different times. Thus, the room impulse response is multidimensional. Merimaa et. al. [MLPK01] presented a visualization of the measured impulse response using two-dimensional plots in the horizontal and median plane. The directional intensity is depicted with vectors on top of a sound pressure related spectrogram.

Omoto and Uchida [OU04] visualized the incidence direction and strength of the measured sound intensity using circles. The circles are mapped onto the surface of a rectangular wire-frame box approximating the room shape. This way the incidence direction is represented. The radii of the circles vary with the intensity. An extension of this approach using photographs of the enclosure instead of the wire-frame box is described in [FSO06].

Weyna [Wey05b, Wey05a] used flow visualization methods in order to study acoustic flow fields in front of and behind a thick rectangular plate. Measured intensity is visualized using hedgehogs and color coded streamlines. Furthermore the intensity is depicted by means of isosurfaces.

The impulse response of the room characterizes the acoustic quality of the room. Several objective metrics are derived depending on the purpose of the room, the use for speech or musical representations. Visualizations addressing the acoustical behavior of the room also exist. Stettner et. al. [SG89] visualized clarity and definition as well as spatial impression by use of specific icons. Furthermore, the

authors represent the overall strength of sound by displaying global pressure levels as color maps at the room boundaries for different time steps.

Monks et al. [MOD00] introduced an interactive optimization system for acoustic design. The system solves the inverse problem. After the user provides constraints for the surface properties and geometric variations for a range of architectural components, as well as desired acoustic performance defined by acoustic metrics, the system searches the configuration space in order to satisfy the target configuration. Simulating annealing followed by a steepest descent algorithm is used for this purpose. The authors visualized the results using icons for different acoustic metrics. Furthermore, the sound strength was visualized at room surfaces using color to indicate the sound-level data at different time moments. The authors show not only the simulated or optimized values of acoustic quantities but also the difference values between the simulation, the optimization, and specified target. Two real concert halls were investigated applying this system.

A number of commercial systems²³⁴ provide several tools for visualizing measured or computed acoustic quantities.

1.3 Overview

In this part of the thesis visualization techniques for the evaluation of room acoustics are proposed. The underlying data is simulated using two different methods to overcome the shortcomings of both wave based and geometric acoustics simulations, which are the high computation expenses for high frequencies in wave based methods and the neglected effects, like diffraction for low frequencies, in geometric methods.

For low frequencies a Finite Element (FE) Method is applied which uses a reduced state space model to efficiently evaluate complex pressure fields. Mid and high frequencies are simulated using different variations of phonon tracing depending on the effects to visualize, i.e. sound energy, sound pressure or scattering.

²Bose modeler: <http://www.bose.com>

³CATT-Acoustic: <http://www.catt.se>

⁴ODEON: <http://www.odeon.dk>

To answer the crucial question which method is appropriate for which frequency range is answered by a comparison of the FE method and phonon tracing which takes the accuracy of the computed results into account.

The proposed visualizations are split into two groups. The first group uses the simulation results to give a global view on the propagation within, and the interaction of sound with the room boundaries. From these visualizations a first insight on the influence of different material properties on the overall sound can be achieved.

The second group of visualizations is based on a listener position and thus give a view on the acoustics of a room from a distinct point. The presented listener based visualizations cover the identification of amount and direction of the received sound, the visual analysis of surface importance for certain acoustic metrics which gives direct advice on how to improve the acoustic quality of the room for the chosen metric, and an acoustic rendering equation which is used to visualize interference effects and phase changes for different frequencies. Furthermore novel ideas for the visualization of low frequency FEM simulations are presented which can help to identify topological changes of the sound pressure field for changing frequencies.

The remainder of the room acoustics part of the thesis is as follows. In the next chapter the used simulation methods are briefly introduced and compared. Chapter 3 presents the visualization approaches split into global, listener based and low frequency visualization. This room acoustics part of the thesis closes with a conclusion in chapter 4.

Chapter 2

Simulation

For the simulation of room acoustics exist a number of approaches as presented in section 1.2, which can be divided into geometric and wave-based methods. However, the arising problem when using only one specific method (geometric or wave-based) is, that a single method is not capable of simulating the acoustics of a room for all frequencies with the same quality or only with high computation costs due to the following reasons:

Geometric acoustics (e.g. ray tracing or the mirror image method) fail in the low frequency range for two reasons:

1. Wavelengths are of the order of typical dimensions of the room. Hence, diffraction and interference can no longer be neglected.
2. Damping is typically low at low frequencies and reverberation times become too long to be represented by a convolution kernel of reasonable length.

Therefore, wave acoustics need to be used to simulate the low frequency part of the sound field.

On the other hand wave based methods, like FEM simulations, cannot be used for high frequencies because they approximate the oscillating pressure field by smooth, e.g. piecewise quadratic ansatzfunctions. To resolve a wave, at least three or four elements per wave are needed. This leads to a FE model of about

$$N = \left(\frac{nLf}{c_0} \right)^3 \quad (2.1)$$

degrees of freedom, where n is the number of elements per wave, L a typical diameter of the room, f the evaluated frequency, and c_0 the velocity of sound. Note that the required number of unknowns, and thus the computation costs, increases as the third power of the frequency.

Therefore two different approaches (geometric and wave-based) are used for the simulation of room acoustics and a comparison of both methods is done to decide for which frequency ranges which method is appropriate for the simulation of room acoustics.

To simulate mid- and high frequency sound *phonon tracing*, a simulation approach based on geometric acoustics, was applied. An overview of the algorithm and different modifications to it is given in section 2.1. For a more detailed description see [BDM⁺05, DBM⁺06, Dei07].

To simulate low frequency sound, especially the behaviour of room eigenmodes, a wave based method approximating the solution of the wave equation (see appendix A.1) using a finite element method (FEM) was applied. The method uses a reduced parametric state-space model to evaluate the complex pressure field for arbitrary low frequencies. The algorithm is described in section 2.2.

Section 2.3 compares the results of the two applied methods numerically and visually using sound strength and interference patterns in order to decide when phonon tracing or FEM is appropriate for simulating the room acoustics.

2.1 Phonon tracing

Photon mapping [Jen96, JC98] is often used for rendering photorealistic images, supplementing unidirectional ray tracing by a variety of visual effects, like color bleeding and caustics. Phonon tracing adopts a similar approach to the simulation of sound, therefore naming the "acoustic particles" *phonons* instead of photons. Depending on the effects to simulate different versions of the algorithm are used, i.e. tracing energy for impulse response calculation, tracing pressure for interference

effects or incorporating scattering on room boundaries. The following sections give a brief description of the algorithms for tracing energy (2.1.1) and the modifications necessary for tracing pressure (2.1.2) and to include frequency dependent scattering coefficients (2.1.3).

2.1.1 Phonon tracing for sound energy

The idea of the algorithm is the separation of tracing and filter calculation processes. This way, only one tracing step is needed for a given sound source, followed by multiple impulse response calculation steps for different listener positions. Of course, when the source position has been changed the particle tracing has to be re-executed. Thus the phonon tracing algorithm consists of two steps: the phonon emission step where the particle traces are calculated and the phonon collection step used to determine the impulse response at given listener position. As result of the emission step the phonon map is obtained which represents all reflections of an emitted wave front by a large set of particles (phonons).

Problem specification. The simulation algorithm requires the following input information:

- position of sound source s
- emission distribution E of sound source
- number of phonons n_p to be traced from the sound source
- one or more listener positions l_i
- a triangulated scene with tagged material m_j
- an absorption function $\alpha_j : \Omega \mapsto (0, 1]$ for each material
- an acoustic BRDF for each material (if applicable)
- an energy threshold ϵ and maximum number of reflections n_{refl} for terminating the phonon paths

The output of *phonon tracing* is a finite response filter (FIR) f_i for each listener's position l_i corresponding to the impulse response with respect to the sound source and the phonon-map containing for each phonon the energy spectrum e_p , the traversed distance d_p , the phonon's position pt_p at the reflection point, its outgoing direction v_p , and the material m_p at the current reflection.

The two steps of the algorithm, the *phonon emission* step constructing the phonon map, and the *phonon collection and filtering* step collecting the phonon's contribution to a FIR filter for every listener position, are summarized in the following.

Phonon emission Every phonon p emitted from the sound source carries the following information:

- an energy spectrum $e_p : \Omega \mapsto \mathbb{R}^+$
- the distance d_p traversed from the source
- the phonon's current position pt_p
- the normalized outgoing direction v_p

The absorption and energy functions α_j are represented by $n_e = 10$ coefficients associated with the frequencies 40, 80, 160, ..., 20480 Hz. The basis functions for the energy spectrum are wavelets adding up to a unit impulse. Every phonon is composed of different frequencies, which is more efficient than tracing a single phonon for each individual frequency band.

Phonons are emitted from the source s according to the emission probability distribution E , and have at the starting point a unit energy spectrum $e_{p,i} = 1$ ($i = 1, \dots, n_e$). At the intersection of the phonon ray with the scene, the virtual source q_p is calculated as follows:

$$q_p \leftarrow q_p + 2 \cdot \langle (pt_p - q_p), n \rangle \cdot n \quad (2.2)$$

where n is the surface normal at the intersection point pt_p . The phonon direction v_p is calculated with respect to the virtual source q_p and the absorbed energy is subtracted according to the local material m_j . The distance d_p is set to the traversed

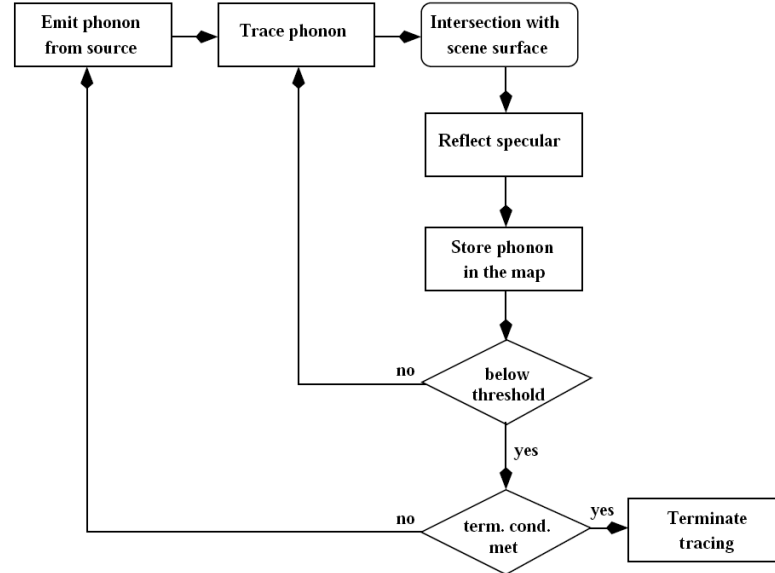


Figure 2.1: Flow chart diagram of the phonon emission step.

distance. The phonon information is stored at the intersection point, contributing to a global phonon map.

If the maximum energy of the phonon still exceeds the defined energy threshold, i.e. $\max\{e_{p,i}\}_{i=1}^{n_e} > \epsilon$, the next phonon continues the path and energy of the preceding one, saving computation time. It is started at the current position with respect to the outgoing direction v_p and contributes to the phonon map at the next surface intersection. If the threshold is not exceeded and a minimum number of reflections have been computed, a new phonon is started from the source. After a prescribed number n_p of phonons have contributed on the global phonon map, the tracing is terminated. Figure 2.1 depicts the *phonon emission step*.

Phonon collection and filtering The remaining task of the phonon tracing method is collecting the phonon's contribution to a FIR filter f for every listener position l_i . This filter corresponds to the impulse response from the source, recorded at l_i , such that convolution with an anechoic signal reproduces the perceived signal.

In the case of uniform absorption for all frequencies, the contribution of a phonon visible from the listener is simply a scaled, translated unit impulse (Dirac). The Dirac is shifted by the time elapsed between emission and reception of a phonon and

scaled by the phonon's energy $e_{p,i}$ multiplied by a Gaussian weighting the distance of the ray to the listener. In classical acoustic raytracing [Kro68, Kul84], a sphere is used to collect rays at a listener position. Using a Gaussian, however, provides much smoother filters, since more phonon rays contribute to the filter, weighted by their shortest distance.

In the more general case of frequency dependent absorption, the unit impulse is subdivided into wavelets representing the individual frequency bands. The filter becomes then a sum of these wavelets scaled by $e_{p,i}$ and shifted by the elapsed time. In the implementation 10 frequency bands and absorption coefficients for the frequencies $\omega_i = 20 \cdot 2^i$ Hz ($i = 1, \dots, 10$) were used.

A more detailed description of the phonon tracing algorithm, especially filter design and corresponding band pass filters (wavelets), can be found in [BDM⁺05].

2.1.2 Phonon tracing for sound pressure

The results obtained from tracing the sound energy are sufficient for the evaluation of acoustic metrics based on the impulse response of the room. However, due to the fact that energy can only be positive it is impossible to analyse interference effects or phase changes of the signal. To enable the analysis and visualization of these effects the improved phonon tracing simulation using sound pressure instead of sound energy was developed ([DBM⁺06]).

The idea is, analogous to section 2.1.1, to trace sound particles propagating from the sound source through the given scene contributing to the phonon map now enabling the observation of interference effects due to the extended information obtained using pressure instead of energy.

In addition to the algorithm in section 2.1.1 the following input information is needed:

- reference pressure p_0 at 1m distance for the sound source s
- a lower pressure threshold ϵ and a maximum number of reflections n_{refl} for terminating the phonon paths

Every phonon p emitted from the sound source carries, analogous to section 2.1.1, the following information:

- a pressure spectrum $p_p : \Omega \mapsto \mathbb{R}^+$
- the distance d_p traversed from the source
- the phonon's current position pt_p
- the outgoing direction v_p

The *phonon emission* step is adjusted to account for differences in energy and pressure attenuation. The resulting phonon map now contains the necessary information to look at interference effects. The *collection and filtering* step results in a FIR filter corresponding to the impulse response received from the sound source analogous to section 2.1.1.

2.1.3 Phonon tracing with scattering

In the phonon tracing algorithm described in the previous section only specular reflections are considered. In fact for virtual acoustic applications surfaces are generally assumed to reflect the sound wave specularly. This assumption is true if the surface structure is significantly smaller in contrast to the wave length. Otherwise, the sound wave is reflected diffusely. This section describes the reflection model used in the modified phonon tracing algorithm.

In room acoustics, in order to model diffusion, a scattering coefficient $\delta_i \in [0, 1]$ for each scene surface is introduced. The *phonon emission step* of the phonon tracing algorithm is then modified as follows. If the sound particle hits a scene surface, a number $\xi \in [0, 1]$ is randomly chosen. If $\xi > \delta_i$ the phonon is reflected diffusely, otherwise the reflection is specular. In case of diffuse reflection the outgoing direction v_p is determined assuming ideal (Lambertian) diffuse reflection where the direction of the reflection is perfectly random over a hemisphere surrounding the phonon's position pt_p (intersection point of the ray with the surface) [Kut71]. The azimuth angle θ is a random number ξ_1 in the interval $(-\pi, \pi)$ and the polar angle ϕ is given

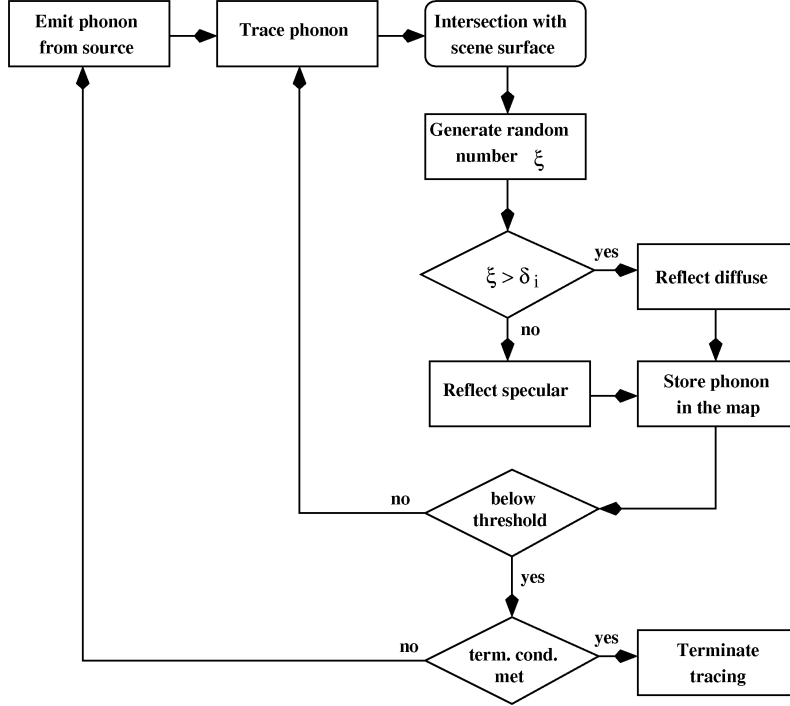


Figure 2.2: Flow chart diagram of the phonon emission step including diffuse reflections.

by the arc-cosine of the square root of a random number ξ_2 chosen in the interval $(0, 1)$:

$$\theta = \xi_1 \quad \phi = \arccos(\sqrt{\xi_2}) \quad (2.3)$$

In the phonon tracing algorithm the virtual source in equation 2.2 can now be calculated as follows:

$$q_p = pt_p - d_p \cdot v_p \quad (2.4)$$

Figure 2.2 depicts the *phonon emission step* including the diffuse reflection modeling.

Since the scattering coefficients δ_i are frequency dependent, either performing a tracing step for each frequency band or using an average scattering coefficient for all frequencies has to be applied.

2.2 Finite Element Model

In the following an efficient algorithm to use wave based methods in a transient acoustic simulation is summarized. This approach was developed at the Fraunhofer ITWM within the scope of a collaborative work and has been published in [DBM⁺06] and [Moh08]. This method is later used to compute the complex pressure values throughout a room for arbitrary low frequencies.

For closed rooms the wave equation is preferably solved by the finite element method (FEM), which approximates a solution of the wave equation by a large system of ordinary differential equations (ODEs), the unknowns of which are the pressures at grid points covering the room. In general, there are by far too many unknowns to solve these systems of ODEs in real time. Hence, the system needs to be reduced to a concise state-space model with similar input-output behaviour as the ODEs in the frequency range of interest.

There are many different approaches to model reduction [AS01]. The common observation is that system dynamics can often be represented quite well by a superposition of a few (generalized) eigenmodes. The coefficients of these modes are the unknowns of the new reduced system.

In the following, the steps to get from the wave equation (2.5) to a reduced state-space model describing the transient response of a room to an acceleration of a loudspeaker membrane are listed. The wave equation and associated boundary conditions read:

$$\begin{aligned}
 \frac{\partial^2 pr}{\partial t^2} - c_0^2 \Delta pr &= 0 \quad \text{on } G \\
 c_0 \frac{\partial pr}{\partial n} &= -\frac{1-r}{1+r} \frac{\partial p}{\partial t} \quad \text{on } \Gamma_w \\
 \frac{\partial pr}{\partial n} &= -\rho_0 \frac{\partial^2 x_m}{\partial t^2} \quad \text{on } \Gamma_m .
 \end{aligned} \tag{2.5}$$

$pr = pr(t, x)$ denotes pressure, $c_0 = 343\text{m/s}$ the velocity of sound, and $\rho_0 = 1.2\text{ kg/m}^3$ the density of air at room temperature, G the interior of the room, and Γ_w and Γ_m the surfaces of walls and membrane, respectively. x_m is the deflection of the

membrane and r is a reflection coefficient. It may depend on the particular wall, but is constant for all frequencies. This is a minor problem, as the model is used only for a small frequency band.

Approximating the pressure distribution by a superposition of, for instance, piecewise quadratic ansatzfunctions $p(t, x) = \sum_{i=0}^N p_i(t) \varphi_i(x)$ and integrating (2.5) with respect to the φ_i gives a FE model of the form:

$$\begin{aligned} M\ddot{p} + R\dot{p} + Kp &= Fu \\ y &= Pp. \end{aligned} \quad (2.6)$$

The real matrices M, R, K are called mass, damping, and stiffness matrices. $p = p(t)$ is a vector composed of the coefficients p_i . $u = u(t)$ is the input, e.g. the acceleration of the membrane. F transforms this input into a force. P is a projection matrix extracting certain interesting pressures y_i . Setting

$$\begin{aligned} x &= \begin{bmatrix} p \\ \dot{p} \end{bmatrix}, \quad E = \begin{bmatrix} I & 0 \\ 0 & M \end{bmatrix}, \quad A = \begin{bmatrix} 0 & I \\ -K & -R \end{bmatrix}, \\ B &= \begin{bmatrix} 0 \\ F \end{bmatrix}, \quad \text{and} \quad C = \begin{bmatrix} P & 0 \end{bmatrix} \end{aligned} \quad (2.7)$$

the FE model may be rewritten as a generalized state-space model:

$$\begin{aligned} sEx &= Ax + Bu \\ y &= Cx. \end{aligned} \quad (2.8)$$

where $s = 2\pi if$ for a frequency f .

In [DBM⁺06] and section 2.3, the *rational dual Arnoldi* algorithm described in [Ols02] was used for reduction. For the visualization method in section 3.3, the generalized modal reduction described in [Moh08] was employed.

2.3 Comparison of phonon tracing and FEM results

As stated in the introduction to chapter 2 it is not sufficient to only use one method (geometric or wave-based) to simulate room acoustics.

The crucial question is at which frequency geometric and wave based methods provide similar results and the simulation method can be switched from wave based to geometric. In the following the method used for the comparison of phonon tracing (section 2.1) and the FE method (section 2.2) is presented ([DBM⁺06]).

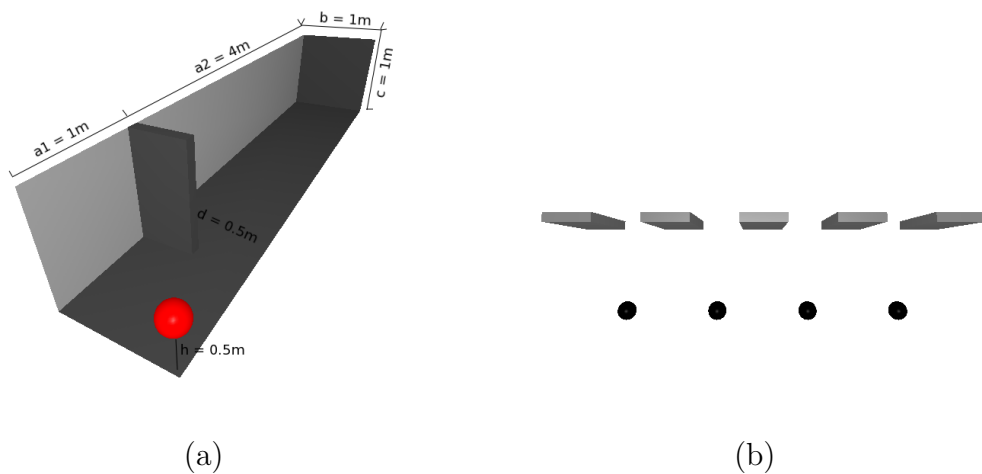


Figure 2.3: Geometry of the room (a) and simulated scenario (b).

Test Scenario In order to compare the two simulation approaches described in sections 2.1 and 2.2 the following test case, designed to produce interference patterns, was considered. Phonon tracing and FEM are used to simulate a room of 5 meters length, 1 meter width, and 1 meter height with an opening of 0.5 meters (see figure 2.3 (a)). The sound source is placed in the corner of the room. The two long walls are perfect reflectors, whereas the remaining room surfaces are perfect absorbers. Choosing the characteristics of the room in this way an array of sound sources as outlined in figure 2.3 (b) is modeled. Now interference effects as well as diffraction effects behind the gap can be observed.

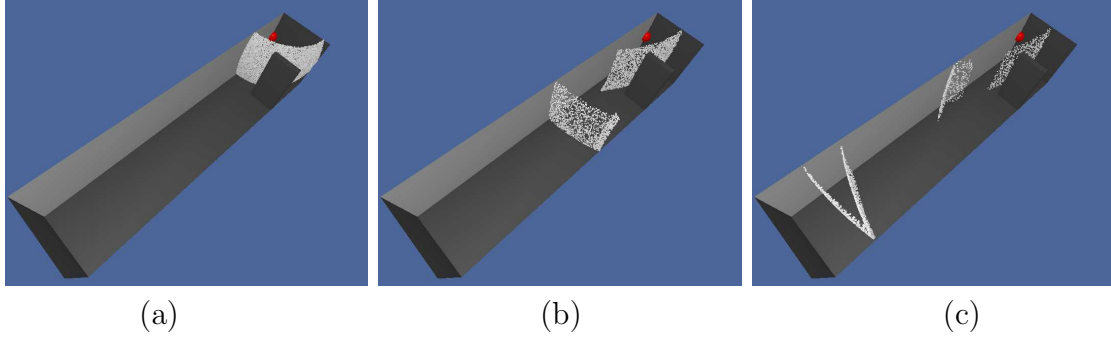


Figure 2.4: Visualization of particle (phonon) propagation from the sound source in three consecutive time steps.

For phonon tracing, the pressure inside the room was simulated on a regular grid (561 points in total), tracing 100000 phonons from the sound source in order to calculate the room impulse responses f_i at the grid points. Figure 2.4 shows the wave propagation from the sound source for three consecutive time steps. Afterwards, to determine the pressure at a grid point g_i for a given frequency ω , a sine signal of frequency ω is convolved with f_i to obtain the pressure at g_i at the position $le_{f_i} + 1$ of the resulting signal. le_{f_i} is the length of the room impulse response at the i -th grid point.

Comparing the results of phonon tracing and FEM, stationary sound fields originating from a source emitting only one particular frequency are considered. The corresponding FEM solution is computed in terms of the reduced continuous time system:

$$y(s) = C (sE - A)^{-1} B \quad (2.9)$$

where $s = 2\pi if$. The mean squared pressure at the i -th grid position reads:

$$p_i^2 = \frac{1}{T} \int_0^T p_i(t)^2 dt = \frac{1}{2} |y_i|^2 \quad (2.10)$$

For the visualization, the results are interpolated to the same grid as used for phonon tracing. The simulation results for different wave numbers $k = \frac{2\pi}{\lambda} = \{3, 6, 9, 12, 15\}$, where λ is the wave length, were compared. Note that choosing the shifts in the

Arnoldi algorithm to match the above wave numbers, i.e. $s_j = ik_j c_0$, the reduced model is exact at these wave numbers and results coincide with those of the full FEM simulation.

Interference pattern visualization In the first step the pressure distributions have been compared to validate whether similar interference patterns appear. In case of similar interference patterns the two simulation methods are equivalent for this frequency and phonon tracing can be used from this frequency upwards computing accurate results. For visualization a quad mesh with the following color coding was used. Positive pressure values are mapped to red and negative pressure values to blue. The saturation of the color is reduced, depending on the absolute pressure value at the considered position. Additionally, all pressure values with an absolute value less than the hearing threshold level ($2 \cdot 10^{-5}$ Pa) are mapped to grey color. The resolution of the displayed mesh is higher than that of the simulation mesh, therefore the pressure values of the additional points are bilinearly interpolated. Figure 2.5 shows examples of the interference pattern visualization for wave number $k = 12$ and $k = 6$. The results show that both methods faithfully reproduce matching interference patterns, where the results obtained by FEM appear to be somewhat smoother. The patterns at $k = 12$ are closer to each other than that at $k = 6$.

The wave propagation is illustrated more intuitively when pressures are mapped along the normal to the listening plane as shown in figure 2.6.

Sound strength visualization For a more detailed comparison an acoustic metric, sound strength (see A.2), was used, which is essentially the logarithm of the mean squared pressure [ISO97]:

$$G = 10 \log_{10} \left(\frac{\sum_{i=0}^m p_i^2}{\sum_{i=0}^m p_{10_i}^2} \right) \quad dB \quad (2.11)$$

Since sources have been modeled differently (point source in phonon tracing and small membrane in FEM), the sound fields are normalized by a linear fit excluding the direct neighborhood of the sources. For visualization of sound strength and error, a quad mesh color coded from red (maximum value) to blue (minimum value) was used. Therefore the hue value of the HSV color space is interpolated according

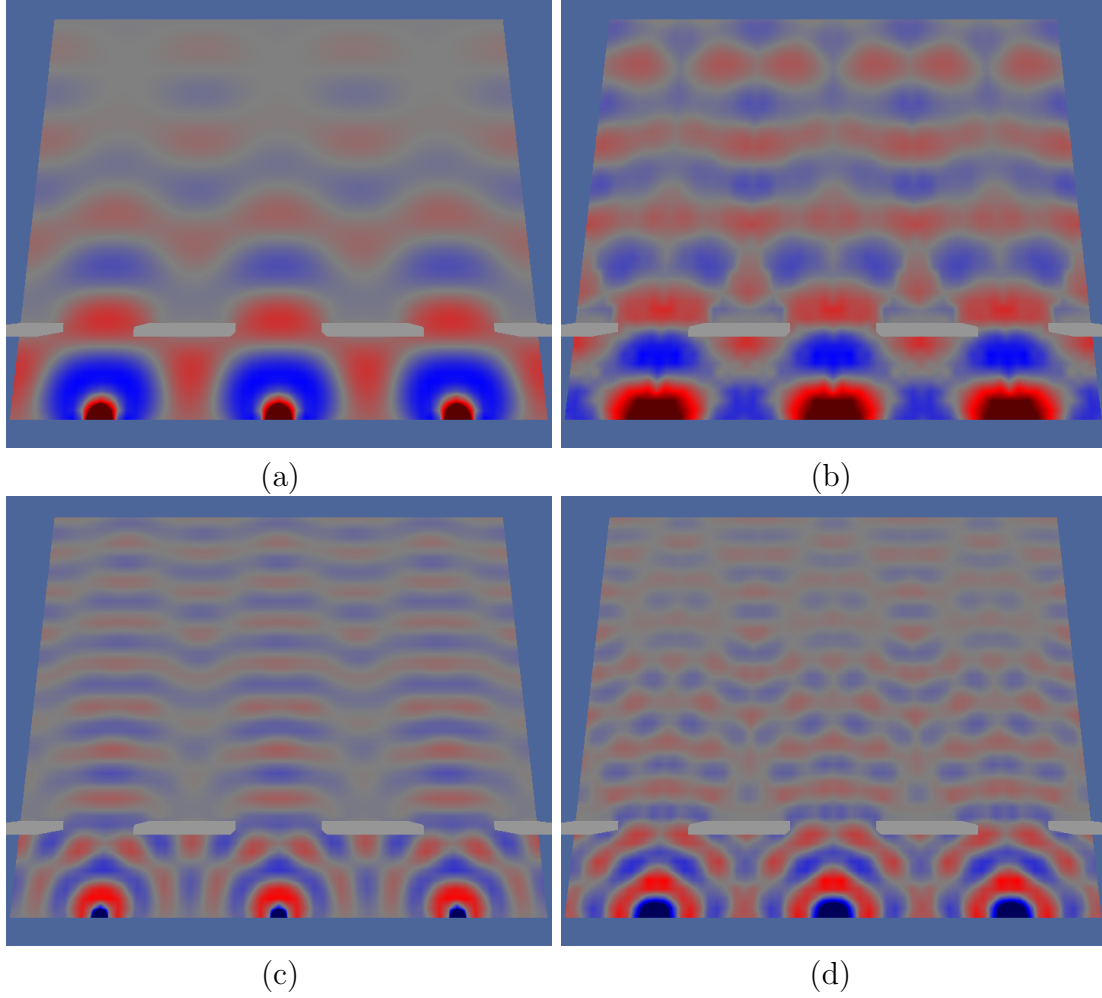


Figure 2.5: Interference pattern. FEM simulation (a, c) and phonon tracing (b, d) for the wave number $k=6$ (a, b) and $k=12$ (c, d).

to the sound strength and error, respectively. Values for additional mesh points for rendering are bilinearly interpolated as mentioned before. To ensure better comparison, the same color range for different simulation types at same frequencies was used for G . The same color range was used for all error plots too. As the sound strength is a logarithmic measure the relative error of the pressures is proportional to the difference of the sound strength values and can be calculated as:

$$\epsilon = \delta \frac{\ln(10)}{20} \quad \text{with} \quad \delta = \|G_{ph_j} - G_{fem_j}\| \quad (2.12)$$

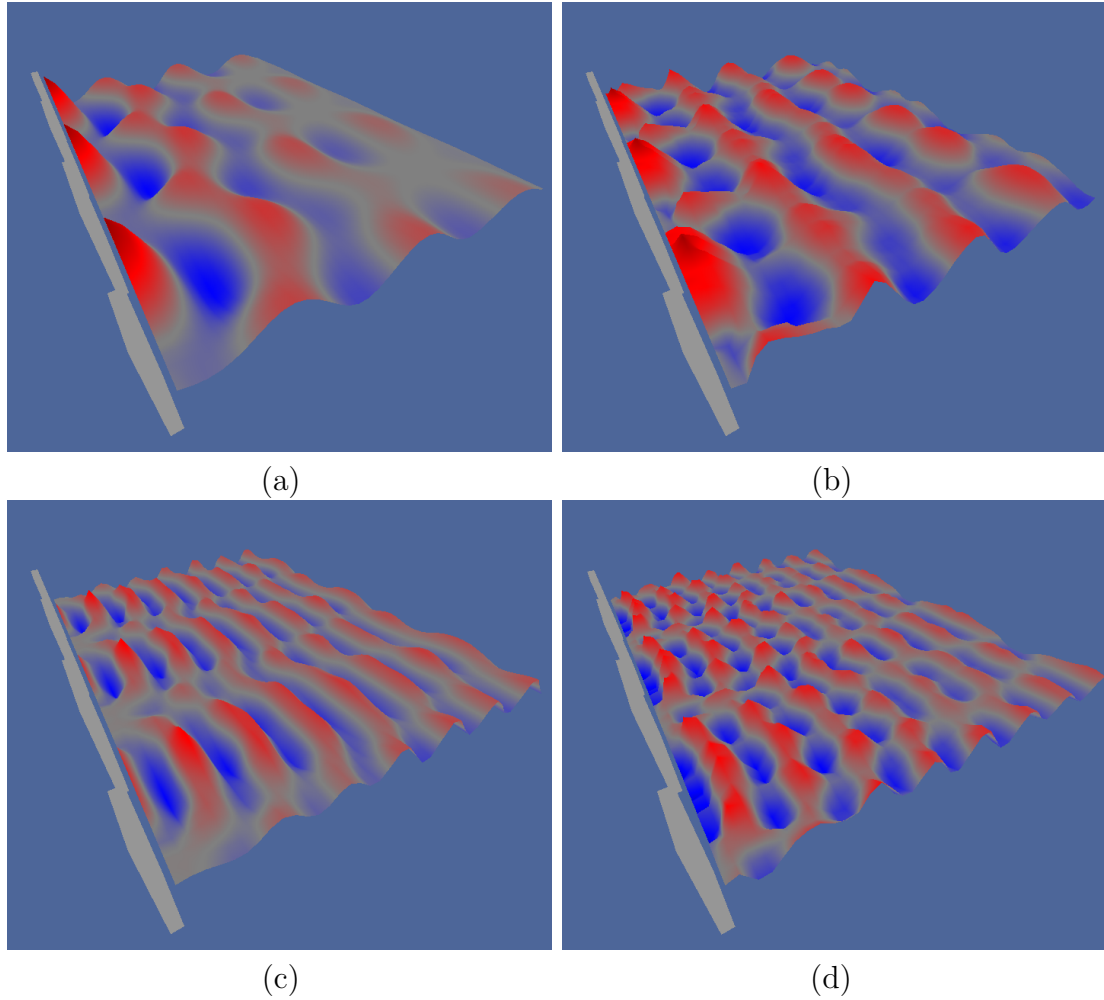


Figure 2.6: Visualization of wave propagation. FEM simulation (a, c) and phonon tracing (b, d) for the wave number $k=6$ (a, b) and $k=12$ (c, d).

where G_{ph_j} and G_{fem_j} is the sound strength at grid point j calculated with results from phonon tracing and FEM, respectively. The results are summarized in table 2.1. It can be observed that the error decreases until $k = 12$. That is because the diffraction effects not captured by the phonon tracing approach become smaller. Due to the shortcomings of the FEM method at higher frequencies the error increases again. Considering the results it can be said that both simulation methods are matched best at wave number $k = 12$. In figures 2.7 (c), 2.7 (f), and 2.7 (i) it can be noticed, that the blue regions on the error plots are predominant indicating overall error decrease. The gain plots of FEM and phonon tracing results at $k = 12$ (figure 2.7 (g and h)) are closer as those at $k = 3, 6$ (figures 2.7 (a and b), 2.7 (d and e)).

The FEM approach is the mathematically correct method in the frequency spectrum that can be represented by the grid (due to the Nyquist limit). In order to keep the calculation cost of the FEM appropriate, the grid size needs a limit. If the wave length reaches the order of the grid size, FEM becomes inaccurate. Phonon tracing is the more efficient method with a constant cost for all frequencies and provide at $k = 12$ similar results as the FEM, thus it can be used for the simulation of the acoustics at the frequencies above $k = 12$.

k	3	6	9	12	15
δ	8.216	5.164	3.989	3.784	4.903
ε	0.946	0.595	0.459	0.436	0.565

Table 2.1: Absolute and relative error in dB between FEM and phonon tracing.

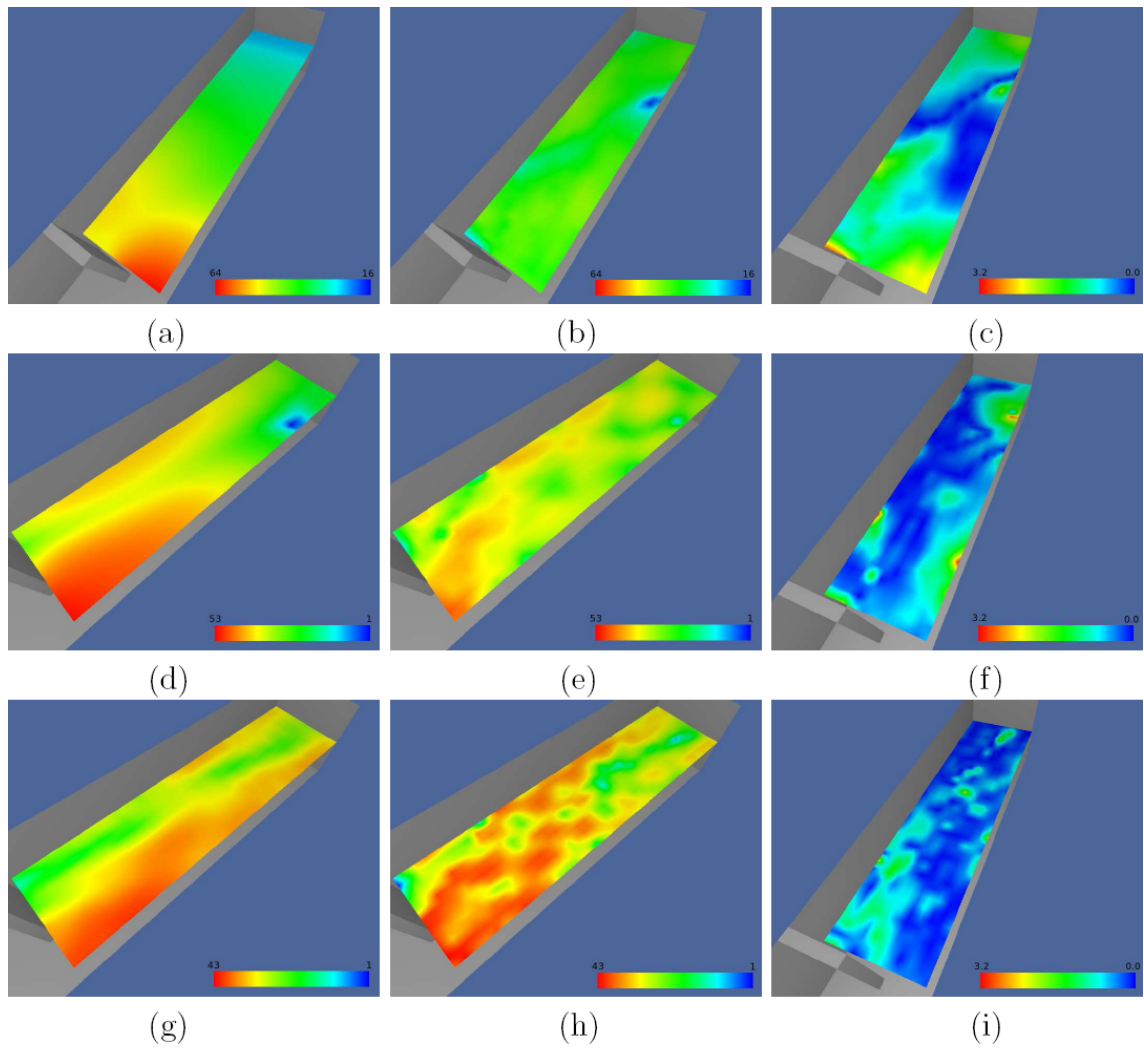


Figure 2.7: Sound strength visualization (values in dB). (a, d, g) FEM simulation, (b, e, h) phonon tracing, and (c, f, i) the relative error by wave number $k=3, 6$ and 12 . (top to bottom)

Chapter 3

Visualization

Simulating room acoustics is an important tool for the analysis and evaluation of existing and planned rooms. Modern computer technology with high computation power enables the extensive simulation of acoustics leading to a great amount of data which cannot be displayed in charts or tables.

Therefore visualization techniques need to be introduced which present the simulated data in a clear and comprehensible way. These techniques can be classified into two groups. The first considers the propagation of sound inside the room and the interaction of sound with the room boundaries, thus giving a global view on the overall sound behaviour. The second group focuses on given listener positions evaluating the impulse response calculated there.

This chapter presents different approaches for the visualization of simulated room acoustics. In section 3.1 novel techniques for the visualization of global sound behaviour are discussed. They evaluate the phonon map computed with phonon tracing (see section 2.1) to display sound propagation and interaction with the geometry and different material properties. The approaches for the visualization of sound behaviour and acoustic metrics based on a distinct listener position are covered in section 3.2. These techniques take the impulse response at the listener position into account and cover the detailed view on the impulse response itself, the importance of surface elements for certain acoustic metrics, and the visualization of sound interference and phase shift calculated with an acoustic rendering equation. Furthermore

novel approaches for the visualization of low frequency FEM simulation (see section 2.2) results are presented in section 3.3.

3.1 Visualizing the phonon map

This section presents visualizations which are based on the phonon map directly [DMB⁺06], thus showing the distribution, propagation and interaction of sound with the room geometry from a global standpoint. These visualizations, as they are based on the phonon map, show only the results of the emission step of the phonon tracing algorithm.

The phonon map characterizes the acoustic behaviour of a scene, considering the location of a specific sound source. It consists of the reverberations of a unit pulse, coming from different directions with different time delays and specific energy distributions. How can this complex information be visualized?

3.1.1 Phonon map

Given the phonon map as the result of the acoustic simulation using phonon tracing, the first naive attempt of visualization would be the display of all the particles or particle traces stored within. However, the number of particles in the map can be very high and thus the phonon map is too dense and no information can be extracted from the visualization. Figure 3.1 depicts the visualization of the particles in a phonon map with an increased number of particles displayed. Additionally to the occurring occlusion the representation of all the phonons depicts neither the sound propagation from the source nor the impact on a listener position.

Visualizing the phonon traces is also unsuitable because of the increasing occlusion and clutter when displaying more than a few traces at once. In figure 3.2 the visualization for an increasing number of traces can be seen.

The first approach to get an insight into the phonon map is now, to visualize not only a percentage of the phonons, but certain phonons with the same properties, like

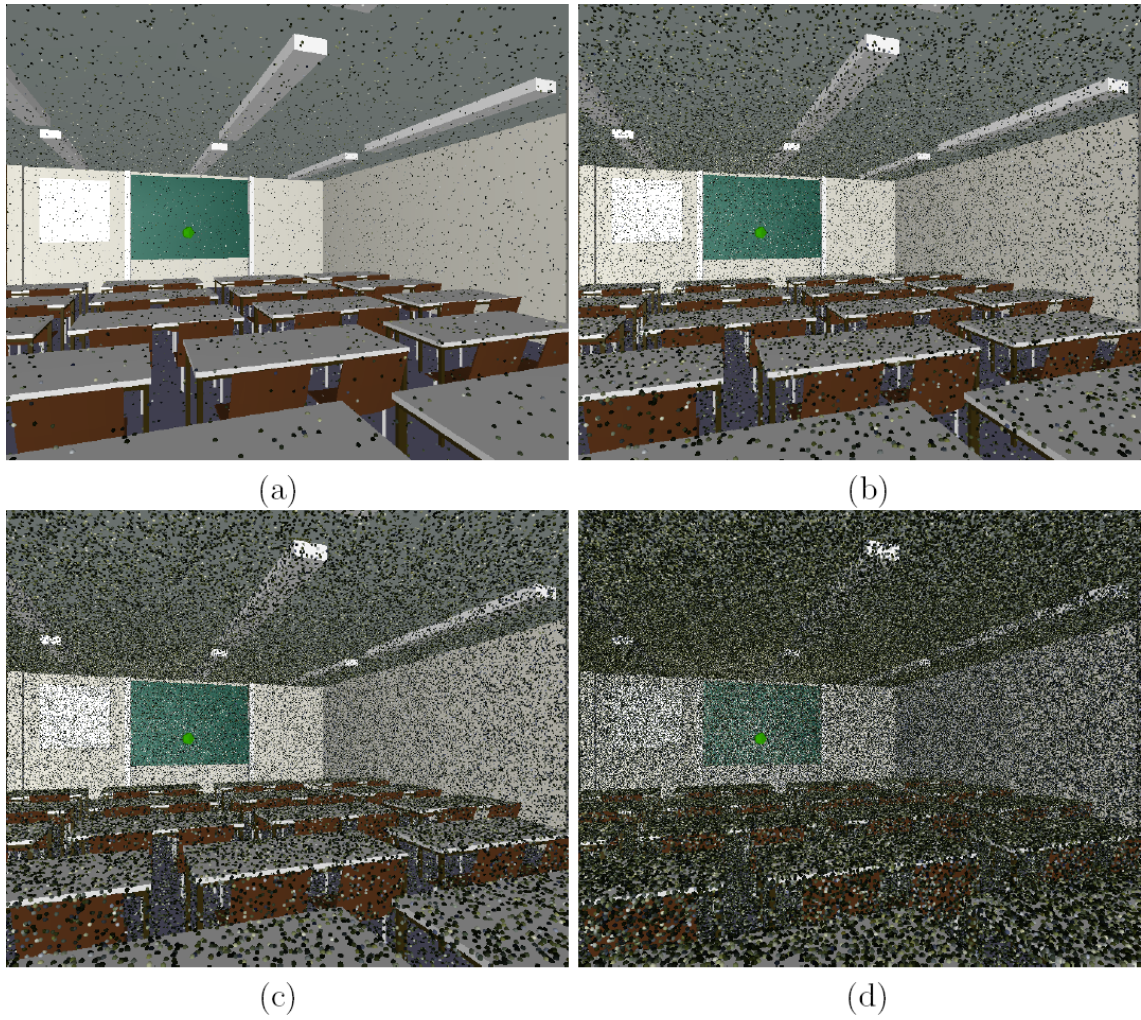


Figure 3.1: Phonon map representation with increasing number of phonons in the map from (a) to (d).

number of reflections or specific histories. This leads to the visualization of phonons on surfaces which is presented in the next section.

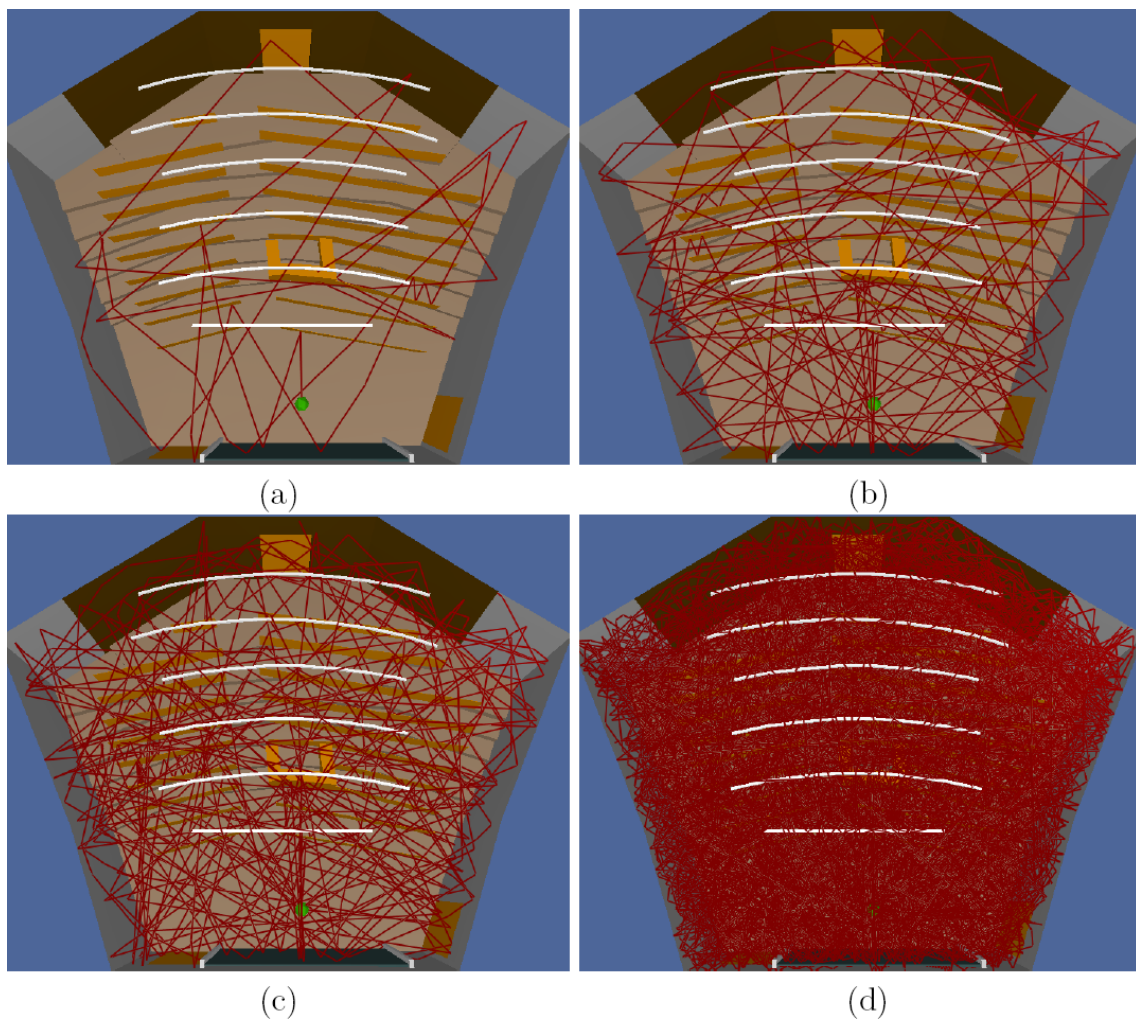


Figure 3.2: Particle paths represented by line segments. One (a) path, five (b), ten (c) and one hundred (d) paths.

3.1.2 Phonons on surfaces

Coloring For the visualization of single phonons two different schemes are used depending on the spectral energy of the phonon and the considered frequencies:

- All frequencies simultaneously: RGB model. The average of high, mid and low frequency ranges are mapped to the red, green and blue components, respectively.

Frequencies	Color component
5120, 10240, 20480 Hz	red
640, 1280, 2560 Hz	green
40, 80, 160, 320 Hz	blue

- Single frequencies: HSV model. The energy of the phonon in the chosen frequency is interpolated between red (full energy) and blue (energy equals zero)

The first approach to examine the phonon map is the visualization of certain phonons at their position on the surface inside the given scene. Each phonon is rendered as a sphere and is colored according to its spectral energy using the coloring scheme described above. In order to show the phonons outgoing direction v_p a cone whose peak is rotated towards v_p is rendered. The color of the cone corresponds to the phonon's energy, too.

Since the number of phonons in the phonon map is large only phonons with a given number of reflections n_p are rendered simultaneously. With this approach it can be examined how the surfaces of the considered scene affect the overall acoustic of the room.

Figure 3.3 shows an example of the visualization approach. The complete phonon map consists of one million phonons. In figures 3.3 (a) and (b) the overall frequency spectrum of the phonons after one (a) and four (b) reflections is depicted using the RGB components. As can be seen in figure 3.3 (a) the walls, the bottom and the canvas absorb high frequencies more than low frequencies which results in a bluish color due to more remaining energy in the low frequencies. The door (right side of figures) for example, reflects all frequencies equally resulting in a grey color

because of similar energy level left in all frequencies. After four reflections at the scene surfaces we can observe a shift towards lower frequencies. Sliding through the frequency bands we can observe the absorption for each individual frequency band using the HSV model to color the spheres. Figure 3.3 (c, d) shows the energy at 160 Hz and figure 3.3 (e, f) at 10240 Hz after one and four reflections, respectively. After four reflections there is about 75% of the energy of the phonons left at 160 Hz, whereas the energy at 10240 Hz is nearly completely absorbed by the room. By depicting the outgoing direction we can guess which object the phonon will hit next. Displaying the phonons on the surfaces gives a first insight into the phonon map and the characteristics of the room. But due to the amount of phonons in the map only fractions can be displayed at once to circumvent occlusions. Choosing the particles to display by means of common history or same number of reflections provides understanding of the influence of material properties on the acoustic of the room. However, the visualization is time independent and thus the propagation of the particles as well as the interaction with the geometry cannot be observed. This is overcome by visualizing the propagation of the particles as wavefronts which are not only time dependent but can also show the interaction with the geometry.

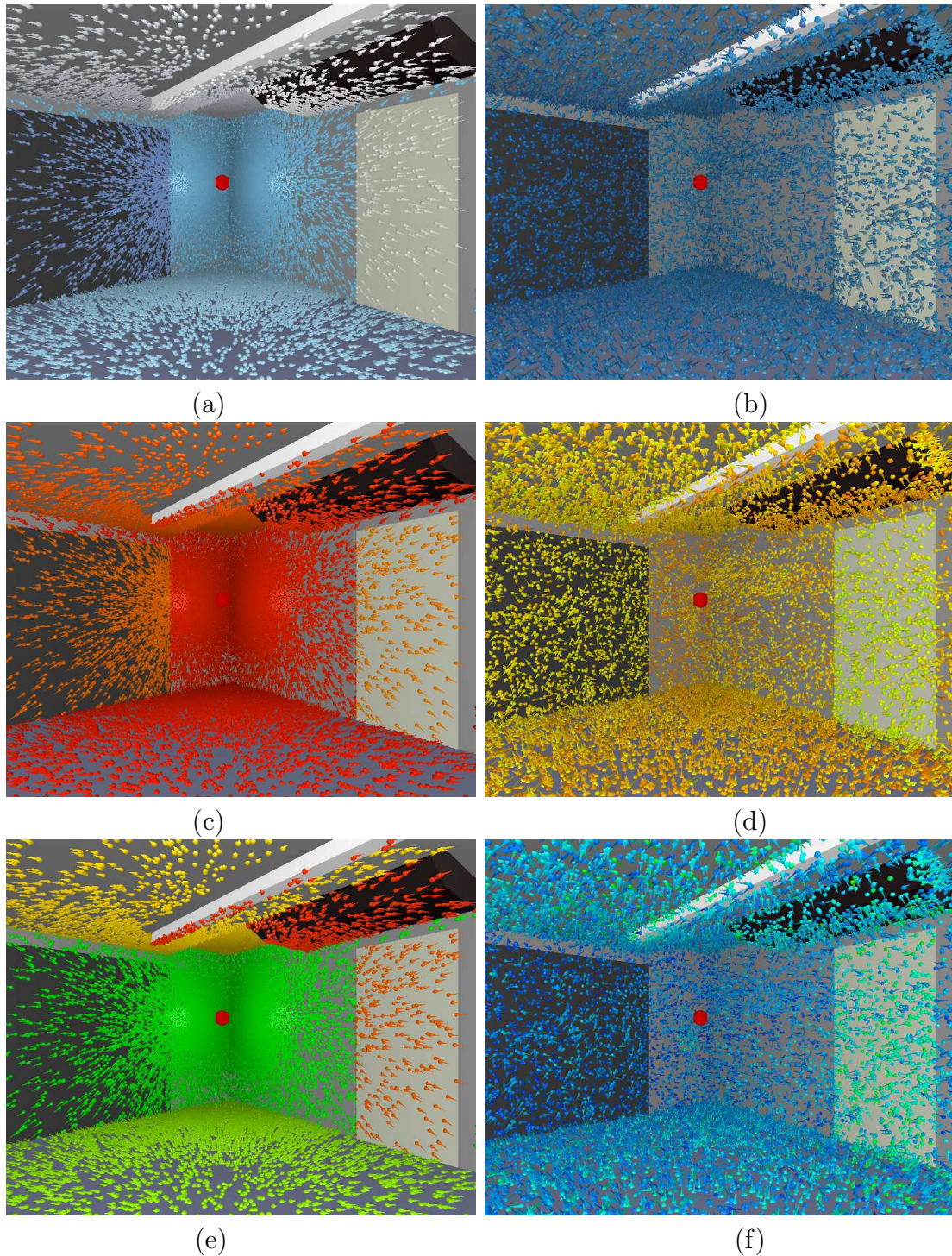


Figure 3.3: Visualization of particular phonons. First (a) and fourth (b) reflection using all frequencies for coloring (RGB). First (c, e) and fourth (d, f) reflection colored using single frequencies (HSV). 160 Hz and at 10240 Hz.

3.1.3 Phonon propagation

3.1.3.1 Particles

This visualization approach focuses on the spatial propagation of a Dirac impulse from the sound source. The corresponding wave front traverses the room and is reflected at surfaces, altering its intensity and energy spectrum. This wave front is visualized by rendering a small sphere for every phonon path with color coded spectral energy. All frequencies are considered simultaneously and the spheres are color coded using the RGB model as described above.

When moving through time, the spheres follow the phonon paths. At small time values, the reflected wave fronts are clearly visible. When the number of reflections increases, however, it becomes more difficult to recognize individual fronts. In order to tackle this problem, the following functions are integrated into the interactive visualization system:

- varying the percentage of phonons to be rendered
- rendering only the phonons reflected from a selected material
- exchanging selected materials
- varying time / traversed distance.

The data structure supporting this visualization is an array of phonons carrying their energy spectrum e_p , the traversed distance d_p , the phonon's position pt_p at a reflection point, and its outgoing direction v_p . In addition, the number of reflections r_p and the material m_p at the current reflection are recorded.

Since all phonons sharing the same path are listed consecutively in the array, it is simple, for example, to select all consecutive pairs p_i, p_{i+1} where the current time t satisfies $t_{p_i} \leq t < t_{p_{i+1}}$ and to draw a sphere on the line segment $p_{p_i}, p_{p_{i+1}}$, corresponding to a phonon's location at time t . In addition, certain predicates can be used, for example selecting all phonons whose path was reflected at the first (or at any) reflection on a selected material.

The change of a certain material requires only the phonons energy to be re-evaluated, where the phonon paths remain fixed. To allow the exchange, it is necessary to

enforce a minimum number of reflections for every path in advance, since otherwise materials with high absorption coefficients cannot be replaced.

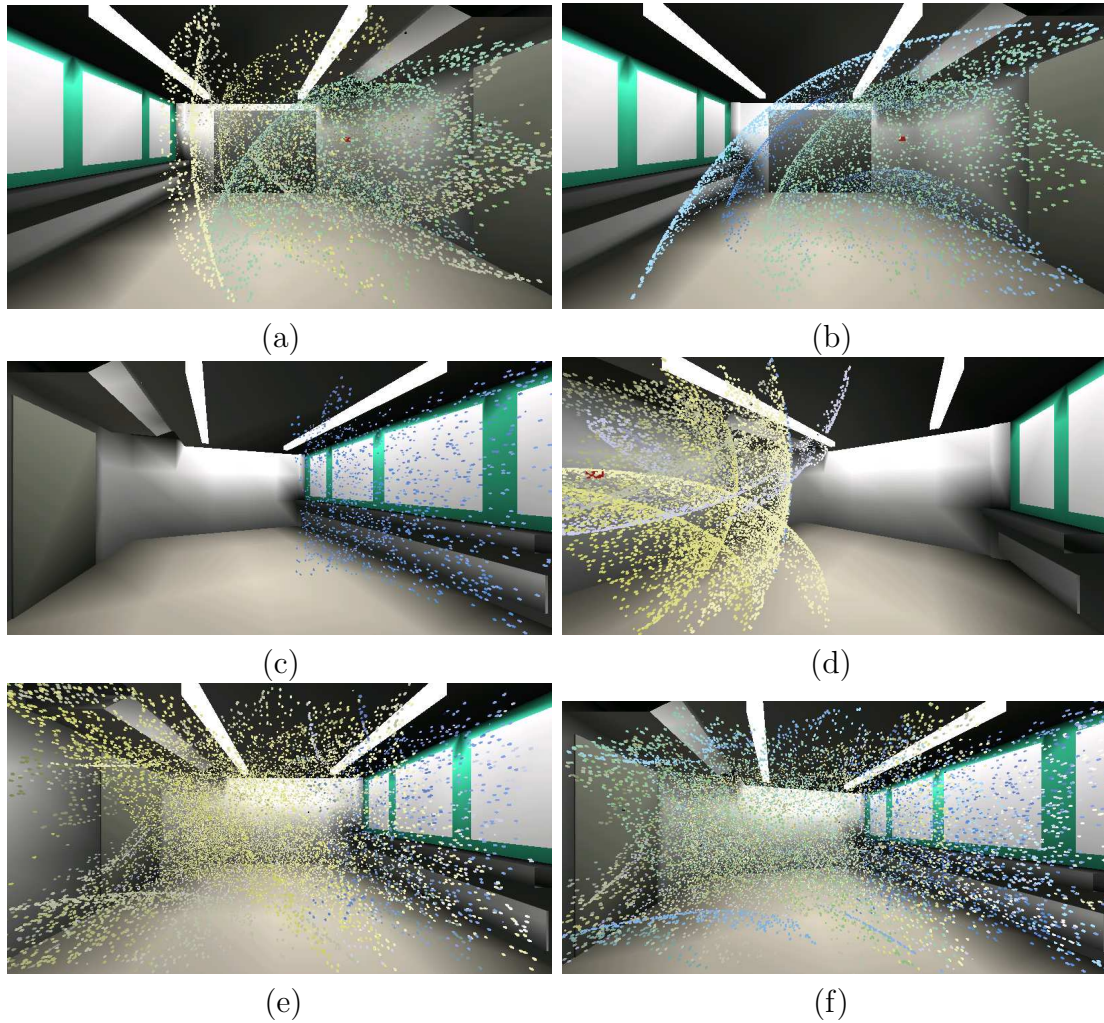


Figure 3.4: *Selecting wave fronts by material reflection.* (a) Phonons reflected at least once by a wall (b) phonons reflected from floor (c) phonons reflected from canvas (behind viewpoint). *Changing material of the floor.* (d) all phonons at $d = 1.5m$ (e) phonons at $d = 4.5m$ (f) same as (e) with old material.

Figure 3.4 depicts some examples of the visualization approach and the selection options. Figures (a) - (c) show the phonons reflected from the wall (a), the floor (b) and the canvas (c). On one hand the spatial propagation of the phonons can be observed and wave fronts can be identified. On the other hand the effects of the different materials can be seen from the coloring of the spheres. For example, figure 3.4 (c) clearly shows that the canvas absorbs nearly all energy in the high

and mid frequencies (R and G values reduced) but not in the low frequencies (B value still high), thus the resulting blue color. Figures (d) and (e) depict all phonons at $1.5m$ and $4.5m$ respectively but with a changed floor material (tiles instead of carpet and thus less absorption of high and mid frequencies). For comparison the phonons at $4.5m$ distance are shown using the old floor material (carpet) in figure (f). Comparing figures (f) and (e) clearly shows the shift in the spectral energy from blue (mainly low frequencies) to yellow (all frequencies present) and thus a better spectral distribution by changing the floor to a more reflective material.

The visualization of phonons as propagating spheres gives insight into the time dependent behavior of wave fronts inside the room and the coloring of the spheres a good view on the influence of different materials on the overall spectral distribution. An enhanced perception can be achieved by emphasizing the wave fronts using triangulated surfaces. This is presented in the next section.

3.1.3.2 Triangulated wave fronts

To further enhance the perception of wave fronts the next approach is to visualize wave fronts reflected at the room surfaces by use of triangulated surfaces. In order to build these surfaces knowledge about which phonons belong to a common wave front is needed. Therefore the phonons are subdivided in clusters of equal history, such that phonons in the same cluster satisfy the following criteria:

- equal numbers of reflections n_p
- and for each reflection:
 - equal material indices m_p (same object of the scene)
 - equal surface normals n at the reflection position

Consequently all phonons inside a cluster have equal energy spectra.

In order to build the cluster the phonons need to be traced back to the sound source and their histories need to be compared. This is not a difficult task since the phonon p_i re-uses the path and energy of the preceding one (see section 2.1). The normal of the surface hit by p_i can be easily computed as:

$$n = \begin{cases} v_{p_i} - (p_{p_i} - s) / \|v_{p_i} - (p_{p_i} - s)\| & \text{if } n_{p_i} = 1 \\ v_{p_i} - v_{p_{i-1}} / \|v_{p_i} - v_{p_{i-1}}\| & \text{else} \end{cases} \quad (3.1)$$

where s is the position of the sound source. The material index m_p is stored in the phonon map.

The surface of the wave front coming from the sound source is then constructed as a convex hull of phonons on the unit sphere and the neighborhood relationship of particular phonons is obtained. This relation does not change in time for a set of phonons in the same cluster, so the polygonal representation of the wave front must be calculated only once. For the construction of the convex hull on the unit sphere providing a Delaunay-triangulation the CGAL library¹ is used. The wave front surfaces reflected at the objects inside the considered room are built by keeping only triangles of the initial wave front whose vertices (phonons) reside in the according cluster. Figure 3.5 shows the wave front coming from the source. Where it hits the canvas, for example (figure 3.5 (b)), the faces that now belong to the wave front of the reflection at the canvas are separated from the initial surface.

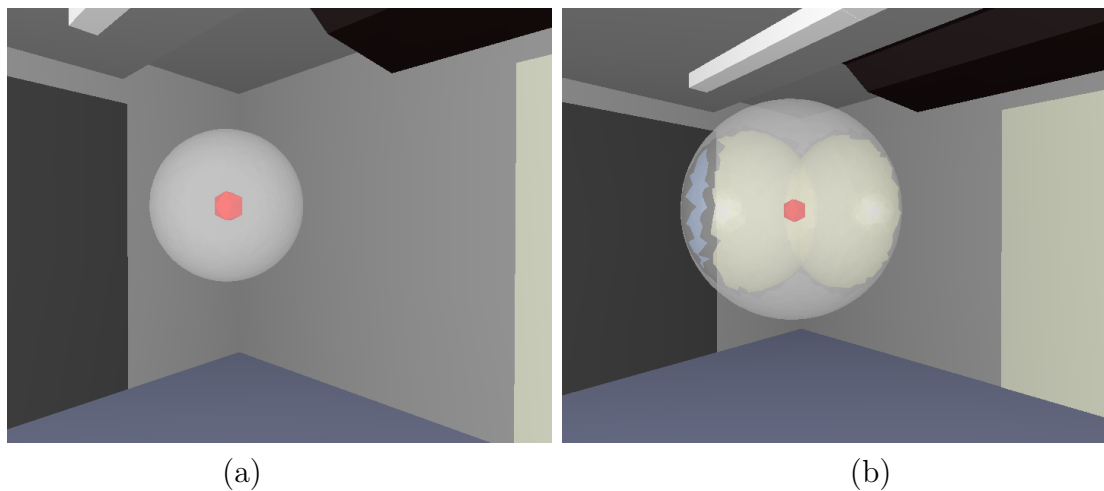


Figure 3.5: Wave front traversed from the sound source (a), separated after reflections (b).

Now the resulting surfaces for the visualization of the wave fronts reflected from the scene objects can be rendered. To illustrate where the wave front hits the object first and in which direction it propagates the phonons traversed distances d_p is used

¹<http://www.cgal.org>

to deform the surface. First, the maximum traversed distance d_{max} of all phonons inside the cluster is determined. Then, the phonons (which are the triangle vertices of the wave front surface) are rendered in an offset from the according scene surface:

$$p_p \leftarrow p_p + \left(1 - \frac{d_p}{d_{max}}\right) \cdot n \quad (3.2)$$

where n is the scene surface normal. This way, the offset between the original surface and the according visualized wave front is at most one unit. The wave fronts are color coded according to the energy spectra of the corresponding phonons. Depending on whether all frequency bands or each of them separately should be examined the RGB model or the HSV model as described in the previous sections is used. Furthermore, the surface transparency is set according to the average energy of the wave front.

For better clarifying the propagation direction of the wave fronts and the traversed distance, the option to draw colored cones at the position of the phonons is provided. The peaks of these cones are rotated towards the phonons outgoing directions. Their color corresponds to the traversed distance and is calculated by use of the HSV model as follows:

$$(1 - \alpha) \cdot H_{red} + \alpha \cdot H_{blue} \text{ with } \alpha = \frac{d_p}{l_{max} \cdot n_p} \quad (3.3)$$

where l_{max} is the maximum distance of the scene. In this case red corresponds to $d_p = 0$ and blue to the maximum possible distance depending on number of reflections n_p . Using the above equation for color mapping the cones the traversed distance of wave fronts reflecting at different objects for a given number of reflections can be compared. Since displaying all wave front surfaces becomes complex, the implementation provides the alternative to select wave fronts by number of reflections, material(object) or history.

Figures 3.6 and 3.7 show examples of the described visualization approach. The red sphere in the corner of the room represents the sound source. Figure 3.6 depicts the wave fronts of first reflections coming from the bottom, the wall and the canvas. In image 3.6 (a) and (b) the wave fronts color coded using the RGB model and overall frequency spectrum as described above are displayed. It can be observed that the bottom and the canvas predominantly absorb more high frequencies, whereas the

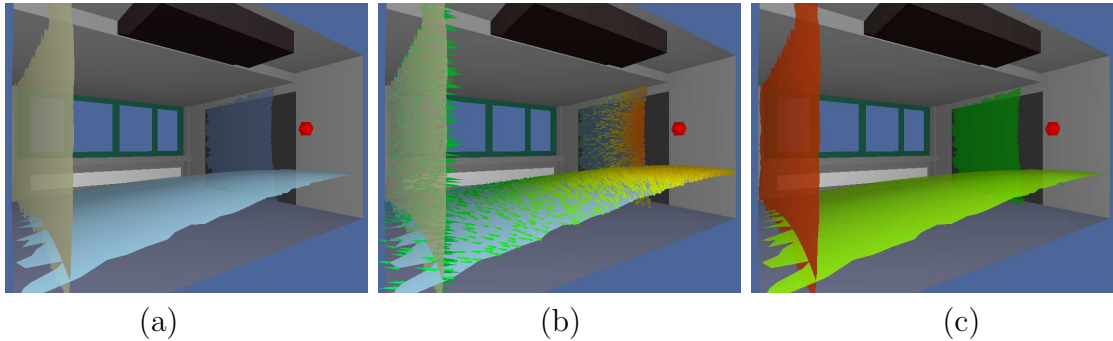


Figure 3.6: Clustered wave fronts. (a) first reflection color coded using the overall frequency spectrum. (b) Traversed distance represented by use of cones. (c) first reflection color coded using the frequency band at 10240 Hz.

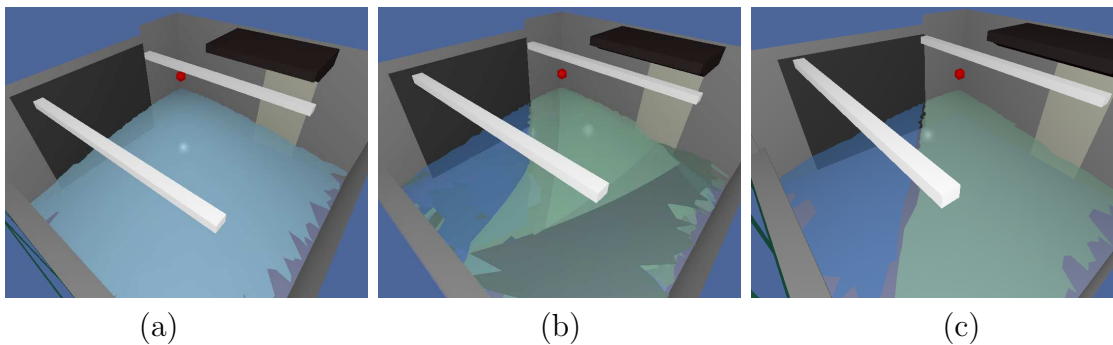


Figure 3.7: Clustered wave fronts. First (a) and second (b) reflections at the bottom. (c) Second reflections at the bottom reflected before at the wall and canvas, respectively.

wall absorbs more low frequencies. Figure 3.6 (c) shows the wave front surfaces color coded by use of HSV model and the frequency band at 10240 Hz. This frequency band is absorbed by the canvas and bottom, but is reflected almost completely by the wall.

The surfaces are deformed according to the traversed distance of the phonons belonging to the clusters. Here, we can observe where the wave fronts hit the room surfaces first and in which direction they will further spread. A representation of the traversed distance by use of colored cones (figure 3.6 (b)) shows that the wave front propagated from the sound source hit the canvas and the bottom before the wall.

Figure 3.7 presents the wave front reflecting at the bottom the first (a) and the second time (b,c). Since reflections coming from all objects inside the scene can

overlap (fig. 3.7 (b)) the option to select different wave fronts is provided. In figure 3.7 (c) the second reflection at the bottom reflected first at the wall and the canvas, respectively is shown. In this picture it can be observed how the energy spectrum of the wave front changes and how it is split during the reflections at the room surfaces. This way the interaction of the single objects inside the room can be examined.

However, since the wave front traversed from the sound source is split after each reflection, the visualization approach described in this section is applicable only to the first few reflections because of increasing clutter and nonconnected wave fronts.

Having dealt with the visualization of the phonon map itself from an overall standpoint in the last sections, the next sections will provide information about the room acoustics from a distinct position within the room, using the so called listener based visualization.

3.2 Listener based visualizations

In contrast to the visualizations in the last section, the following visualizations are based on a location, namely the listener position and thus give a "view" of the sound behavior in the room from a distinct point.

3.2.1 Listener spheres

The approaches described above visualize the phonon map considering the surfaces of the room and their acoustic properties. In this section the visualization method depicting the received energy at a listener position is presented. With this approach it can be detected from which direction the most energy reaches the listener and the energy spectrum can be visualized.

For this purpose a triangulated sphere is deformed according to the weighted phonons received at the listener position. The phonons are collected using the collection step described in section 2.1. For each phonon which contributes to the total energy at the listener position, first the intersection point $p_{intersec}$ of the ray from the center c_s of the sphere to the phonons position pt_p is calculated and the intersected triangle determined. Then the energy e_{sp} and the displacement $disp_{sp}$ of the triangle vertice sp with minimal distance to $p_{intersec}$ is increased as follows:

$$e_{sp} \leftarrow e_{sp} + fac \cdot \begin{pmatrix} (e_{p,8} + e_{p,9} + e_{p,10})/3 \\ (e_{p,5} + e_{p,6} + e_{p,7})/3 \\ (e_{p,1} + e_{p,2} + e_{p,3} + e_{p,4})/4 \end{pmatrix} \quad (3.4)$$

$$disp_{sp} \leftarrow disp_{sp} + fac \cdot \frac{1}{10} \sum_{i=1}^{10} e_{p,i}$$

$e_{sp} \in \mathbb{R}^3$, $disp_{sp} \in \mathbb{R}$ if all frequency bands are considered and

$$e_{sp} \leftarrow e_{sp} + fac \cdot e_{p,i} \quad (3.5)$$

$$disp_{sp} \leftarrow disp_{sp} + fac \cdot e_{p,i}$$

$e_{sp} \in \mathbb{R}$, $disp_{sp} \in \mathbb{R}$ if a certain frequency band is chosen. Thereby fac is the gaussian distance described in section 2.1. In order to smooth the sphere representation, the energy of the points sp_j around sp is increased, if $arccos(\langle c_s - sp_j, c_s - sp \rangle) < \alpha$ for a given angle α as follows:

$$\begin{aligned} e_{sp_j} &= w \cdot e_{sp} \text{ where} \\ w &= 1 - (arccos(\langle c_s - sp_j, c_s - sp \rangle) / \alpha) \end{aligned} \quad (3.6)$$

Afterwards, the energy and the displacement of the sphere points are normalized. Therefore the maximal displacement $disp_{max}$ and energy e_{max} (in all three components) of all points is determined the values normalized according to:

$$\begin{aligned} e_{sp_j} &\leftarrow \frac{e_{sp_j}}{e_{max}} \\ disp_{sp_j} &\leftarrow \frac{disp_{sp_j}}{disp_{max}} \end{aligned} \quad (3.7)$$

In order to consider occlusion of the listener position, the energy values of the sphere points sp_j are scaled as follows:

$$\begin{aligned} e_{sp_j} &\leftarrow e_{sp_j} \cdot \frac{n'_{ph}}{n_{ph}} \\ disp_{sp_j} &\leftarrow disp_{sp_j} \cdot \frac{n'_{ph}}{n_{ph}} \end{aligned} \quad (3.8)$$

where n_{ph} is the number of phonons in the phonon map and n'_{ph} the number of phonons which are seen from the listener.

Now after the calculation of the displacement factors and energy at each point of the sphere the spheres at given listener positions can be deformed and rendered. The new position of the point sp_j results in:

$$sp_j \leftarrow sp_j + disp_{sp_j} \cdot \frac{c_s - sp_j}{\|c_s - sp_j\|} \quad (3.9)$$

The color of the sphere points is calculated by use of the RGB (for overall frequency spectrum) or the HSV (certain frequency band) model as mentioned in the previous sections.

To assess the acoustic quality at a listener position it is important to know at which time the reflections arrive at the listener. Therefore the option to set the lower and upper time limits for phonon selection is available.

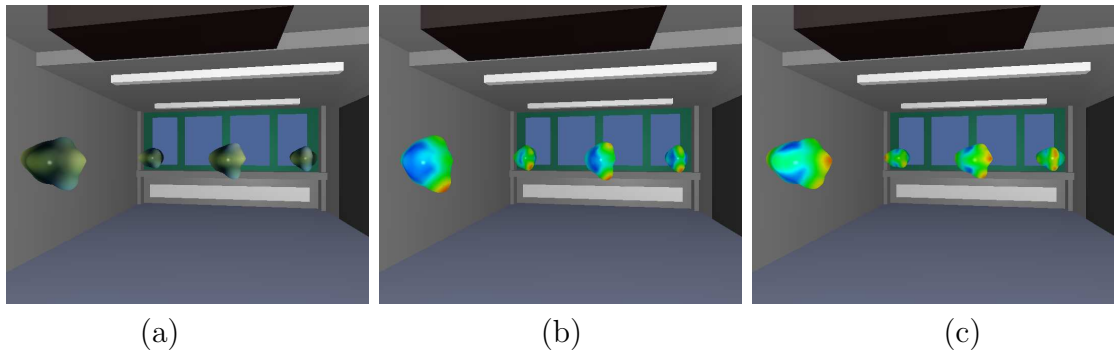


Figure 3.8: Deformed spheres representation at four listener positions. (a) color coded using the overall frequency spectrum (b) by 80 Hz and (c) by 1280 Hz.

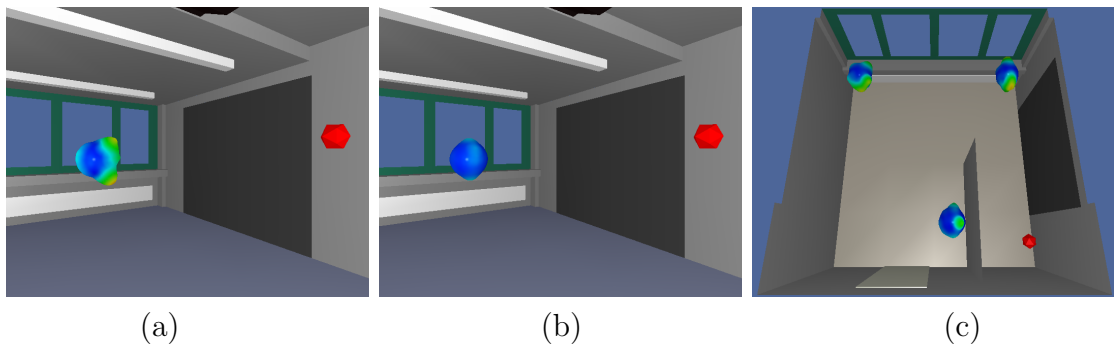


Figure 3.9: Deformed spheres representation at 80 Hz collected before (a) and after (b) 50 msec at one listener position. Deformed spheres representation at 5120 Hz at three position in a room with a separating wall with total absorption (c).

The following figures present the results of the presented visualization approach. Figure 3.8 (a) shows spheres at four positions in the considered room. The energy is collected over the entire time interval. The spheres are deformed and color mapped by using the overall energy spectrum. It can be seen that the most energy of low frequencies arrives at the listener from the bottom and the ceiling, since they do not absorb low frequencies. Whereas middle and high frequencies reach the listener from the walls. Considering the energy at 80 Hz (figure 3.8 (b)) and at 1280 Hz (figure 3.8 (c)) it can be observed that most part of the energy at 80 Hz reflects at the bottom and ceiling, and at 1280 Hz most part is reflected at the walls.

The depicted spheres in figure 3.9 (a) and (b) are deformed and color coded using the energy at 80 Hz of phonons that reached the listener position before and after 50 msec, respectively. It can be observed that the whole energy of the reflections at the room surfaces arrives at the listener before 50 msec. In this way the amount of early to late reflections can be compared.

Figure 3.9 (c) shows the same room with a separating wall with total absorption. This wall prevents most reflections from the surfaces on the left side of the room to the right side and vice versa. One listener position is placed behind the wall and two in the corners of the room. The spheres for the frequency band at 5120 Hz are rendered. As can be seen, no reflections are received from the separating wall and only few reflections reach the listener from the left and right room surfaces.

The visualization approach presented in this section enables the inspection of the directional aspect of sound from a listeners point of view. From the deformed and colored listener spheres the amount of incoming energy as well as the direction can easily be perceived. By choosing time limits for the collection a first insight into the ratio of early to late received energy can be achieved. The visualization also gives a first hint on how the acoustic of the room can be improved for a certain position by showing when, how much and from where energy is received. However, only the "last" direction can be observed by using the listener spheres. The next section introduces an approach which computes importance values for the geometry depending on a chosen acoustic metric. These importance values give a direct hint how the room acoustic can be improved at certain positions and throughout the whole room.

3.2.2 Surface importance

This section describes a visualization approach that uses the phonon tracing method to calculate the contribution of the reflection surfaces to the impulse response for different listener positions [MDHB⁺07]. This data is used to compute importance values for the geometry. Here importance denotes how much a certain scene surface contributes to an acoustic quality measure (see section A.2). To get a visual insight into the directional aspect, the importance is mapped to the reflecting surfaces of the geometry. This visualization indicates which parts of the surfaces need to be

changed to enhance a certain acoustic quality measure at different listener positions or the complete audience.

Importance values The intention is to visualize which parts of the scene surface are most important for a certain acoustic measure at every listener position l_i . To calculate an importance value for a phonon the pressure contribution of the phonon ph_j to the impulse response at a given listener position l_i is used.

Because the phonon tracing method re-uses particle paths for multiple phonons (a phonon is stored at every reflection, tracing a large number of reflections until the energy contribution drops below a threshold) subsequent phonons on the same path have to be taken into account when calculating the pressure contribution for a certain phonon ph_j (see figure 3.10 (a)). Figure 3.10 (b) depicts one phonon paths throughout the room.

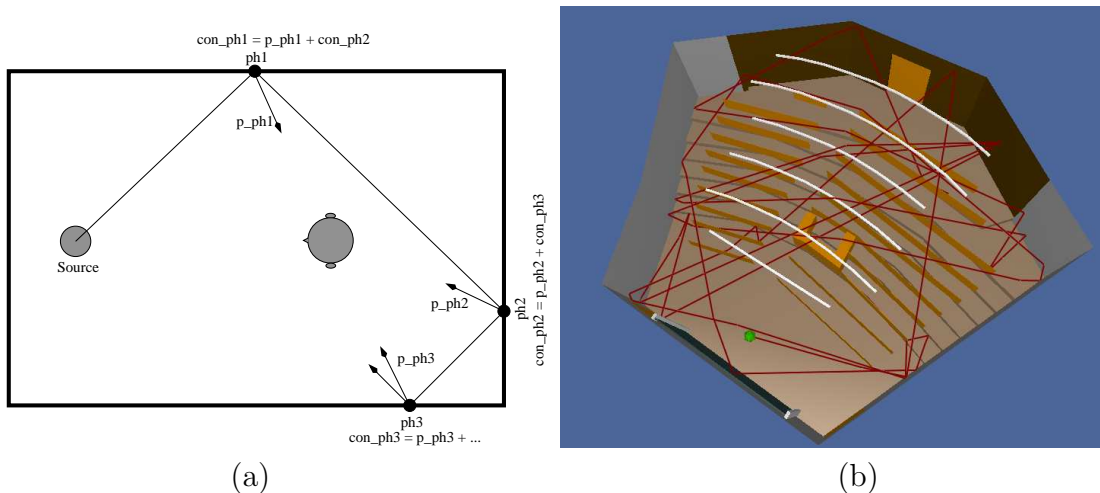


Figure 3.10: (a) Calculation of the contribution con_{ph} for phonons sharing the same path. (b) Illustration of one phonon path.

The contribution of a single phonon ph to the impulse response is denoted in sections (2.1.2 (pressure)) and (2.1.1 (energy)). All phonons corresponding to one reflection path are listed in consecutive order within the phonon map, say $ph_{k_0}, ph_{k_0+1}, \dots, ph_{k_n}$. The pressure and energy contribution of a phonon ph_j to the impulse response at listener position l_i is then the accumulated contribution of itself and its successors as stated in equation (3.10) for pressure con_p and energy con_e .

$$\begin{aligned}
con_p(ph_j, l_i) &= \sum_{k=j}^{k_n} p_{ph_k}(t, l_i) \\
con_e(ph_j, l_i) &= \sum_{k=j}^{k_n} e_{ph_k}(t, l_i),
\end{aligned} \tag{3.10}$$

where p_{ph_k} , e_{ph_k} are the pressure and energy received at listener position l_i from the single phonon ph_j .

Due to the fact that all phonons sharing the same path are listed consecutively in the phonon map, the contribution of a phonon can easily be computed by forward summation of the contribution of subsequent phonons. In addition to the importance of the phonon to one listener position l_i , the contribution of the phonon to all listener positions in the scene (or to a selected subset) is also calculated:

$$\begin{aligned}
con_p\ all(ph_j) &= \sum_{i=0}^{n_l} con_p(ph_j, l_i) \\
con_e\ all(ph_j) &= \sum_{i=0}^{n_l} con_e(ph_j, l_i)
\end{aligned} \tag{3.11}$$

where n_l is the number of listeners, $con_p(ph_j, l_i)$ and $con_e(ph_j, l_i)$ are the contribution of a phonon to a single listener position l_i .

To calculate an importance value $imp_e(ph, l_i)$ and $imp_p(ph, l_i)$ for a phonon ph and listener position l_i the fraction between the contribution of the phonon ph to the pressure or energy at the listener position l_i and the total received pressure or energy at the listener position (i.e. percentage of pressure received at position l_i from phonon ph) is calculated.

$$\begin{aligned}
imp_p(ph_j, l_i) &= \frac{con_p(ph_j, l_i)}{p_{tot, l_i}} \\
p_{tot, l_i} &= \sum_{k=0}^{n_{ph}} p_{ph_k}(t, l_i)
\end{aligned}$$

$$\begin{aligned}
imp_e(ph_j, l_i) &= \frac{con_e(ph_j, l_i)}{e_{tot, l_i}} \\
e_{tot, l_i} &= \sum_{k=0}^{n_{ph}} e_{ph_k}(t, l_i)
\end{aligned} \tag{3.12}$$

where n_{ph} is the total number of phonons, p_{tot, l_i} and e_{tot, l_i} are the total pressure and energy received at l_i .

To evaluate speech comprehensibility in room acoustics, for example, it is important to analyse the ratio between early received sound to the later received reverberations. Therefore, an option to choose a time limit t_{end} such that the contribution of each phonon that reaches the listener after t_{end} is set to zero is provided. By means of the importance values for each phonon in the map the impact of reflection surfaces in the scene for a chosen range of listeners is visualized.

Visualization In the following the visualization approach conveying the importance of particular room surfaces for the received sound signal at a listener position is described. The goal of the visualization is to highlight the surfaces of the scene that reflect the most energy of a sound wave to a given listener position and therefore are most important for the evaluation of acoustic behavior regarding acoustic measures such as definition ("Deutlichkeit" [DIN00]) and clarity. These acoustic metrics consider the amount of early received energy to the amount of entire and late received energy respectively (see section A.2).

Definition ("Deutlichkeit") is defined without regards to the direction where the sound energy came from. The visualization system allows to observe the origin of the early and entire energy, respectively, and relate them visually to each other.

First, some preprocessing steps are performed in order to prepare the scene geometry for the visualization. The 3D room models used for simulation and visualization are defined in Wavefront obj format. The scene consists of triangulated objects. After the tracing process we know the phonons' positions and connect each phonon to the reflecting scene object. The triangulation of the scene used for the acoustic simulation is low in resolution to keep the computation moderate. For a detailed visualization more sample points are needed to provide the correct approximation of the surface importance. Therefore the triangles are refined using a subdivision

algorithm as outlined in Fig. 3.11. The subdivision is terminated when all edges of a triangle have a smaller length than a given threshold λ .

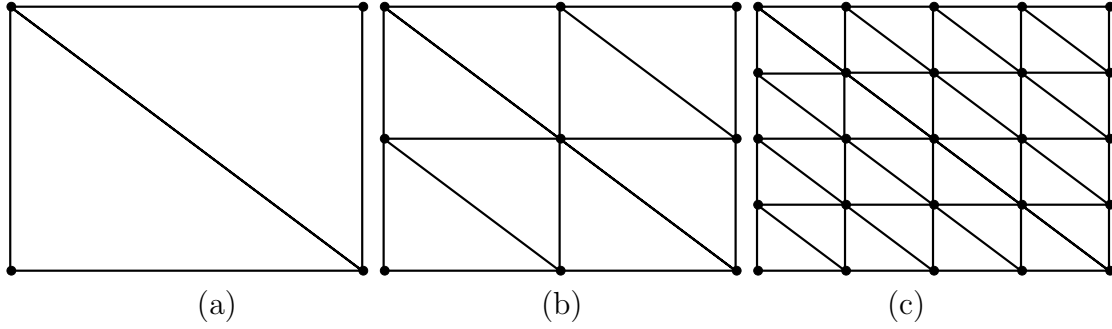


Figure 3.11: Surface subdivision. (a) initial triangulated surface. (b) triangulation after first subdivision step. (c) triangulation after second subdivision step.

In order to obtain the desired level of detail for the visualization color values are mapped to the vertices depending on the contributions of the phonons associated with adjacent triangles. Since we have many more phonons than vertices we use a scattered data approximation approach

$$\begin{aligned} imp_{v_i} &= \frac{\sum_{k=0}^m \omega \cdot imp(ph_k)}{\sum_{i=0}^m \omega} \\ \omega &= \frac{1}{\sigma\sqrt{2\pi}} \cdot e^{-\frac{d^2}{2\sigma^2}} \end{aligned} \quad (3.13)$$

where σ is proportional to the edge length and d is the distance between the phonon's position and the vertex v_i . Furthermore we consider only phonons ph_k which satisfy the condition

$$\langle n_t, n_{v_i} \rangle > 0 \quad (3.14)$$

to neglect phonons residing on a different face of an object. Here n_t is the normal of the triangle containing the phonon ph_k and n_{v_i} denotes the normal at v_i . The latter can be calculated as interpolation normal of the corresponding triangle normals.

The second approach which is utilized to calculate the importance of the vertices takes only phonons ph_k into account which are located in a tight neighborhood of

v_i (the distance of the phonon's position to the considered vertex is smaller than a given threshold). The importance value of v_i is then the average of the importance values $imp(ph_k)$ of the phonons ph_k :

$$imp_{v_i} = \frac{\sum_{k=0}^m imp(ph_k)}{m} \quad (3.15)$$

Additionally, the condition in 3.14 has to be satisfied for two-sided scene elements. Now, since the importance values for each vertex in the scene are calculated the corresponding color is assigned to each v_i . The color value for v_i is calculated as follows:

$$\begin{aligned} c_{v_i} &= \alpha \cdot hue_{max} + (1.0 - \alpha) \cdot hue_{min} \\ \alpha &= \frac{imp_{v_i} - imp_{min}}{imp_{max} - imp_{min}} \end{aligned} \quad (3.16)$$

where imp_{min} and imp_{max} are the minimum and maximum importance values in the scene and hue_{min} and hue_{max} denote the minimum and maximum hue values, respectively. Red color was chosen for hue_{max} and blue color for hue_{min} and the color for the vertices v_i is interpolated from red to blue in HSV color space. Now that the refined triangulated geometry of the considered scene, and color values for each v_i corresponding to the importance values is available we can render the entire scene using OpenGL texture mapping techniques or simple primitives rendering.

Furthermore, the visualization system provides some additional options for user interaction:

- selection of break-off time t_{end} for early reflections
- selection of start time t_{start} for late reflections
- selection of one listener position l_i
- selection of one object o_j inside the scene

Results In the following results of the listener-based analysis of surface importance for acoustic metrics presented above are shown. The method is applied to the acoustic improvement of a lecture hall at the university. A main acoustic measure for a lecture hall is the comprehensibility of speech which is expressed with the acoustic metric clarity (C_{50}). The C_{50} values alone only show the current acoustic state but give no insight how it can be improved (e.g. where to put absorbing material). The listener-based analysis of surface importance overcomes this drawback by visualizing the directional aspect by means of mapping importance values to the room surfaces. In the case of clarity the importance is based on energy received in the first 50ms after the primary wave front and energy received after the first 50ms, respectively. The visualization of these importance values give a clear advice which parts of the room geometry need to be changed (by means of exchanging material) to improve the chosen acoustic metric (clarity).

Glyphs In order to visualize this metric (clarity C_{50}), glyphs analog to the approach described in [SG89] are used. The representation of the glyphs is as follows. The early reflections and late reverberations are represented as semicircles where the semicircle for the early reflections is placed above that for late reverberations. The radii of the semicircles correspond to the early and late received energy, respectively. Thus, the direct comparison of early and late reflections is possible. In addition to the ratio the glyphs also show if the clarity is above a certain threshold (e.g. $C_{50} > 3dB$). This is visualized by coloring the lower semicircle green for above or red for below the chosen threshold respectively. Examples are depicted in figure 3.12.

These glyphs are used to assess the value of the visualization. The C_{50} values are derived from the simulated impulse responses for each position. Nevertheless, this metric is independent of the direction of the arriving sound wave at a listener position and gives only insight in the current acoustic state. However, the glyphs can be used to evaluate the results of the listener-based importance visualization.

Lecture hall The university lecture hall subject to acoustic optimization is presented in figure 3.13. The materials used in this hall are as follows:

- concrete (floor, ceiling, gray walls)

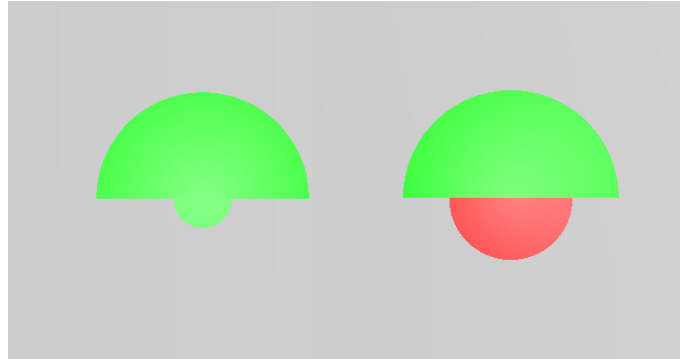


Figure 3.12: Example for clarity (C_{50}) visualization using glyphs. Left: C_{50} above given threshold (green lower semicircle). Right: C_{50} below given threshold (red lower semicircle).

- metal (doors, blackboard frame)
- wood (desk, benches, brown walls)

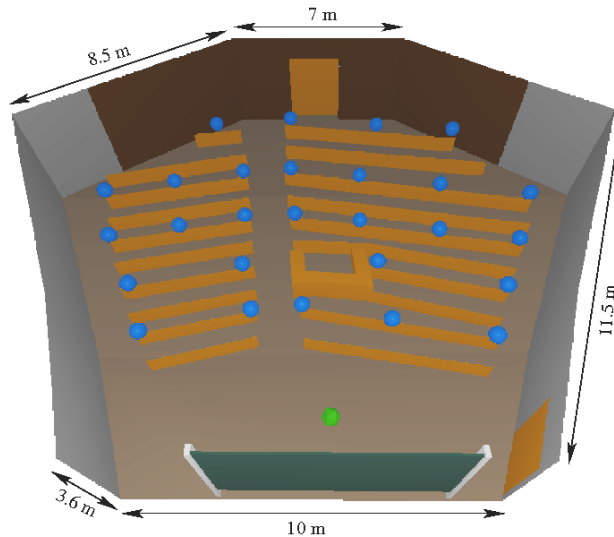


Figure 3.13: Lecture Room setup. Green: speaker, blue: audience

Speaker and audience are depicted by the green and blue spheres, respectively. Phonon tracing for sound pressure (section 2.1.2) is used to calculate the impulse response and thus the definition and clarity values at the listener positions.

Since the comprehensibility of the human speech, which has a frequency range from 150 Hz - 4 kHz with a main focus around 1kHz [CM78], should be improved, the 1

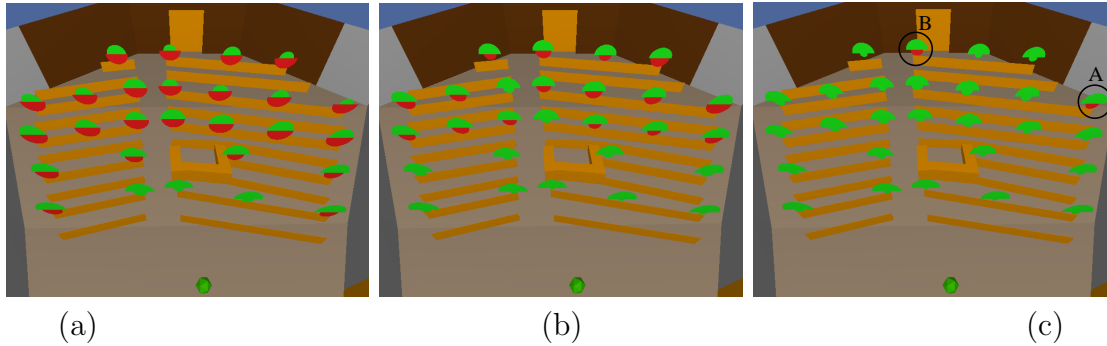


Figure 3.14: C_{50} Glyphs at listener positions in the lecture hall. (a) Actual materials/absorption coefficients. (b) Glyphs at listener positions for changed ceiling (above speaker) material with highly absorbing material (sound absorbing foam). (c) Glyphs at listener positions for changed backwall material with sound absorbing foam.

kHz octave band is used for the evaluation. If improving a music hall, one has to adjust and use more octave bands because music spans a wider range of frequencies than human speech. To get an overview of the current acoustic state of the room glyphs for the clarity (C_{50}) measure are rendered at all listener positions. The C_{50} values for the 1kHz frequency band are shown in figure 3.14 (a). These values are derived from the impulse responses at the different listener positions. For the simulation of the impulse responses the actual material/absorption coefficients were used. The threshold for C_{50} was set to $3dB$.

Figure 3.14 (a) clearly shows that the desired clarity is only reached at the three closest positions to the speaker (green lower semicircles of the glyphs). Depending on the individual hearing ability of the listeners the second and third row could be acceptable (red lower semicircle but smaller than upper green semicircle) whereas the clarity in the last two rows is unacceptable (red semicircle is bigger than green semicircle). This clearly indicates the need of acoustic improvement, but the glyphs cannot give any cue how to alter the room so that the acoustic situation is acceptable.

Analysis of surface importance To get insight into the directional aspect of the current acoustic situation, importance values based on the chosen acoustic metric (clarity C_{50}) are calculated. As clarity describes the ratio between early ($< 50ms$) and late ($> 50ms$) received energy the break-off time t_{off} for early and the start time t_{start} for late reflections were set to $50ms$. All values were calculated for the

1kHz frequency band with all listener positions taken into account. The importance values are then mapped to the room surfaces as shown in figures 3.15 (a) + (b) (topview) and 3.16 (a) + (b) (sideview). In addition to the importance for early and late reflections we calculate a difference image by subtracting the importance for early reflections from the importance for late reflections (figures 3.15 (c) + 3.16 (c))

As described in section 3.2.2 the highest importance value imp_{max} is mapped to hue_{max} (red) and the lowest importance value imp_{min} to hue_{min} (blue). Thus red areas in figures 3.15 (a) + (b) and 3.16 (a) + (b) depict the parts of the room surface which contribute most to early (a) and late (b) reflections.

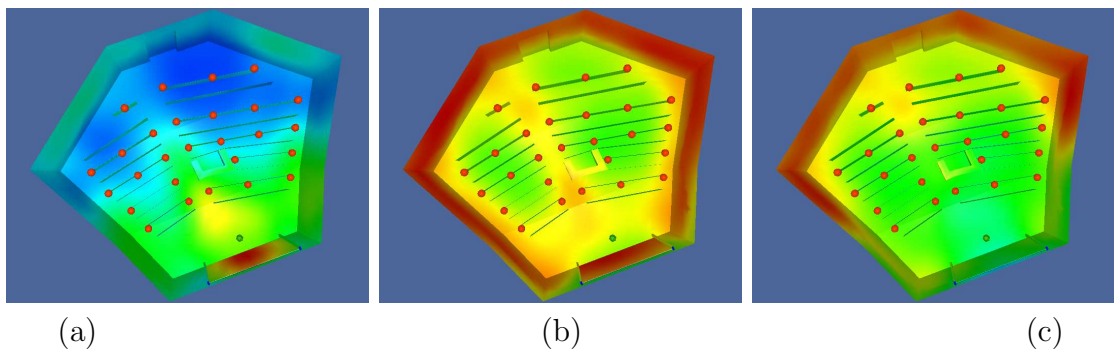


Figure 3.15: Importance values whole audience and 1kHz mapped to the room surfaces (topview). (a) Importance for early reflections ($< 50ms$), (b) Importance for late reflections ($> 50ms$) red: highest importance, blue: unimportant. (c) Difference (importance for late reflections - importance for early reflections) red: only important for late reflections blue: only important for early reflections.

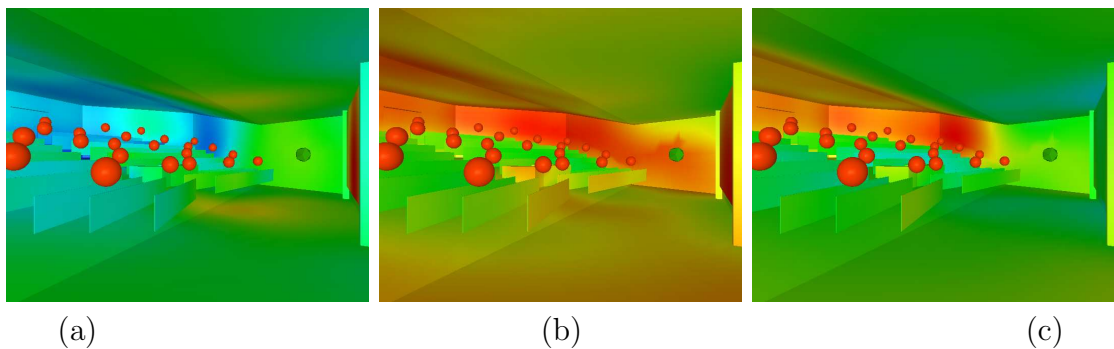


Figure 3.16: Same as figure 3.15 from side view.

In figures 3.15 (c) and 3.16 (c) red areas depict parts of the geometry which are important for late reflections but unimportant for early reflections and blue vice versa. Light green areas are equally important for early and late reflections. Thus the absorption coefficients of the surfaces in the red areas can be changed to alter the amount of late received energy without large affect to the amount of early received energy and vice versa.

To enhance the C_{50} values throughout the lecture hall it is necessary to reduce the amount of late received energy at the listener positions. The visualization of the surface importance for early and late reflections gives a direct cue how to improve the overall clarity in the given room by simple changes. When looking at figures 3.15 (b) and 3.16 (b) one can directly locate the most important surfaces for late reflections which are the sidewalls of the room (red). An inspection of the difference images (figures 3.15 + 3.16 (c)) indicates that the change of the back wall material will not influence the early reflections too much (also red color of the back wall). Therefore we exchanged the material of the back wall (wood) with highly absorbing material (sound absorbing foam) to reduce the late reflections throughout the audience without cutting out the early reflections.

To evaluate the changes the impulse responses for the listener positions are simulated and the C_{50} values recalculated according to the new material/absorption coefficients. Figure 3.14 (c) shows the improvement in clarity at the listener positions throughout the audience. The C_{50} values for almost all listener positions exceed the chosen threshold (green lower semicircles). A closer look has to be taken at the two positions which did not satisfy the desired threshold (marked as *A* and *B* in figure 3.14 (c)).

Figures 3.17 and 3.18 (a)-(c) show the importance values when only the single listener positions *A* and not the whole audience is taken into account (importance for (a) early and (b) late reflections, difference image (c)). From figure 3.17 it is directly apparent that the change of the back wall material only has a medium impact on the clarity for listener position *A*. The main contribution to the late received energy is received from the rightmost corner of the room (which was not changed) rather than from the back wall. Thus if we want to enhance the clarity for listener position *A* only and not for the whole audience we need to change the material in the red areas in figure 3.17 (c). When looking at figures 3.18 (a)-(c) (importance for listener

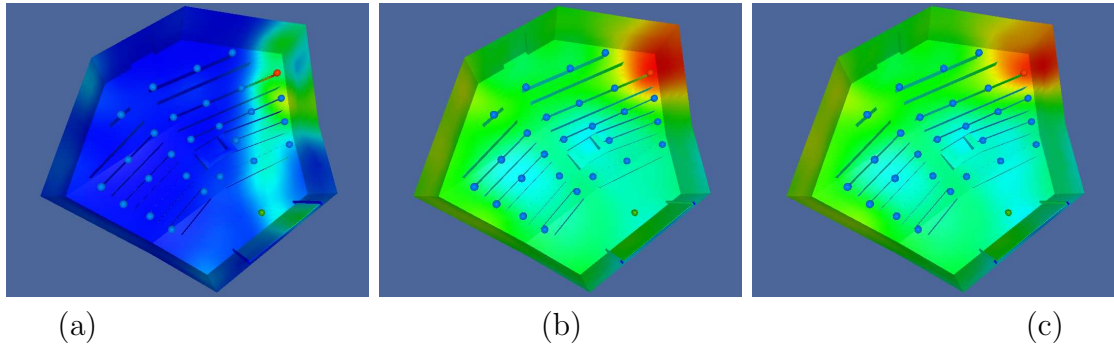


Figure 3.17: Importance values for listener position A and 1kHz mapped to the room surfaces (a) Importance for early reflections. (b) Importance for late reflections. (c) Difference. (Same as figure 3.15 for single listener).

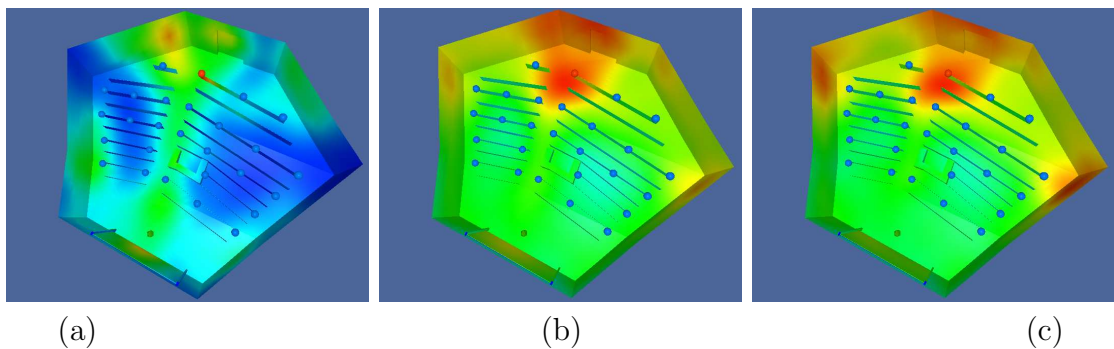


Figure 3.18: Same as figure 3.17 for listener position B .

position B) we can see a problem which occurs when we take the whole audience into account. While the back wall is important for late reflections but nearly unimportant for early reflections to the whole audience, it is important for early and late reflections when taking only listener position B into account. The exchange of the back wall material resulted in a decrease of late reflections to this position (which was intended) but also reduced the amount of early reflections. Thus the clarity (depending on the early to late reflection ratio) only improves slightly compared to the rest of the audience. To improve the clarity at this single position it would be most effective to alter the absorption of the floor material (red area in figure 3.18 (c)) for example exchanging the flooring material but the impact on the whole audience would not be as good as the conducted changes to the back wall.

For evaluation purposes the material of a surface (ceiling above speaker) which is on the one hand only medium important for late reflections and on the other hand

also has some influence on the early reflections had been replaced. The resulting C_{50} glyphs are visualized in figure 3.14 (b). As expected the improvement in clarity is only partial because the chosen surface is only medium important for late reflections taking the whole audience into account, whereas it is more important for the listeners in the first two rows (C_{50} reaches the desired threshold, i.e. green lower semicircles). Overall the listener-based analysis of surface importance proves to be a useful tool to understand application specific data and to get insight into the directional aspect of the acoustic situation in a room for a certain acoustic metric, which is not apparent when looking at the resulting values only. Through the visualization of surface importances for a certain metric the parts of the room surface which affect this metric the most could be easily identified. Thus the current acoustic situation could be improved with selective changes to the most important surfaces of the room.

3.2.3 Sound tracing using an acoustic rendering equation

In the previous sections different approaches for the visualization of the results of phonon tracing were presented. In section 3.1.3.1 the sound wave propagation was visualized by use of color coded spheres representing particular phonons, where the color of the spheres corresponds to the energy decomposition of the phonons. Section 3.1.3.2 introduced additional techniques using the phonon map to visualize wave fronts on the scene surfaces using geometric primitives and triangulated surfaces. In sections 3.2.1 and 3.2.2 a more local view on the acoustics of a room was given by visualizing the results at a listener position using a color coded sphere which is deformed according to the direction and amount of the received energy and the visual analysis of acoustic quality at listener positions utilizing acoustic quality measures.

However, all previous visualization approaches are based on graphical primitives (spheres, arrows, surfaces, etc.) and do not make use of an acoustic rendering equation. This section presents the adaption of photo-realistic rendering techniques to the visualization of acoustic simulation results ([BMD⁺08]). Therefore, a pressure based acoustic rendering equation is established which is applied to an array of frequencies. Since the auditive environment of a scene is by far more complex than its visual environment regarding the number of base frequencies that can be distinguished, the method produces a set of images in each rendering pass. For

each frequency, the corresponding image conveys the pressure amplitude (mapped to brightness) and its phase shift (mapped to color). From this visual representation, local details of the directional impulse response are conveyed spatially much sharper than possible with auditive methods, complementing the valuable analysis by means of auralization.

Visualization algorithm To visualize phase and pressure of sound arriving through the individual pixels of the viewing window, a pressure-based sound-rendering equation is established. The corresponding relation between the sound-pressure $p(S, t)$ at a source at position S and the sound-pressure $p(L, t)$ at a listener-position L is computed by convolution with a proper impulse response g ,

$$p(L, t) = g(t) * p(S, t) = \int_{\tau} p(S, \tau) g(t - \tau) d\tau. \quad (3.17)$$

Adaption of the ray tracing approach Based on the local pressure representation at scene surfaces obtained from simulation, a pressure signal is calculated for every pixel. Therefore, the following assumptions of linear geometric acoustics are made:

- linear spread of a wave front with sound speed $c = 343 \frac{m}{s}$
- linear attenuation of sound pressure $p \sim \frac{1}{d}$
- the total pressure is the sum of all reflected pressure fields

Linear acoustics is only applicable to wavelength $\lambda \ll \xi$, with ξ as a measure for the dimensions of the simulated environment. The second assumption of linear attenuation with the traversed distance d is valid for pressure, whereas energy is subject to quadratic attenuation.

To calculate equation (3.17) by ray tracing the pressure response needs to be formulated geometrically. This is done by the sound rendering equation

$$p(L, t) = \lim_{\rho \rightarrow 0} \left(\frac{1}{4\pi\rho^2} \int_{S_\rho} P_E(B, t) dB \right), \quad (3.18)$$

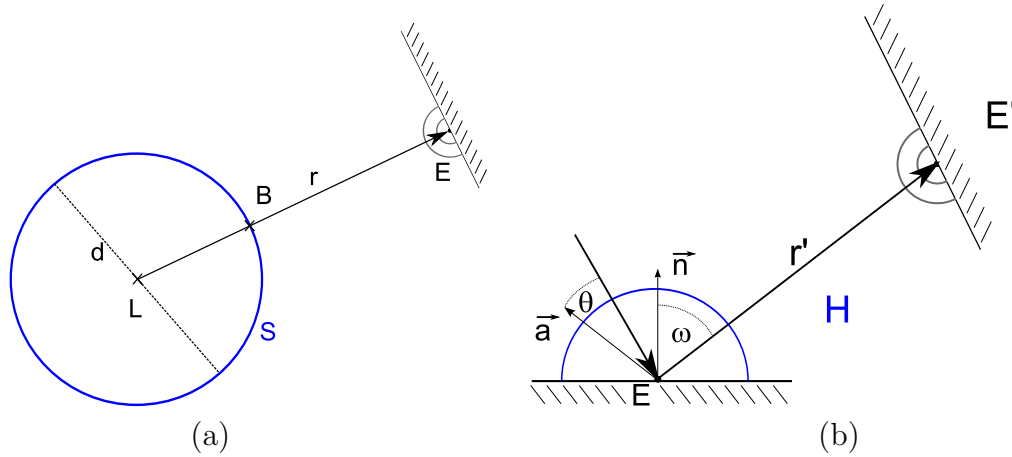


Figure 3.19: The pressure at the point L can be calculated by the pressure on the surface of an infinitesimal sphere S around L with diameter $d = 2\rho$ (a). In analogy, the pressure at the surface point E can be calculated by the pressure on an infinitely small hemisphere H around E with diameter d (b).

calculating the pressure on an infinitesimal sphere with radius ρ around L by integrating the incoming pressure $P_E(B)$ on its surface. As illustrated in figure 3.19, B is a point on S_ρ and r denotes the ray from L through B to its intersection point E with the scene.

Based on Huygens' principle, the pressure field on a reflecting surface can be represented by an infinite set of infinitesimal spherical sources, see figure 3.20. The incoming pressure at L may thus be represented by integrating the pressure contributions of all reflecting surfaces E .

When considering a specific frequency ω , the incoming pressure $P_E(B, t)$ can be represented by a complex function

$$\bar{p}_E(B, t)dB = \bar{g}(B, E) \cdot \bar{p}_{out}(E), \quad (3.19)$$

where $\bar{g}(B, E)$ denotes the complex transfer function of the direct transmission line between B and E , given by equation (3.20). The harmonic pressure wave and the complex description reduce the convolution with g to a simple multiplication with

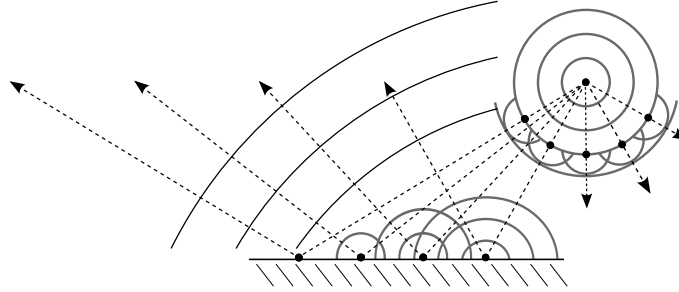


Figure 3.20: Huygens' principle: A reflected sound wave corresponds to an infinite set of point sources. When adding the individual pressure fields, shape and direction of the wave front are preserved.

\bar{g} . The phase α and amplitude A of the pressure $p(X)$ are expressed by a complex number $\bar{p}(X)$.

$$\bar{g}(L, E) = \frac{1}{\|L - E\|} e^{i\alpha(\|L - E\|)} \quad (3.20)$$

$$\begin{aligned} p(X, t) &= A \cdot \cos(\omega t + \alpha) = \text{Re}(Ae^{i\alpha} e^{i\omega t}) \\ &= \text{Re}(\bar{p}(X)e^{i\omega t}) \end{aligned} \quad (3.21)$$

Inserting this into equation (3.18) provides the frequency-specific sound rendering equation

$$\bar{P}refl(L) = \frac{1}{4\pi\rho^2} \int_S \bar{g}(B, E) \cdot \bar{p}_{out}(E, r) dB \Big|_{\rho \rightarrow 0}, \quad (3.22)$$

calculating the total incoming reflected sound pressure.

The direct response from the point source S is not represented here, since it corresponds only to one point in the image. The outgoing pressure $\bar{p}_{out}(E, r)$ at E with respect to the ray direction r is calculated by a simple acoustic bi-directional reflection distribution function (BRDF), as described below.

The discretization of equation (3.22) is provided in equation (3.23), where ψ_i is the solid angle covered by the pixel w_i . The infinitesimal radius ρ is eliminated when considering only the pressure reflected through the viewing window Ψ towards L :

$$\begin{aligned}
 \bar{P}_{refl,\Psi}(L) &\approx \frac{1}{4\pi\rho^2} \sum_{i: \psi_i \in \Psi} \bar{g}(B, E_i) \cdot \bar{p}_{out}(E_i) \rho^2 \psi_i \Big|_{\rho \rightarrow 0} \\
 &= \frac{1}{4\pi} \sum_{i: \psi_i \in \Psi} \bar{g}(L, E_i) \cdot \bar{p}_{out}(E_i) \psi_i \\
 &= \frac{1}{4\pi} \sum_{i: \psi_i \in \Psi} \bar{P}_{refl,\psi_i}(L)
 \end{aligned} \tag{3.23}$$

Recursive ray tracing In geometric acoustics reflection of sound is considered more specular than reflection of light. Diffuse reflections are mainly reduced due to simplifications in the geometric model, for example representing a book shelf by a planar surface. Hence, recursive ray tracing provides a good approximation. The total outgoing pressure \bar{p}_{out} at each intersection point is the weighted sum of specularly and diffusely reflected and emitted sound pressure.

For an intersection point X^k and an incident ray r^k during the recursion, the pressure \bar{p}_{out} , which is emitted in reverse direction of r^k , can be written as:

$$\bar{p}_{out}(X^k, r^k) = \begin{cases} \bar{p}_{out,diff}(X^k) & \text{if } rd = rd_{max} & (a) \\ \bar{p}_{emis}(X^k, r^k) & \text{if } r^k \text{ hits a source} & (b) \\ \bar{p}_{out,refl}(X^k, r^k) & \text{otherwise} & (c) \end{cases} \tag{3.24}$$

with rd being the current and rd_{max} the maximum recursion depth. If the maximum recursion depth rd_{max} is reached only diffuse reflection is used for the last intersection point (3.24,a). The calculation of the diffusely reflected outgoing sound pressure $\bar{p}_{out,diff}$ from the simulation data is shown in the next paragraph. The case that a ray hits a point source (3.24,b) is very unlikely, as a point source has no area. Therefore, it will be neglected. $\bar{p}_{out,refl}$ (3.24,c) is calculated by (3.25) which describes the

outgoing pressure for the first $n - 1$ reflections of a ray with rd intersection points. To ensure the correct reproduction of direct sound in case of specular reflection a shadow ray is traced for each source S_i .

$$\begin{aligned}
 \bar{p}_{out,refl}(X^k, r^k) &= \bar{p}_{out,spec}(X^k, r^k) + \bar{p}_{out,emis}(X^k, r^k) + \bar{p}_{out,diff}(X^k) \\
 \bar{p}_{out,spec}(X^k, r^k) &= R_{spec}(X^k, r^k) \cdot \bar{g}(X^k, X^{k+1}) \cdot \bar{p}_{out}(X^{k+1}, r^{k+1}) \\
 \bar{p}_{out,emis}(X^k, r^k) &= \sum_{\forall S_i \in V^k} R_{spec}(X^k, r^k) \cdot \bar{g}(X^k, S_i) \cdot \bar{p}_{emis}(S_i)
 \end{aligned}
 \tag{3.25}$$

$\bar{p}_{out,refl}$ is the sum of the perfectly specular reflected pressure $\bar{p}_{out,spec}(X^k, r^k)$, the specular reflected direct incoming sound $\bar{p}_{out,emis}(X^k, r^k)$ and the diffusely reflected sound $\bar{p}_{out,diff}(X^k)$. V^k is the set of direct visible sources S_j from X^k , r^{k+1} is the perfectly specular reflected ray and X^{k+1} its next intersection point with the scene. $R_{spec}(X^k, r^k)$ is the specular part of the Bidirectional Reflection Distribution Function (BRDF). It calculates the sound pressure reflected by X^k in one meter distance. This enables us to approximate the reflected sound pressure by that of a point source at E .

Figure 3.21 shows the impact of the recursion depth rd . In Figure 3.21(a) the recursion depth $rd = 1$ is used. Thus, it shows only the information of the phonon map, interpreted as diffusely reflected sound. Figures 3.21(b) and (c) show the same setup, traced with $rd = 3$ and $rd = 20$. A high recursion depth increases the effect of specular reflection and overweighs the diffuse part.

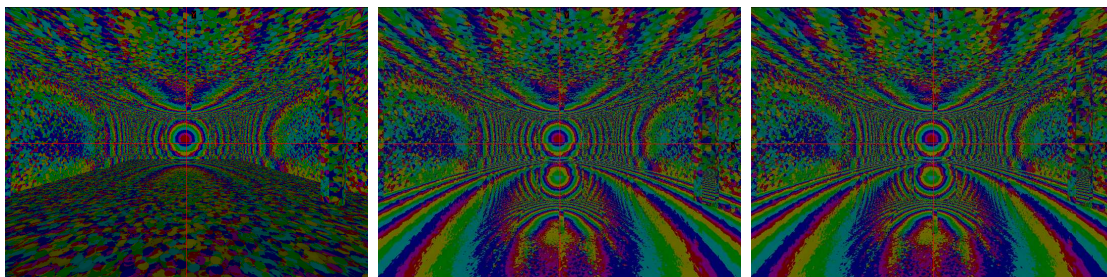


Figure 3.21: The same setup traced with recursion depth $rd=1$, $rd=3$ and $rd=20$ @640Hz. The floor has 1% and the other surfaces 90% scattering. The impact of the recursion depth can be clearly observed.

$\bar{P}_{refl,\psi_i}(L)$ in equation (3.23) can be calculated by:

$$\bar{P}_{refl,w_i}(L) = g(L, X_i^1) \cdot \bar{p}_{out}(X_i^1, r^1) \quad (3.26)$$

Local evaluation of the phonon map for diffuse reflection In contrast to the previous sections frequency-dependent effects like interference need to be visualized. Therefore some additional information like phase of the reflected sound is needed to calculate \bar{P}_{emis} . As explained in section 3.2.3, this is done by expressing the phase and pressure spectrum for each phonon by a complex pressure spectrum.

Each intersection point E can be considered as a point source, as described in section 3.2.3. For diffuse reflection the sound-pressure and phase of this source is determined by interpolating the phonon map. This is done by a gaussian weighted sum, equation (3.27), as proposed in section 2.1.2, or standard Shepard interpolation. A comparison is depicted in Figure 3.22. As in this case the reflection is assumed as perfect diffuse, each \bar{p}_j is weighted by $R_{diff}(\beta) = \cos(\beta)$ for lambertian reflection. β is the angle between surface-normal and incident direction of the Phonon j .

$$\bar{p}_{out}(E, t) = \sum_{j=0}^m w(\gamma(P_j, E)) R_{diff}(\beta) \bar{p}_j \quad (3.27)$$

For correct interpolation of the pressure at E the phonons on different surfaces need to be distinguishable. Therefore, for each phonon, the normal and material-index of the corresponding surface is added to the map.

In Figure 3.22 (a) the left half of the image is rendered using Shepard and the right half using equation (3.27). Even if the results obtained by gauss interpolation are more blurry than those by Shepard interpolation, the error can be accepted as a trade off between quality of the results and physical correctness. As contribution of diffuse reflected sound pressure is much smaller than that of specular reflected sound pressure, the overall error is negligible. Therefore gaussian interpolation is preferred.

Color mapping Phase and amplitude convey the most important information in this approach. Therefore the phase is mapped on discrete color intervals in order to

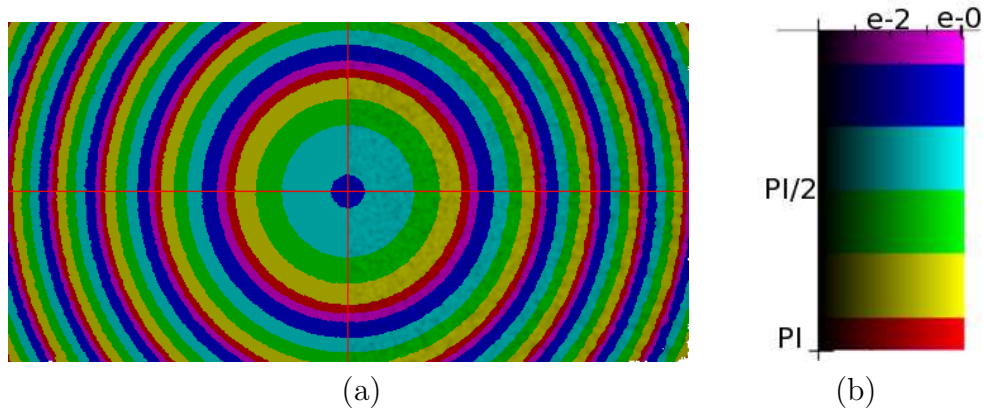


Figure 3.22: (a) Phonon map of simple wall with point source in front of it. The left half is interpolated with Shepard, the right half with gauss interpolation. (b) Legend for $min_{ampl} = 10^{-4}$

display the isolines of the phase shift. The amplitude is logarithmically mapped on the value channel of the HSV color model. As in most simulations the amplitude values are concentrated on a small interval, therefore a lower clipping level min_{ampl} is defined. For values below min_{ampl} the amplitude is set to zero. Figure 3.22 (b) shows the legend for $min_{ampl} = 10^{-4}$. As the ray tracer creates a complex pressure spectrum for each pixel in one run, also the color mapping is done in a single run. For each middle frequency of a frequency band a single picture is mapped.

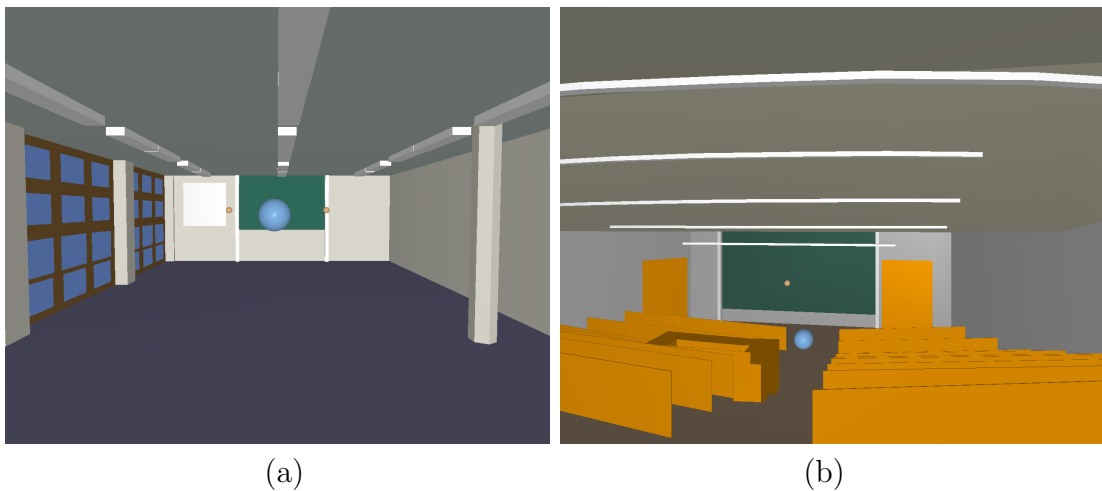


Figure 3.23: Configuration of the simulation scenario in two different lecture rooms. Orange spheres mark the sources and blue sphere marks the listener position.

Comparison of different visualization methods In virtual acoustics scattering is used to model diffuse reflection of structured surfaces. In order to show the scattering effect the phonon map is visualized with this approach and by use of the method described in section 3.1.2 with the addition of scattering (section 2.1.3). The phonon map is build for scattering of 1% and 50%, respectively. For the rendering only phonons which are reflected two times at the scene surfaces are considered. The virtual scene is depicted in figure 3.23 (a). The visual results achieved by use of the sound rendering equation show the global influence of the scattering coefficient at 320Hz (see 3.24 (a+b)). The resulting phase pattern becomes more blurry with increased scattering coefficient, recognizable in figure 3.24 (b) as distorted phase color borders. The more blurry the total phase of a surface is the more uncorrelated is the reflected sound wave front. This global influence of the scattering coefficient can not be seen in figure 3.24 (c,d), which shows particles on room surfaces (section 3.1.2). Nevertheless it gives a good local insight into the scattering effect.

Interference pattern visualization Interference is a disturbing effect of standard speaker setup. While the interference pattern of the first reflection at scene surfaces can be easily calculated, the determination of the pattern after several reflections is not that trivial. In order to visualize the interference phenomenon the following scenario (see Figure 3.23(a)) has been simulated. Inside the virtual model of a university lecture room ($13 \times 6 \times 3$ m), two sources are placed in a distance of approximately three meters between each other (orange spheres). The listener (blue sphere) is positioned centered to the sources at the same height several meters away. Using this setup interference patterns should be visible, at least for the early reflections. The sound pressure and phase has been calculated using the sound tracing algorithm for different frequencies without scattering. The used phonon map contains about 2M phonons. Figure 3.25 shows the occurring interference patterns on the scene surfaces for 452Hz (a,d), 640Hz (b,e), and 1280Hz (c,f) considering only the first reflection (a-c) and the early six reflections (d-f). The interference patterns due to the constructive interference (full color intensity) and the destructive interference (zero color intensity) are clearly recognizable.

Application examples Figures 3.23 (b) shows a model of a lecture room at the University. The shape and the materials inside this room are chosen in order to

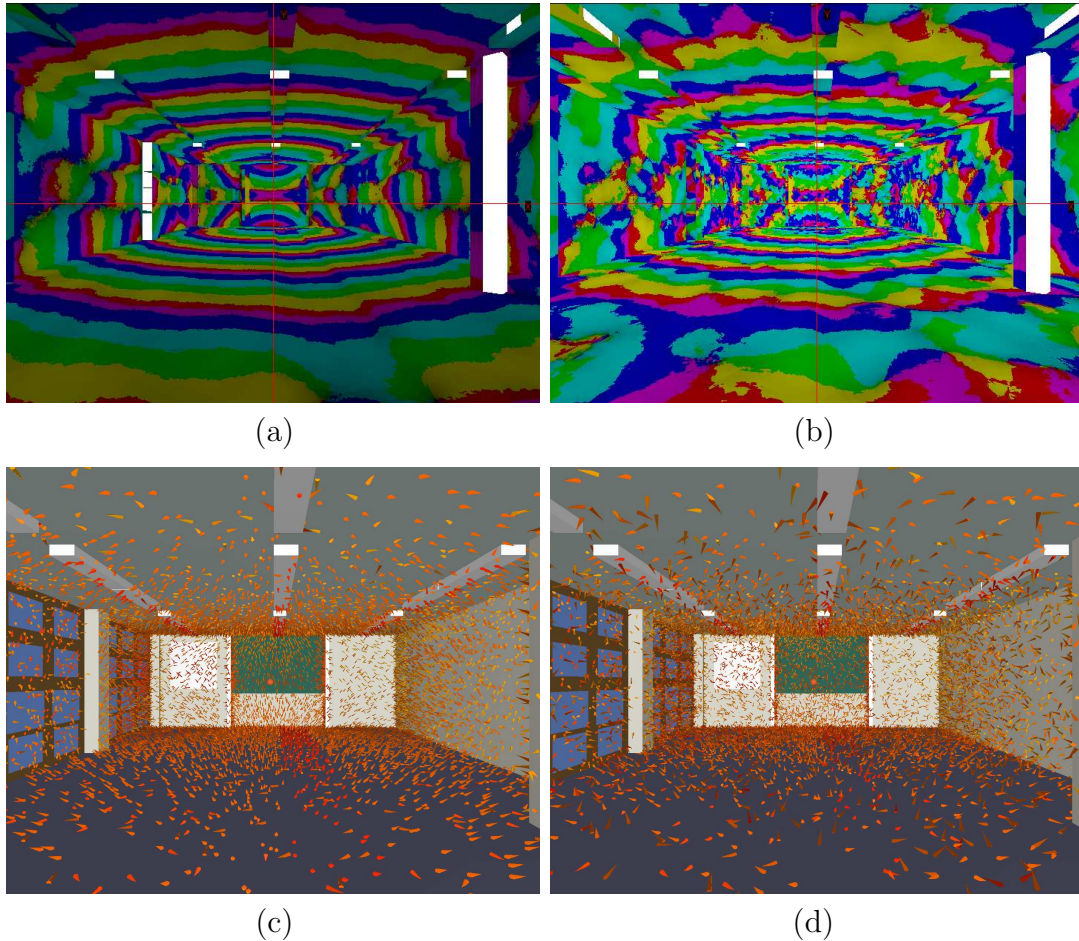


Figure 3.24: The visualization of the phonon map using the described approach (a,b) and the phonon visualization described in section 3.1.2 (c,d) for the second reflection showing the global (a,b) and local (c,d) influence of scattering. Pictures (a,c) are traced with a scattering coefficient of 1% and (b,d) with a scattering coefficient of 50%

satisfy its usage for speech. The pressure amplitude and phase are calculated approximating the real absorption coefficients. Rays have been traced until the recursion depth of twenty using a phonon map with 2.5M phonons. Figure 3.26 depicts the resulting visualization at 452Hz frequency, corresponding to a low frequency of speech. As expected the visualization shows that the lecture room is suitable for speech presentations. The side walls on both sides of the blackboard are mainly responsible for this fact. The big green spots in the figure show that a large sur-

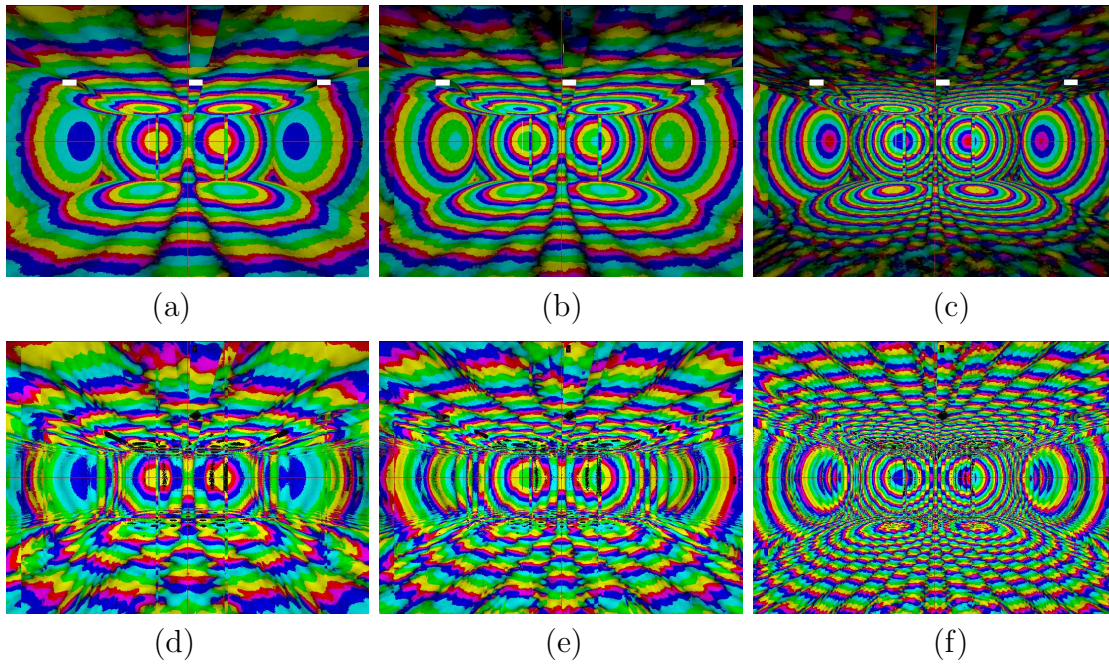


Figure 3.25: Phase visualization of sound received at one listener position for the frequencies 452Hz (a,d), 640Hz (b,e), and 1280Hz (c,f) for the first reflection and after six reflections (d-f) for the scenario shown in Figure 3.23 (a).

face of them reflects sound with equal phase as that reflected off the middle of the blackboard. Therefore sound at this frequency will be amplified by these reflections.

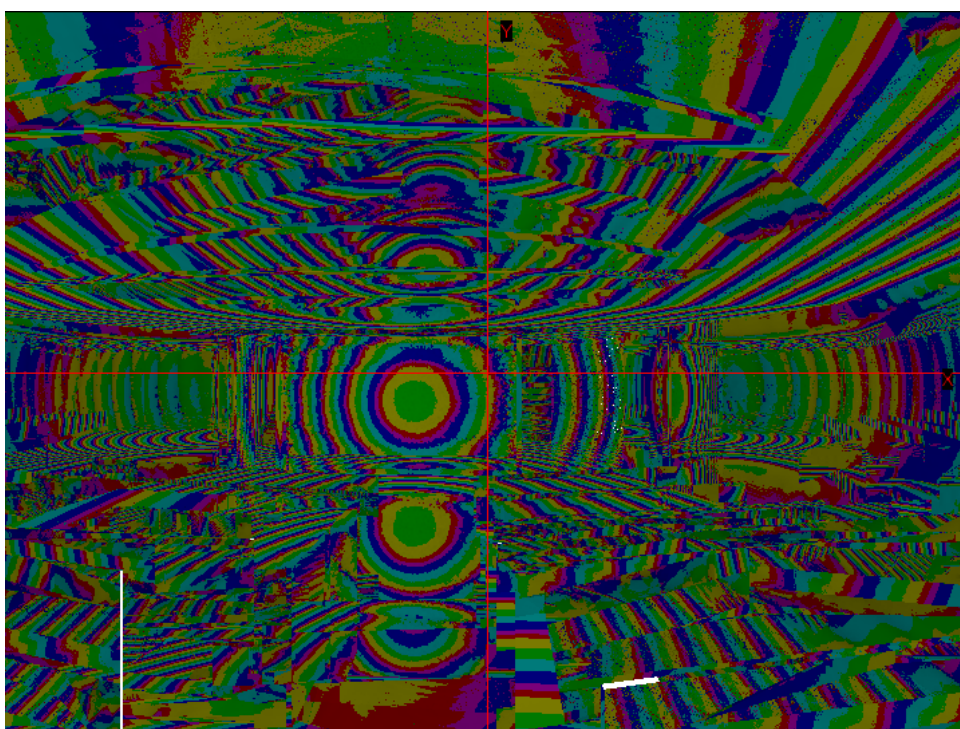


Figure 3.26: Room HS46-110 at the university @452Hz

3.3 Visualizing low frequency sound

When it comes to low frequency sound phonon tracing cannot be used for the simulation because some features like diffraction which are not computable with phonon tracing cannot be neglected anymore (see section 2.3 for a comparison). Therefore, the FE method introduced in section 2.2 is used to simulate low frequency sound and calculate a pressure distribution throughout a room for arbitrary frequencies.

3.3.1 Simulation

The simulation for low frequency sound is done in Comsol/FemLab². Therefore the geometry of the room to be examined is converted to a supported format or directly modeled inside Comsol. This includes reflection coefficients for room surfaces and the position of the membrane. The FEM mesh is then constructed by Comsol and the state-space model for different excitation frequencies is calculated by solving the wave equation considering damping.

The resulting state-space model is then fed into Matlab³ which computes a given number of eigenfrequencies, e.g. 80, and the reduced state-space model for the mesh points. The result is equation system 3.28 which takes the frequency f ($s = 2\pi if$) as input and delivers the complex pressure at all mesh points. Despite using only the eigenfrequencies the complex pressure values can be calculated for arbitrary frequencies embedded in the range of the eigenfrequencies, e.g. up to 350Hz. This equation system can be solved nearly in realtime on commodity PC hardware and enables the interactive visualization of the pressure distribution.

$$y(s) = (C(sE - A)^{-1}B + D)u \quad (3.28)$$

To compare different reflection coefficients the above steps have to be redone to generate a new equation system. This has to be done once for every combination of reflection coefficients. The resulting systems can then be chosen in the visualization system to calculate the corresponding pressure fields.

²<http://www.comsol.com>

³<http://www.mathworks.com>

Certain problems arose from the use of the Comsol/Matlab combination. In order to get an equation system for the reduced state-space model at all grid points, all mesh points had to be fed into Comsol as solution points which then calculates the full-resolution state-space model. In order to avoid memory problems (because of matrix sizes) the grid points had to be decomposed and the resulting models reassembled to compute the reduced state-space model. Another problem was the different order of mesh points exported from Comsol and the solution from the Matlab equation system. Therefore a post processing step of the mesh had to be done to "fit" the mesh points to the solution vector.

3.3.2 Visualization

Using the resulting system of equations the solution for arbitrary frequencies at all mesh points can now be calculated and visualized. From the complex pressure value the phase and the amplitude of the pressure field is computed. As mentioned before the calculation is done nearly in realtime, so it is possible to interactively "slide" through the frequencies and observe the changes in the pressure field.

To examine the behavior of the pressure field different visualization techniques were implemented.

Single isosurfaces can be drawn for selectable isovalues or multiple isosurfaces throughout the whole range of values. An example of the isosurface visualization in a box shaped room is shown in figure 3.27a.

Furthermore we explore the pressure field by determining the local extrema of the pressure scalar values (real/imaginary parts, amplitude, phase). We compute the extrema as critical points of the gradient field of the scalar values. To determine the gradients a Moving Least Squares (MLS) approach [Lev98] is used. MLS is a weighted, local generalization of the well-known "Least Squares" technique which fits a function of given degree to a set of points while minimizing the squared distance to the corresponding field points. After computing the gradients it is possible to visualize the topology of the scalar pressure field by drawing arrows at the position of the mesh points corresponding to the direction of the gradient. The visualization of the field topology is enhanced by integrating random number of streamlines started in the vicinity of the saddle points of the gradient field. An example of the streamline

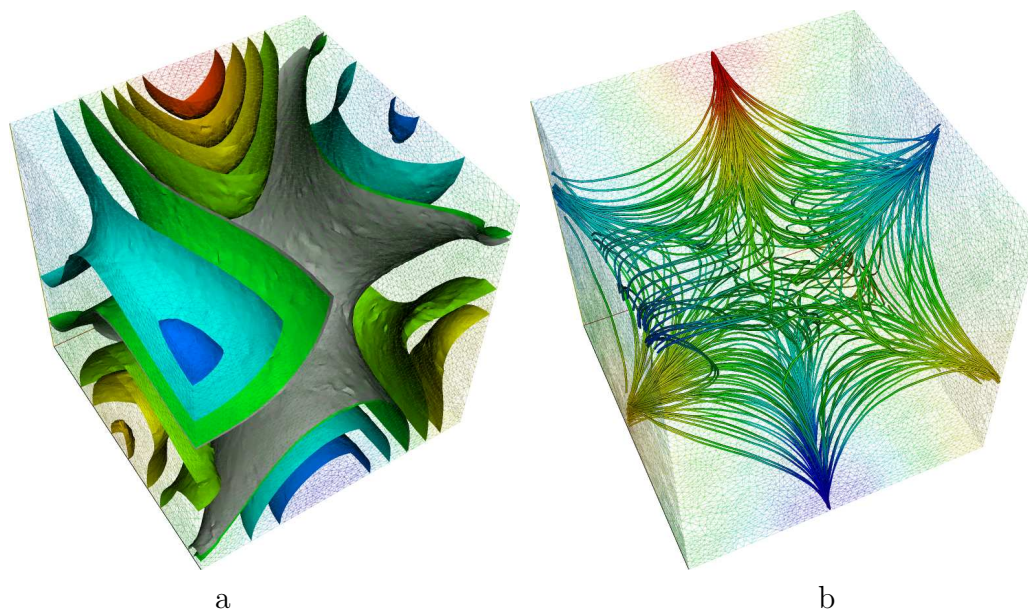


Figure 3.27: Visualization methods implemented to visualize the pressure field. Iso-surfaces (left) and streamlines(right). The streamlines make use of the additionally computed gradient field.

visualization is depicted in figure 3.27b. The streamlines as well as the gradient vectors (the arrows mentioned above) are color coded corresponding to the values of the considered scalar field.

Using the different visualization techniques gives a first visual insight into the topological structure of the pressure field. Being able to continuously slide through the different frequencies enables the observation of correlations between frequency and for example annihilation. Changing the underlying equation system, meaning different absorption/damping coefficients, one can examine the shift of min/max/null regions within the room.

3.3.3 Results

The test geometry for the low frequency visualizations is a small completely tiled reference room with two doors and a radiator on one side. In figure 3.28 the room geometry and the finite element mesh used for the simulation is shown. The sound source in this case is the membrane of the loudspeaker which is visible in the corner

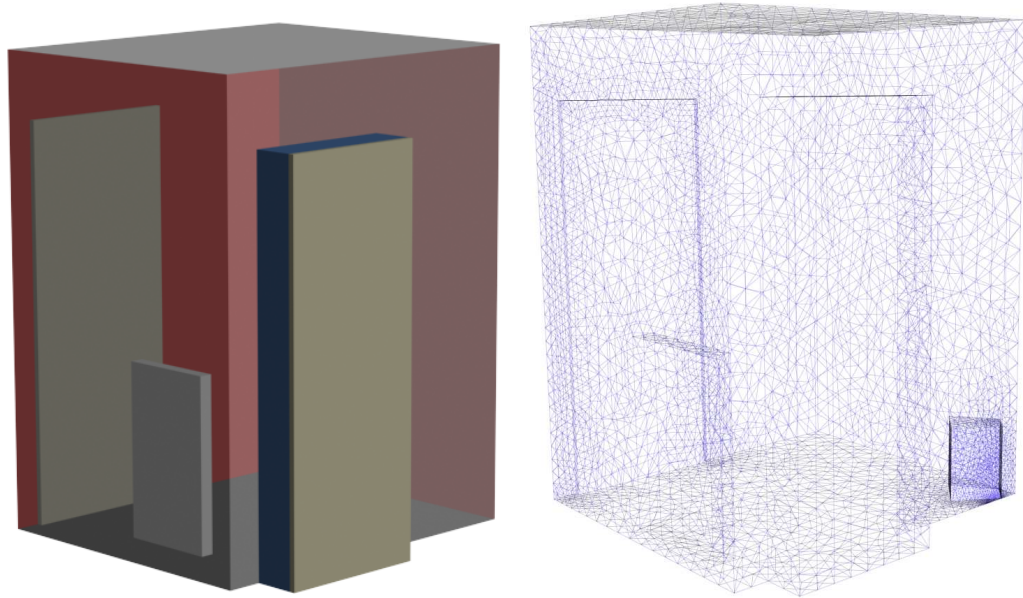


Figure 3.28: Geometry and FEM mesh of the simulated room.

of the room. To see effects of different reflection coefficients the reflectiveness of the radiator, situated on the front left wall in figure 3.28a, is altered.

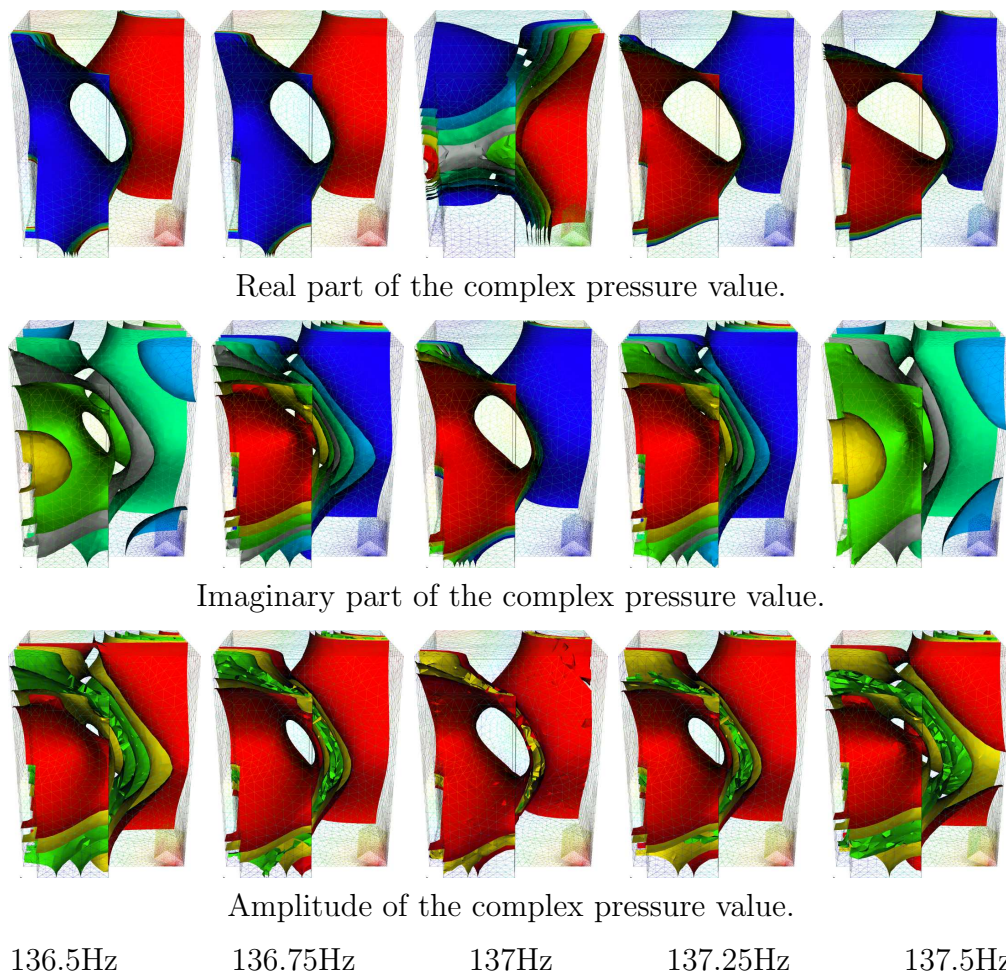


Figure 3.29: Visualization of Isosurfaces for real and imaginary part as well as the amplitude of the complex pressure value spanning over the eigenfrequency of 137 Hz. The values for the isosurfaces are fixed and colored between red (positive) and blue (negative) values. The grey isosurface denotes the zero isosurface. The topological changes of the pressure field can be observed.

In figure 3.29 isosurfaces are used to visualize the real and imaginary part as well as the amplitude of the complex pressure value for frequencies enclosing the eigenfrequency of 137Hz. From left to right the isosurfaces for 136.5 Hz to 137.5 Hz and top to bottom real part, imaginary part and amplitude of the complex pressure are visualized. The values for the isosurfaces are fixed and colored between red (positive) and blue (negative) values. The grey color denotes the zero isosurface. The topological changes of the pressure field can be observed.

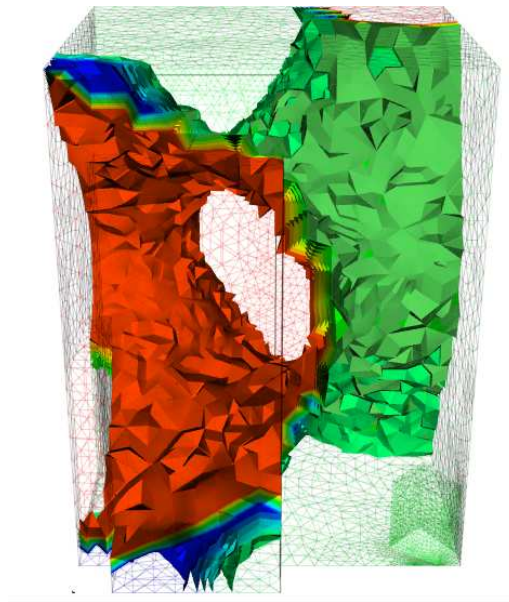


Figure 3.30: Phase of the complex pressure for 137Hz. Red = π , green = 0, Blue = $-\pi$. The phase is nearly a binary function and undefined at the zero crossings and therefore difficult to visualize.

Figure 3.30 shows the problems in visualizing the phase of the complex pressure. Because the phase is nearly a binary function here and undefined at the zero crossings it is difficult to produce clear isosurfaces.

Using the computed gradient field and critical points thereof the gradient field itself can be visualized. Streamlines which help to identify the pressure field's structure can also be applied. In figure 3.31 arrows were used for the visualization of the gradient field (top) and streamlines were started near the saddle points to show the connectivity of minima, maxima and saddles. The saddles are of particular interest because they are located in structural tunnels which connect anti-nodes of the pressure field whose connection is also derivable from the streamlines. The left

column shows, from top to bottom, the gradient field as arrows, streamlines started at a sphere around the saddle point and streamlines started in the direct vicinity of the saddle point for the eigenfrequency at 137 Hz. The right column depicts the same visualizations for a frequency of 276 Hz. The arrows and streamlines are colored according to the values of the underlying scalar field (red/blue = max/min). When a grey isosurface is drawn it always shows an isovalue of zero. The more complex topology of the higher frequency can be clearly seen from the middle and bottom right images by the connecting streamlines between the saddles, maxima and minima of the gradient field.

When using different reflection coefficients for certain materials, which results in different coefficients for the equation systems, the impact on the complex pressure field can be visualized. In figure 3.32, the left column depicts from top to bottom isosurfaces for the amplitude, imaginary and real part of the complex pressure for high absorption (low reflectiveness) at the radiator, the right column for low absorption (high reflectiveness), respectively. In both cases the selected frequency is 169 Hz. The amplitude (top) of the complex pressure is comparable and the real part (bottom) is nearly identical in structure and value. The imaginary part (middle) of the complex pressure field on the other hand is comparable in structure but an increase in value can be observed (left column). This is caused by a phase shift when using a high absorption coefficient on the radiator.

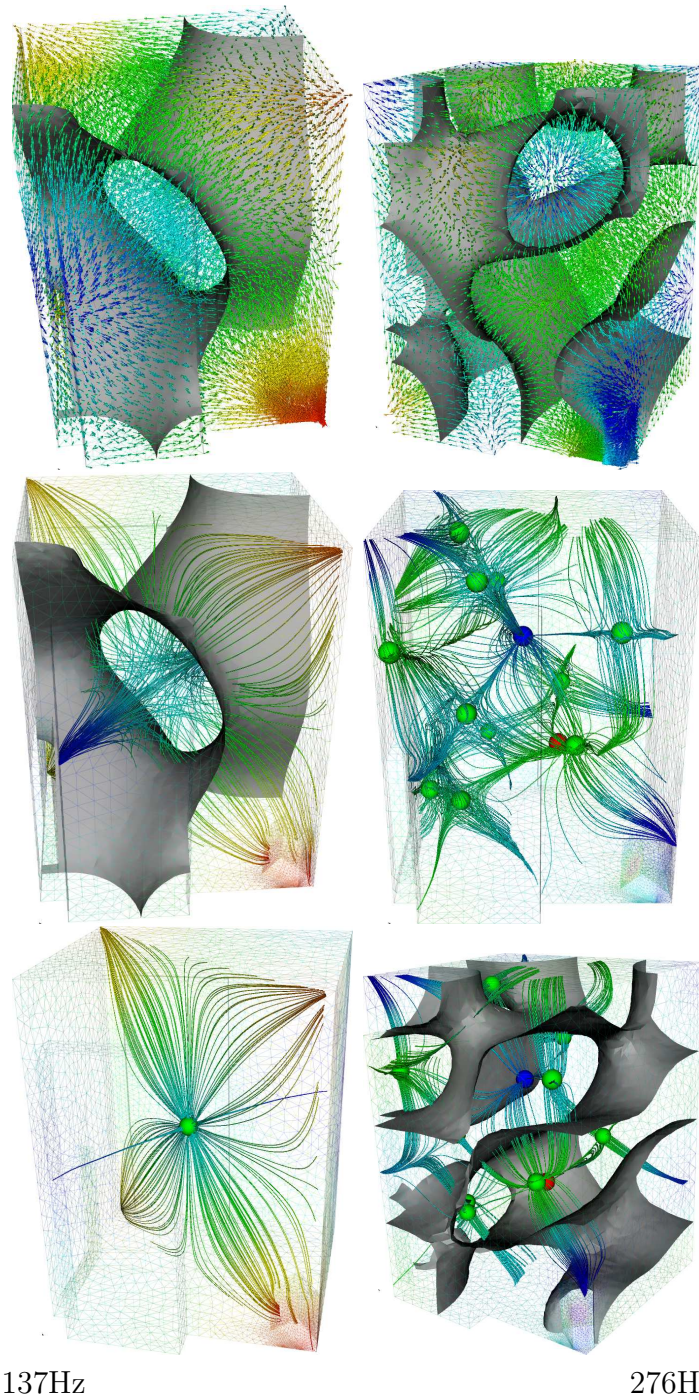


Figure 3.31: Gradient (top) and streamline (middle, bottom) visualization for 137 Hz (left) and 276 Hz (right). The gradient vectors and streamlines are colored according to the value of the underlying scalar field (red/blue = maximum/minimum value). The grey isosurface depicts $\text{isovalue} = 0$. In the middle row the streamlines are started on a sphere around the saddle points of the gradient field.

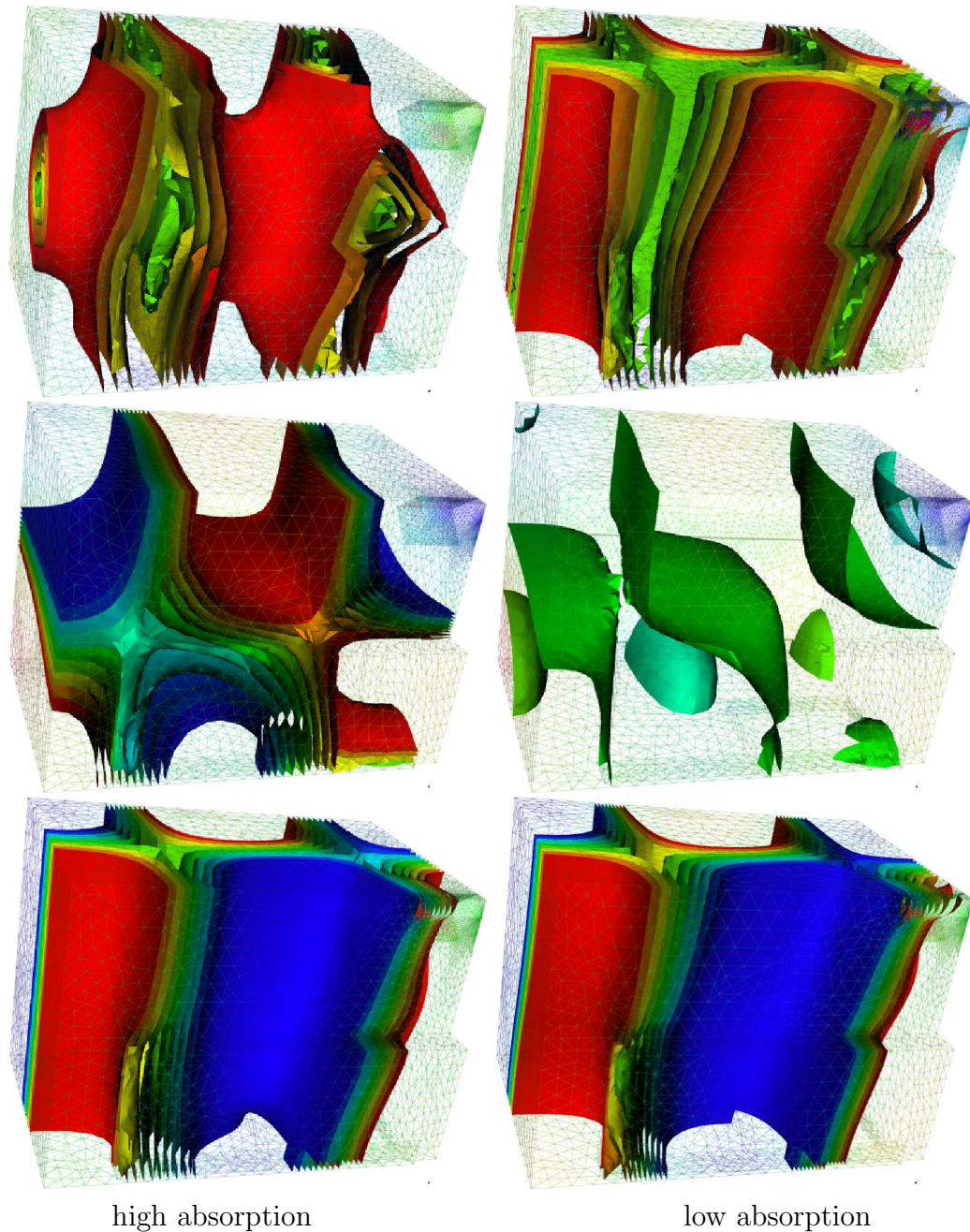


Figure 3.32: Isosurface visualization for 169 Hz using two different reflection coefficients for the radiator (3.28 on front left wall). Left column high, right column low absorption. Top to bottom amplitude, imaginary and real part of the complex pressure. The isovalues are fixed (red/blue = positive/negative). The phase shift is clearly recognizable by the greater imaginary part for the high absorption (left).

Chapter 4

Conclusion and future work

In this part of the thesis various techniques for the visualization of room acoustics were presented. First of all two different simulation methods which were used to calculate the underlying data have been discussed. Phonon tracing, based on geometric acoustics, was applied for the simulation of high and middle frequencies whereas a Finite Element Method, approximating a solution of the wave equation, was used for the simulation of low frequencies. This was necessary because of the inherent shortcomings of the two approaches, geometric and wave based, which are neglectance of low frequency sound effects like diffraction in the geometric case and high computation costs for middle to high frequencies in wave based methods. Therefore a comparison of both methods has been done to decide at which frequencies the shift from the FEM simulation to the faster phonon tracing is acceptable in terms of accuracy.

Based on the simulation results different approaches for the visualization were introduced which can be split into global and listener based views on the sound behaviour inside rooms. The first group gave a global view on the propagation within, and the interaction of sound with, the room boundaries. From these visualizations a first insight into the interaction of sound with the geometrical room structure and the influence of different material properties on the overall sound could be gained. The second group of visualizations were based on a listener position and thus gave a view on the acoustics of a room from a distinct point. The presented listener based visualizations covered the identification of amount and direction of the received sound,

the visual analysis of surface importance for certain acoustic metrics which gave direct advice on how to improve the acoustic quality of the room for the chosen metric, and an acoustic rendering equation which was used to visualize interference effects and phase changes for different frequencies. Furthermore novel ideas for the visualization of low frequency FEM simulations were presented which can help to identify topological changes of the sound pressure field for changing frequencies.

There are still challenging tasks left in the field of room acoustics, especially the problem of optimizing a room for different purposes at the same time. A possibility could be the improvement of the surface importance calculation, for example integrating functions which consider multiple quality measures according to a prescribed weight, and thus giving advice on the optimization of the acoustic quality of a room for multiple usages, like speech and music. Furthermore, research in the visualization of low frequency sound, especially eigenmodes, has to be done. The presented visualization methods could be enhanced to get further insight into the topological structure and correlation between eigenmodes with the objective to find simple descriptions for the complex pressure field.

Part II

Environmental Noise

Chapter 5

Introduction

5.1 Motivation

More and more people in our today's society suffer from noise pollution. Rivas et al. [RHC03] showed in their survey that more than 20 % of the world population live in areas with unacceptable noise levels, and nearly 60 % of the European population are exposed to high noise levels. The main cause for increasing noise levels are the growing population and the connected rise in traffic. Most affected are large cities. In Germany 62 % of the population state that they are annoyed by traffic noise [Umw07].

But noise not only leads to annoyance it can also have serious health effects. These effects are diverse, ranging from sleep disorder and concentration problems to noise induced hearing loss, and can cause cardio vascular diseases and affect the immune system [PB04]. Especially people which are constantly exposed to noise are at risk.

Understanding the negative effects of noise lead to an increase in public interest in this matter. After the release of the 'Green Paper on Future Noise Policy' by the Commission of the European Union in 1996, in 2002 the European Parliament passed a regulation for the abatement of environmental noise [END02]. The goal of the regulation is to inform the public about existing noise pollution and to develop noise abatement measures for highly polluted areas. Furthermore action plans need to be created if certain levels of noise are reached.

The noise maps for the assessment of noise pollution and information of the public proposed by the European Union are two-dimensional. They show the noise level as color coded isobands at a fixed height 4m above the ground. However, in reality noise is not two-dimensional, propagates in all directions and interacts with its surrounding. Additionally these two-dimensional noise maps are not easily comprehensible by laymen in terms of localization and orientation as well as correct interpretation. Due to the static properties of standard maps it is also necessary to compare different physical maps when looking at daytime and nighttime noise pollution or compare pre and post abatement noise levels.

The computation times for noise maps rely on the extent of the observation area, number of objects within this area and the resolution of the immission points where the noise levels should be calculated. These calculations normally take hours up to a day until they are finished and the results can be inspected. This means when planning noise abatement measures or a new building area, a lot of planning has to be done out of experience because you cannot calculate the results on the fly after each change.

To be able to calculate the noise levels interactively, allowing early rejection of bad proposals and easy validation of new ideas, would be a great improvement to the planning process. Also the possibility to change certain objects during the calculation and see the effects in a preview would be a big enhancement.

5.2 Open problems

The open problems arising from the above mentioned issues which are discussed in this part of the thesis can be split in two categories, simulation and visualization.

The first is concerned with improvements to the simulation of noise levels. Therefore it is necessary to review the computation instructions, regulated by national law, to understand the influence of the different parameters used to determine the resulting immission from given noise sources. Additionally it is important to extend the simulation to compute noise volumes which give insight into noise pollution not only in a specified layer but in three dimensional space. Furthermore novel ideas to speed up the calculation process are needed, to allow previewing of the

result and manipulation of objects during the simulation, enabling interactive noise calculations.

The second category, concerning the visualization of the calculation results, contains new ideas to present the underlying data in an easy to comprehend way. Therefore the embedding of the noise data into an interactive three dimensional environment is needed which displays noise within a recognisable environment, for example a city model. To fully understand the data, even by laymen or other user groups, additional information needs to be incorporated into the visualization, and different scenarios, for example planning proposals, need to be easily comparable.

5.3 Overview

This part of the thesis covers the simulation of, and novel visualization techniques for, environmental noise. The focus in this thesis is on traffic noise but the presented simulation and visualization techniques can be easily applied to other noise sources.

Chapter 6 introduces basic terms for environmental noise including different noise sources, definitions for noise parameters, an overview of health effects caused by noise, an historical overview of noise mapping and current regulations concerned with environmental noise. Afterwards chapter 7 discusses the state of the art in noise mapping and presents different commercial and academic tools for noise mapping. Chapter 8 first reviews the current computation instructions in Germany and the effects of different parameters used in the calculation of traffic noise. Furthermore novel ideas for the computation of noise volumes and improvements to the simulation, enabling interactive noise calculations, are presented. The visualization framework and the incorporated techniques used for the visualization of the resulting noise and supplemental data is presented in chapter 9. The environmental noise part of the thesis closes with a conclusion in chapter 10.

Chapter 6

Basics

6.1 What is noise?

The word "noise" originates from the Latin word *nausea* meaning "seasickness", or from a derivative (perhaps Latin *noxia*) of Latin *noceo* = "I do harm", referring originally to nuisance noise.

Today noise is defined as unwanted sound which is a subjective impression of the listener. For example, usually the sound of a violin is referred to as music and is something pleasing. But depending on other factors, like time of day or setting, the sound may be perceived as noise. Therefore factors such as the magnitude, characteristics, duration, and time of occurrence may affect one's subjective impression of the noise.

When talking about environmental noise the main sources are transportation systems, especially motor vehicle noise, but also including aircraft noise and rail noise. Other sources are industrial noise from production facilities or recreational noise. Mistakes made in urban planning may give rise to noise pollution, since side-by-side industrial and residential buildings can result in noise pollution in the residential area, besides the already existing transportation noise.

6.2 Measurement and computation

6.2.1 Definition of sound

Sound is defined as the mechanical oscillations of an elastic medium. The oscillations occur if the medium particles (molecules) are disequilibrated due to an external force. The particles swing periodically around their equilibrium position. The incidence of sound is associated with the existence of a medium. Sound cannot propagate in vacuum. There are three types of sound depending on the transmitting medium:

- Air-borne sound : sound in air and other gases as medium
- Solid-borne sound : sound in solids as medium
- Fluid-borne sound : sound in fluids as medium

6.2.2 Noise parameters

Sound Pressure Level SPL Sound pressure is defined as the difference between the actual pressure (at a given point and a given time) in the medium and the average, or equilibrium, pressure of the medium at that location.

As the human ear can detect sounds with a very wide range of amplitudes, sound pressure is often measured as a level on a logarithmic decibel scale. The sound pressure level (SPL) or L_p is defined as

$$L_p = 10 \log_{10} \left(\frac{p^2}{p_{\text{ref}}^2} \right) = 20 \log_{10} \left(\frac{p}{p_{\text{ref}}} \right) \text{ dB} \quad (6.1)$$

where p is the root-mean-square sound pressure and p_{ref} is a reference sound pressure. Commonly used reference sound pressures, defined in the standard ANSI S1.1-1994, are $20 \mu\text{Pa}$ in air and $1 \mu\text{Pa}$ in water. Without a specified reference sound pressure, a value expressed in decibels cannot represent a sound pressure level.

Since the human ear does not have a flat spectral response, sound pressures are often frequency weighted so that the measured level will match perceived levels more

closely. The International Electrotechnical Commission (IEC) has defined several weighting schemes. A-weighting attempts to match the response of the human ear to noise and A-weighted sound pressure levels are labeled dBA. C-weighting is used to measure peak levels.

A weighted decibel A-weighting is the most commonly used of a family of curves defined in the International standard IEC61672:2003 and various national standards relating to the measurement of sound level, as opposed to actual sound intensity.

Sound level, loudness and sound intensity are not the same things. There is not even a simple relationship between them, because the human hearing system is more sensitive to some frequencies than others, and furthermore, its frequency response varies with level. In general, low frequency and high frequency sounds appear to be less loud than mid-frequency sounds, and the effect is more pronounced at low pressure levels, with a flattening of response at high levels. Sound level meters therefore incorporate weighting filters, which reduce the contribution of low and high frequencies to produce a reading that corresponds approximately to what we hear. Figure 6.1 (a) depicts curves of equal loudness for a human ear and 6.1 (b) the A-weighting filter curve.

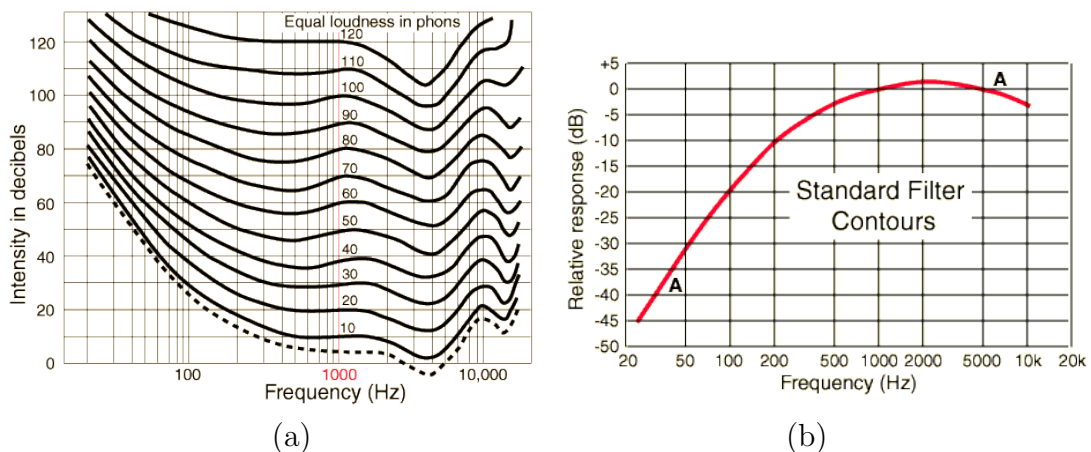


Figure 6.1: (a) Curves of equal loudness. (b) A-weighting filter curve.

The curves were originally defined for use at different average sound levels, but A-weighting, though originally intended only for the measurement of low-level sounds (around 40-phon) is now commonly used for the measurement of environmental noise

and industrial noise, as well as when assessing potential hearing damage and other noise health effects at all sound levels;

Equivalent sound level The equivalent sound level is the most common descriptor for fluctuating sounds. It is used to describe a varying sound level over a certain amount of time and therefore is the notional A-weighted equivalent continuous sound level which, if it occurred over the same time period, would give the same noise level as the actual varying sound level. Due to the equivalence of sound intensity only the time period of exposure and not the distribution in time are relevant. With this averaging single high level sounds have a big influence on the energy equivalent sound level. Figure 6.2 depicts this fact. It shows the resulting equivalent sound levels for a "continuous" event (2000 cars per hour / 60-70dB) and for a "single" train (90dB) passing by in this hour.

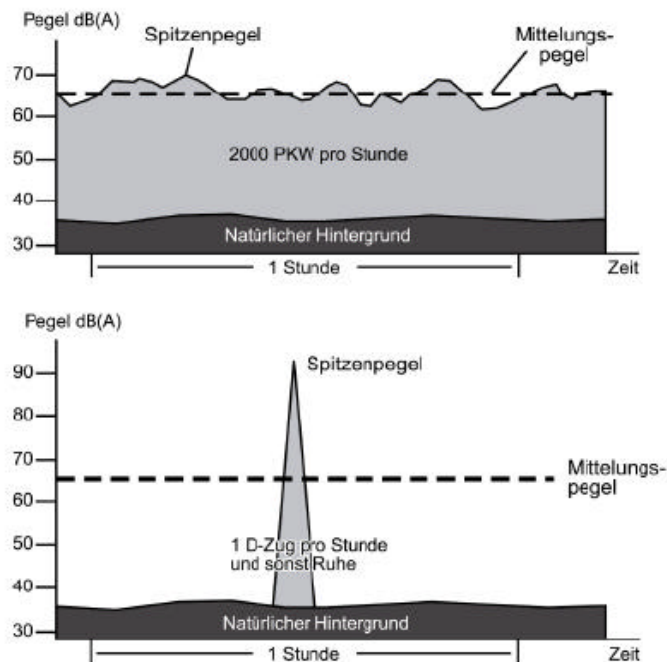


Figure 6.2: Equivalent sound level for car (top) and train (bottom) [Rum06].

Equivalent sound levels are always linked to a time period and are calculated for different parts of the day.

6.2.3 Noise indicators

For the assessment of noise exposure different noise indicators are used. These indicators are A-weighted long-term-average sound levels and are calculated for different daytimes (day, evening, night) as well as a combined indicator L_{den} the Day-Evening-Night level.

Day, Evening and Night levels L_{day} , $L_{evening}$ and L_{night} are the A-weighted long-term-average sound level as defined in ISO 1996-2 [ISO87], determined over all the day, evening and night periods of a year respectively. A year is a relevant year as regards the emission of sound and an average year as regards the meteorological circumstances. The time periods are 12, four and eight hours for the day, evening and night levels. The exact start and end times, for example $Day = 7am \rightarrow 7pm$, $Evening = 7pm \rightarrow 11pm$, $Night = 11pm \rightarrow 7am$, are given by national noise abatement policies, and should be the same for all sources of noise

Day-Evening-Night level L_{den} : The day-evening-night level L_{den} is defined by the following formula:

$$L_{den} = 10 \lg \frac{1}{24} \left(12 \times 10^{\frac{L_{day}}{10}} + 4 \times 10^{\frac{L_{evening}+5}{10}} + 8 \times 10^{\frac{L_{night}+10}{10}} \right) \quad (6.2)$$

where L_{day} , $L_{evening}$ and L_{night} are the A-weighted long-term-average sound level as stated in the previous paragraph. For the evening and night times a penalty of 5 and 10 dB is added to the sound level, because of the heightened sensitivity of human hearing during quiet and night times.

6.2.4 Noise propagation

Sound propagates through air as a longitudinal wave. The speed of sound is determined by the properties of the air, and not by the frequency or amplitude of the sound. How loud a noise, e.g. a 10-ton truck, is perceived at a listener depends on many factors. One has to consider how the noise is emitted from a source, how it propagates through the air, and how it is received at the listener. The most important factors are described below.

Source types Two types of sources are considered. If the dimension of the source is small compared with the distance to the listener, it is called a *point source*. The energy spreads out spherically, the sound pressure level is the same for all points at the same distance from the source and decreases by 6dB per doubling of distance until ground and air attenuation noticeably affects the level. The sound pressure level L_p at any distance r from a point source with sound power level L_W can be calculated as

$$L_p = L_W - 20lg(r) - 8dB$$

If the source is long in one direction and narrow in the other compared with the distance to the listener, it is called *line source*. The energy spreads out cylindrically, the sound pressure level is the same for all points the same distance from the line and decreases 3dB per doubling of distance until ground and air attenuation noticeably affects the level. The sound pressure level L_p at any distance r from a line source with sound power level L_W can be calculated as

$$L_p = L_W - 10lg(r) - 5dB$$

Atmospheric attenuation is a complex process depending on many factors such as distance from the source, frequency spectrum of the noise, temperature, wind, humidity, etc. where distance and frequency are the most influential. The attenuation differs for different frequencies as can be seen in Figure 6.3.

Wind can cause the path of sound to bend. This results in shadow areas and areas where the sound is focused. Wind speed increases with altitude, this causes a shadow on the upwind side and focused sound on the downwind side. The effect of wind speed is depicted in Figure 6.4.

Temperature gradients have effects comparable to the effects of wind gradients but are uniform in all directions from the source. If the temperature decreases with altitude the sound will bend upwards and cause shadow regions. Whereas increasing temperature with altitude (called temperature inversion) bends down the path and results in focused sound on the surface. The effect is depicted in Figure 6.5.

Ground effects are the interferences of the reflected sound with the directly propagated sound. These effects are different for acoustically hard, soft, and mixed sur-

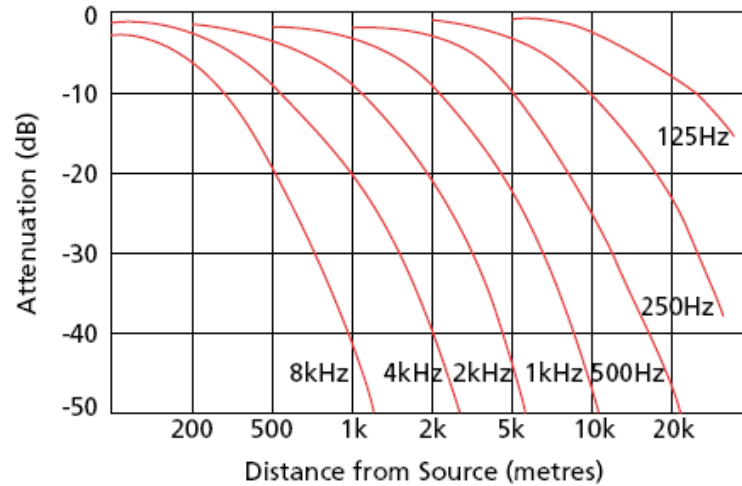


Figure 6.3: Attenuation of sound regarding distance and sound frequency [Brü01].

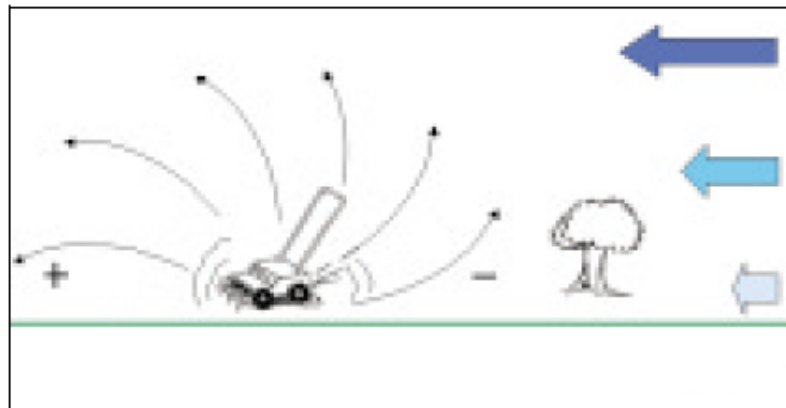


Figure 6.4: Change of sound paths due to wind speeds [Brü01].

faces, e.g. concrete or grass. The attenuation is dependent on the frequency of the noise and the ground type which is depicted in Figure 6.6.

Barriers The effect of noise barriers depends mainly on two factors:

- Path difference between direct and indirect (over the barrier) sound path.
- Frequency of the sound due to diffraction effects.

Because of the ratio between wavelength and size of the barrier, different frequencies are more diffracted than others. Low frequencies for example (wavelength \sim barrier

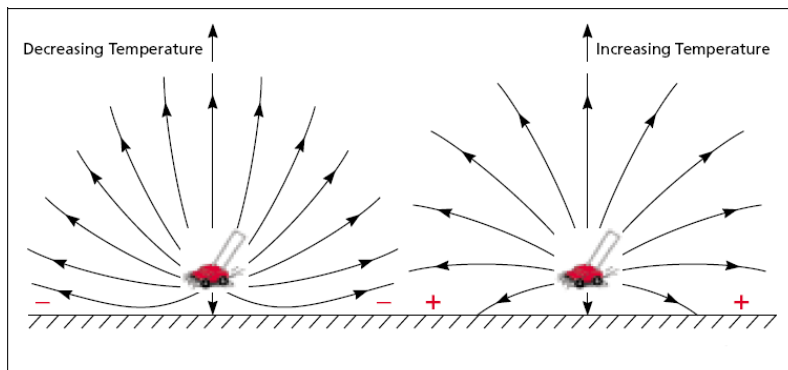


Figure 6.5: Change of sound paths due to temperature gradient [Brü01].

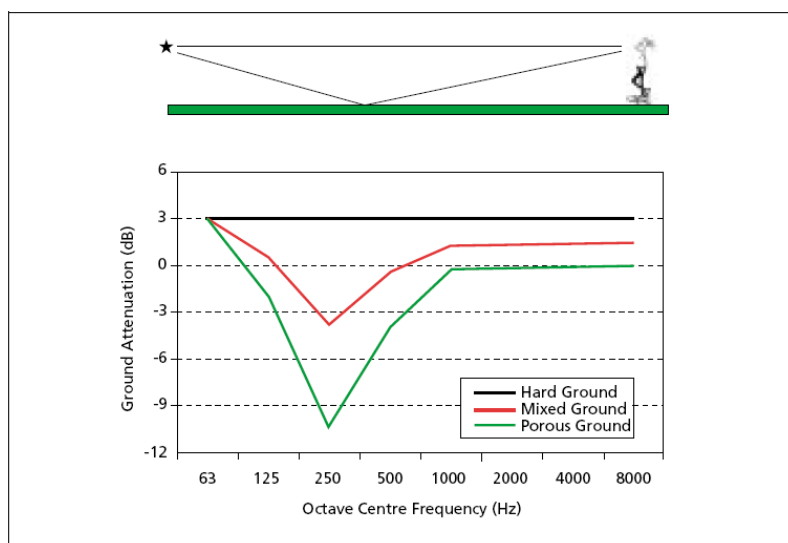


Figure 6.6: Ground attenuation for different frequencies and ground types. Source-receiver distance = 100m, height 2m [Brü01].

dimensions) are not easy to attenuate due to the diffraction effects which occur (the sound bends over the barrier) whereas high frequencies (wavelength \ll barrier dimensions) are nearly not diffracted and thus more attenuated. Attenuation levels for different frequencies and barrier heights are depicted in figures 6.7 and 6.8.

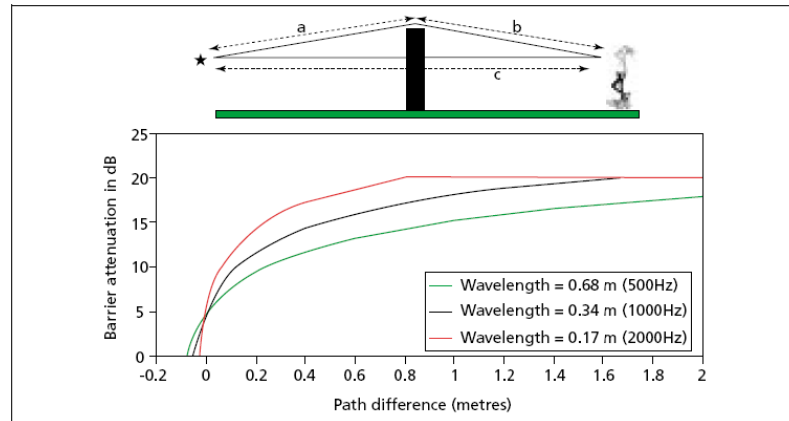


Figure 6.7: Depiction of attenuation on a barrier for different frequencies [Brü01].

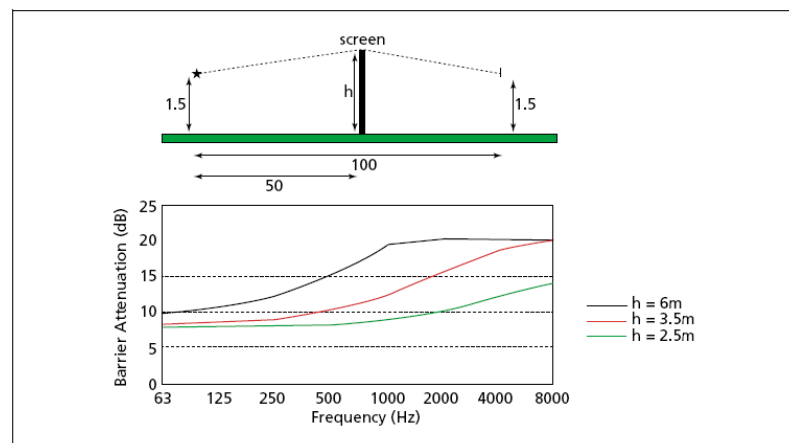


Figure 6.8: Attenuation of a typical noise screen as function of barrier height [Brü01].

6.3 Sources

In environmental planning certain kinds of noise are monitored. This includes mainly traffic, aircraft and railway noise but also industrial and recreational noise.

6.3.1 Traffic noise

Road traffic is the main source of noise in all countries and the most prevalent cause of annoyance and interference. Therefore, traffic noise reduction has the highest priority in noise abatement planning. Traffic noise is the collective sound energy

emanating from motor vehicles such as cars, motorbikes, trucks, and buses. The main sources of traffic noise are:

- Engine noise
- Tire noise
- Aerodynamic noise
- Brake noise

6.3.2 Aircraft noise

Aircraft noise is defined as sound produced by any aircraft on run-up, taxiing, take off, over-flying or landing. Aircraft noise is a significant concern for approximately 100 square kilometers (65 square miles) surrounding most major airports. Aircraft noise is the second largest (after traffic noise) source of environmental noise. While commercial aviation produces the predominate of total aircraft noise, private aviation and military operations also play a role.

Take-off of aircraft may lead to a sound level of more than 100 decibels at the ground, with approach and landing creating lower levels. Since aircraft landing in inner-city airports are often lower than 60 meters (200 feet) above roof level, a sound level above 100 dBA can be realized.

Aircraft noise originates from three main sources:

- Aerodynamic noise
- Engine and other mechanical noise
- Noise from aircraft systems

6.3.3 Railway noise

Railway noise is sound produced by vehicles using a trackbed or rail guidance system. Trains include freight, long haul passenger, commuter rail, metro or mass transit and light rail systems. The noise originates from these main sources:

- Traction noise - For diesel engines, exhaust noise, engine and transmission vibrations. Electric power units are much quieter, though noise is emitted from the traction motor and extra cooling fans. Pantograph noise is significant at high speeds.
- Rail/Wheel noise - Rail and wheel are set into vibration. This produces external and internal noise. Main sources are poorly aligned track joints and the roughness of the wheels and the track.
- Auxiliary equipment noise - compressors, ventilation and brake systems.
- Aerodynamic noise - Produced by passage of the train through the air. Its contribution to the total noise level increases with speed.

6.3.4 Industrial noise

Industrial Noise is the noise related to industrial facilities such as power plants, production facilities, etc. as well as noise from office buildings and noise from construction works. The main sources of industrial noise are for example factory machinery, power tools, external airconditioning and last but not least as consequence a raised amount of traffic leading to and from industrial areas.

6.3.5 Recreational noise

Recreational noise is generally produced by recreational sources such as recreational activities (e.g. ATVs/Quads), lawnmowers, discos, circuses and fairs, private music and open-air concerts and is experienced both indoors and outdoors. In many cases, the noise is unpredictable both in level and in when it occurs. The annoyance from recreational sources is often due to an increase in ambient noise level, but can also be due to information content such as pure tones or impulsive noise, or due to the penetration of deep, bass tones from modern music systems.

6.4 Health effects

Noise health effects are the health consequences of elevated sound levels. Elevated workplace or other noise can cause hearing impairment, hypertension, ischemic heart disease, annoyance, sleep disturbance, and decreased school performance. Noise exposure has also been known to induce tinnitus, hypertension, vasoconstriction and other cardiovascular impacts. Beyond these effects, elevated noise levels can create stress, increase workplace accident rates, and stimulate aggression and other anti-social behaviors. The most significant causes are vehicle and aircraft noise, prolonged exposure to loud music, and industrial noise. Figure 6.9 depicts the noise reaction scheme.

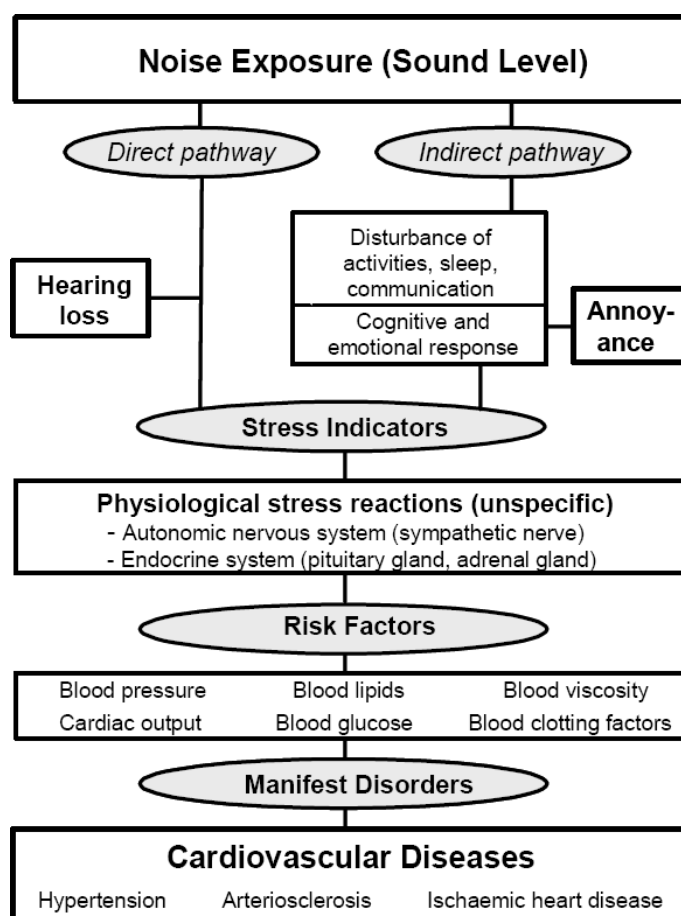


Figure 6.9: Noise effects reaction scheme [Bab02]

6.4.1 Noise-induced hearing loss

Exposure to noise can have several effects on hearing depending on the sound power level of the noise. The main concern related to occupational noise exposure however is noise-induced permanent hearing loss. Different effects of elevated noise levels are:

- Acoustic trauma: Sudden hearing damage caused by short burst of extremely loud noise such as a gun shot.
- Tinnitus: Ringing or buzzing in the ear.
- Temporary hearing loss: Also known as temporary threshold shift (TTS) which occurs immediately after exposure to a high level of noise. There is gradual recovery when the affected person spends time in a quiet place. Complete recovery may take several hours.
- Permanent hearing loss: Permanent hearing loss, also known as permanent threshold shift (PTS), progresses constantly as noise exposure continues month after month and year after year. The hearing impairment is noticeable only when it is substantial enough to interfere with routine activities. At this stage, a permanent and irreversible hearing damage has occurred. Noise-induced hearing damage cannot be cured by medical treatment and worsens as noise exposure continues. When noise exposure stops, the person does not regain the lost hearing sensitivity. As the employee ages, hearing may worsen as "age-related hearing loss" adds to the existing noise-induced hearing loss.

6.4.2 Cardiovascular impact

Noise has been associated with important cardiovascular health problems. In 1999, the World Health Organization concluded that the available evidence showed suggested a weak association between long-term noise exposure above 67-70 dB(A) and hypertension [BLSG99]. More recent studies [Mas03] have suggested that noise levels of 50 dB(A) at night may also increase the risk of myocardial infarction by chronically elevating cortisol production.

Fairly typical roadway noise levels are sufficient to constrict arterial blood flow and lead to elevated blood pressure; in this case, it appears that a certain fraction of the population is more susceptible to vasoconstriction. This may result because annoyance from the sound causes elevated adrenaline levels trigger a narrowing of the blood vessels (vasoconstriction), or independently through medical stress reactions. Other effects of high noise levels are increased frequency of headaches, fatigue, stomach ulcers and vertigo.

6.4.3 Annoyance

Because some stressful effects depend on qualities of the sound other than its absolute decibel value, the annoyance associated with sound may need to be considered in regard to health effects. For example, noise from airports is typically perceived as more bothersome than noise from traffic of equal volume. Annoyance effects of noise are minimally affected by demographics, but fear of the noise source and sensitivity to noise both strongly affect the 'annoyance' of a noise. Even sound levels as low as 40 dB(A) [Gel] can generate noise complaints and the lower threshold for noise producing sleep disturbance is 45 dB(A) or lower [WF98]. Other factors that affect the 'annoyance level' of sound include beliefs about noise prevention and the importance of the noise source, and annoyance at the cause (i.e. non-noise related factors) of the noise. Evidence regarding the impact of long-term noise versus recent changes in ongoing noise is equivocal on its impact on annoyance.

When young children are exposed to speech interference levels of noise on a regular basis (the actual volume of which varies depending on distance and loudness of the speaker), there may develop speech or reading difficulties, because auditory processing functions are compromised. In particular the writing learning impairment known as dysgraphia is commonly associated with environmental stressors in the classroom.

6.5 History of noise mapping

Despite the fact that noise caused annoyance throughout human existence and references to noise can be found in the literature way back to the historical Gilgamesh-

Epic (2600BC) noise mapping / mitigation planning has its beginning in the late 19th and early 20th century. The cause may have been the absence of objective methods to quantify noise or sound intensity in general. In 1882 Lord Rayleigh build the first instrument to measure and thus quantify sound intensity. Combined with new medical insights into the correlation of hearing loss and high sound intensity in production facilities in the late 19th century, noise became of public interest. This lead to the foundation of the "Deutschen Lärmschutzverband" in 1908 and the "Acoustical Society of America (ASA)" in 1929. The "First Symposium on Noise" was held in New York in May 1930.

The definition of Decibel-Thresholds in the 1920s and 30s allowed to express the problem in numbers and identify areas with a high noise exposure. One of the first examples for the visualization of noise is a sound intensity map for a Berlin city district from 1938 (Figure 6.10). In this map streets are shaded according to their intensity levels which were measured at 260 locations for a period of three month.

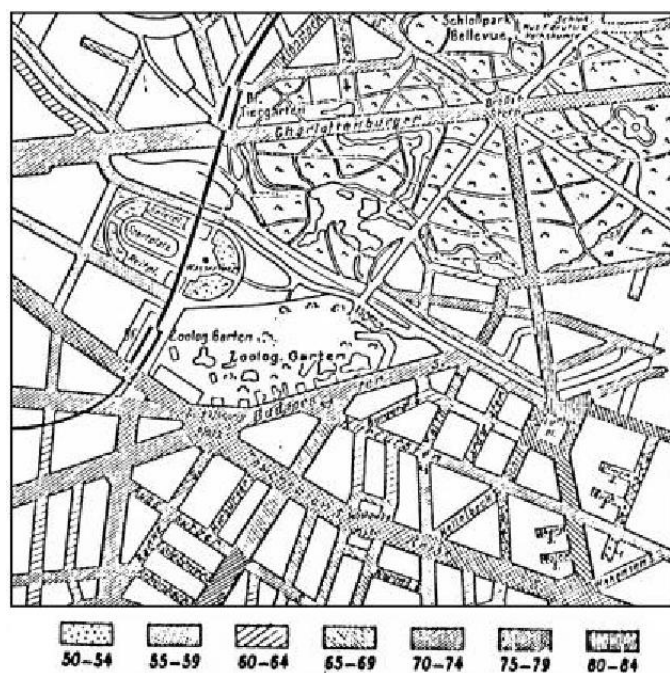


Figure 6.10: Noise map of a Berlin city district (1938) [Glü73]

After the caesura of WWII noise mitigation again came in the view of the public in the late 1950s and early 60s not least because of the increasing number of vehicles and the noise exposure caused by them. Until today many laws and bills for

noise abatement have been passed, the current regulations in state for Europe and Germany are summarized in section 6.6.

6.6 Current regulations

This section gives a brief overview of the current regulations which are in state in the European Union and Germany. The German directive and computation methods will be discussed in more detail in section 8.1.

6.6.1 European Union

In 1996 the Commission of the European Union released the 'Green Paper on Future Noise Policy' which stated, that environmental noise, caused by traffic, industrial and recreational activities is one of the main local environmental problems in Europe and the source of an increasing number of complaints from the public. Generally however action to reduce environmental noise has had a lower priority than that taken to address other environmental problems such as air and water pollution. This 'Green Paper' was the start of a program which resulted in 'The Directive on Environmental Noise' which is aimed at requiring competent authorities in Member States to produce strategic noise maps on the basis of harmonised indicators, to inform the public about noise exposure and its effects, and to draw up action plans to address noise issues.

Directive 2002/49/EC The Directive on Environmental Noise or Environmental Noise Directive (END) [END02] has the goal to provide a common basis for tackling the noise problem across the EU. The underlying principles are similar to those for other overarching environment policy directives:

- Monitoring the environmental problem by requiring competent authorities in Member States to draw up "strategic noise maps" for major roads, railways, airports and agglomerations, using harmonised noise indicators L_{den} (day-evening-night equivalent level) and L_{night} (night equivalent level). These

maps will be used to assess the number of people annoyed and sleep-disturbed respectively throughout Europe

- Informing and consulting the public about noise exposure, its effects, and the measures considered to address noise, in line with the principles of the Aarhus Convention
- Addressing local noise issues by requiring competent authorities to draw up action plans to reduce noise where necessary and maintain environmental noise quality where it is good. The directive does not set any limit value, nor does it prescribe the measures to be used in the action plans, which remain at the discretion of the competent authorities.
- Developing a long-term EU strategy, which includes objectives to reduce the number of people affected by noise in the longer term, and provides a framework for developing existing Community policy on noise reduction from source.

6.6.2 Germany

The Directive 2002/49/EC [END02] was translated into German law in June 2005 as part 6 (§47 a-f) of the 'Bundes-Immissionsschutzgesetz (BImSchG)' (Federal Immission Protection Law) and concretized in March 2006 with the '34. Verordnung zur Durchführung des Bundes-Immissionsschutzgesetzes (34. BImSchV)'.

In May 2006 the 'Interim methods for the calculation of environmental noise' (VBU) [VBU06a] were published. These include calculation methods for street (VBUS) [VBU06d], aircraft (VBUF) [VBU06b], railway (VBUSch) [VBU06e] and industry (VBUI) [VBU06c] noise. The 'Interim methods for the calculation of the number of people affected by environmental noise' (VBEB) [VBE07] was published in February 2007.

Chapter 7

State of the Art

7.1 Noise maps

A map is a symbolic representation of a geographic reality. One has to make a distinction between topographical and thematic maps. Noise maps belong to the latter category and thus depicts the spatial distribution of factual information. In contrast to topographical maps which normally display a realistic geographical situation. However, topographical maps are always the basis for thematic maps.

7.1.1 Types of noise maps

In general noise maps depict measured or calculated noise levels in a region of interest. There have been different types of noise maps which are described in the following.

Noise dots The first type of noise map depicts measured noise levels at distinct receiver positions. Therefore a marker is put on the position in the map. The noise level can be displayed for example as colored dots as shown in figure 7.1 which gives a quantitative view on the noise.

Another example is to visualize the quality of noise using simple icons instead of colored dots. In figure 7.2 smiley faces are used to depict noise levels.



Figure 7.1: Measured air traffic noise in Berlin as colored dots on a map (1968/69) [Glü73].

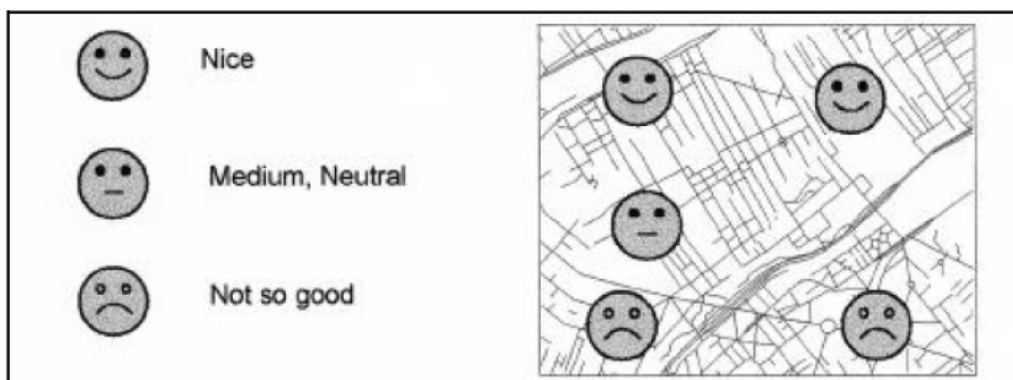


Figure 7.2: Visualizing noise using smiley faces do depict noise 'quality' [Sch02].

Ribbon/Line To visualize traffic noise it is a natural choice to visualize the exposure levels as lines or ribbons around a street, because streets themselves are line objects and therefore the noise sources move along these lines. The most affected buildings are also situated directly besides the street, so the distance to the source can be neglected. To display the amount of noise different colors or varying width of the ribbons are used. An example is given in figure 7.3.

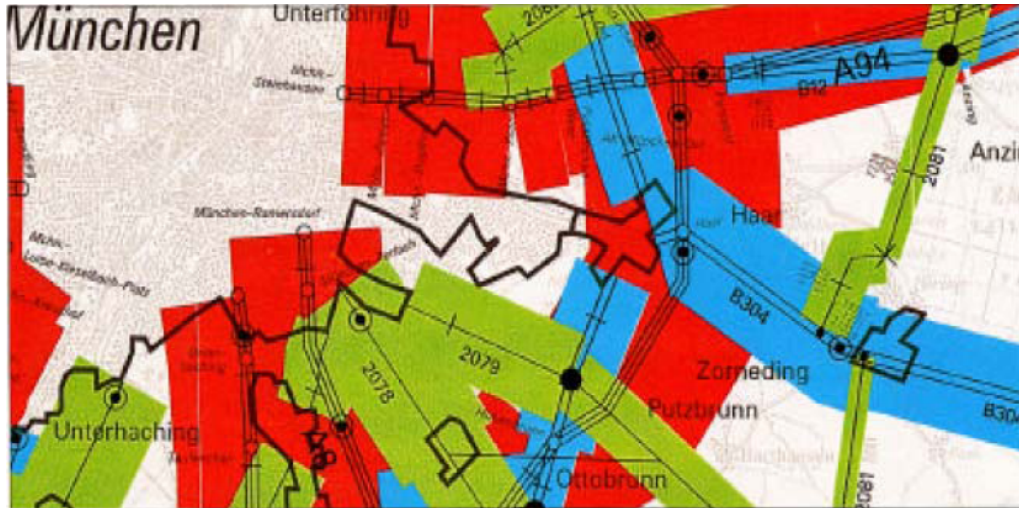


Figure 7.3: Ribbonlike visualization of traffic noise in Munich with varying width and color depicting different noise levels (1990) [Sch02].

2002/49/EC compliant noise maps To satisfy the propagation of sound and therefor noise and to depict noise exposure not only directly at a source but also the whole area of influence current noise maps use a laminar illustration. They are normally not based on single measured but calculated noise values on a grid employing noise prediction software. An example is given in figure 7.4.

With the noise levels separately calculated on a grid for all noise sources (traffic, railway, air, industry) it is easily possible to merge these maps into a single noise exposure map.

7.1.2 Coloring

The coloring of different noise levels in noise maps (figure 7.5) for Germany is defined in the DIN 18005-2 [DIN91].

7.2 Software

For the computation of noise maps there are commercial tools available whose calculation methods and results comply with current standards and which use basic visualization techniques to display the results. However, there are many research

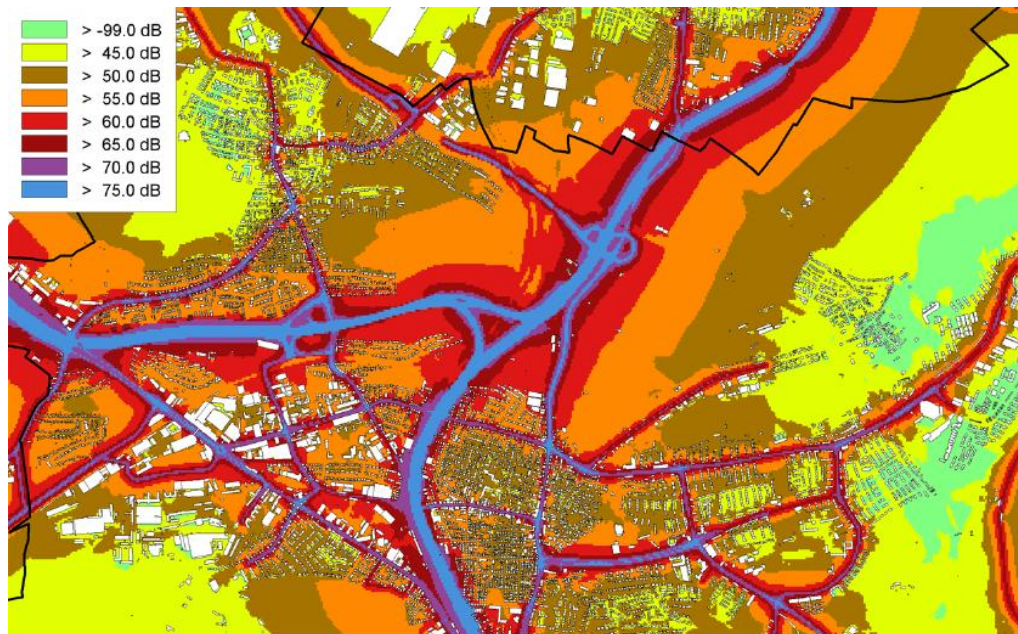


Figure 7.4: 2002/49/EC compliant noise map [KP07].

Beurteilungspegel dB(A)	Farbname	Farben
bis 35	weißgrün	
über 35 bis 40	gelbgrün	
über 40 bis 45	türkisgrün	
über 45 bis 50	schwefelgelb	
über 50 bis 55	braunbeige	
über 55 bis 60	pastellorange	
über 60 bis 65	verkehrsrot	
über 65 bis 70	rubinrot	
über 70 bis 75	verkehrspurpur	
über 75 bis 80	lichtblau	
über 80	capriblau	

Figure 7.5: Default coloring for noise maps [DIN91].

projects which deal with new calculation and visualization methods for noise. A brief overview of common commercial noise calculation software and selected research projects is given in the following.

7.2.1 Commercial tools

Overall, commercial noise calculation software provide many different calculation models, e.g. national instructions like the VBUS (see section 6.6.2 and 8.1), so they can be applied in different states with varying regulations. They also include different visualization methods to display the calculation results. These can reach from plain two dimensional maps or vertical cross-sections to three dimensional city models with projected noise exposures as building textures.

CadnaA developed by Datakustik GmbH¹ is a noise calculation software for the Windows platform. It includes the latest european and international noise calculation standards as well as the interim version of the Imagine project, "Harmonoise"². The calculation model can be completely constructed within CadnaA or imported from various file formats. The noise exposure can be calculated at distinct points, on a two dimensional grid or on building facades.

For the visualization of the calculation results CadnaA offers different possibilities ranging from spreadsheets to 3D models. The spreadsheet view provides a complete list of all important values for each receiver point (Figure 7.6 (a)). It is also possible to view certain values at distinct receiver positions, i.e. nighttime noise in front of a building, in a simple two dimensional map (Figure 7.6 (b)).

If the noise is calculated on a grid, CadnaA offers different configurable styles, i.e. for the coloring of noise levels, to display the resulting noise maps. The resulting maps, which comply with the EU directive (section 6.6.1), are designable and can be exported to various formats. Figure 7.7 depicts two noise maps with different coloring schemes.

The same data can be visualized within a three dimensional city model based on the underlying building information and digital elevation model. Therefore the calculated noise map is projected to the ground surface and used as texture. The examples in figure 7.8 (a) + (b) already show problems arising from this visualization. According to the EU directive the noise has to be calculated 4 meters above ground, but with CadnaA it is possible to compute noise exposure also at different

¹<http://www.datakustik.com>

²<http://www.imagine-project.org>

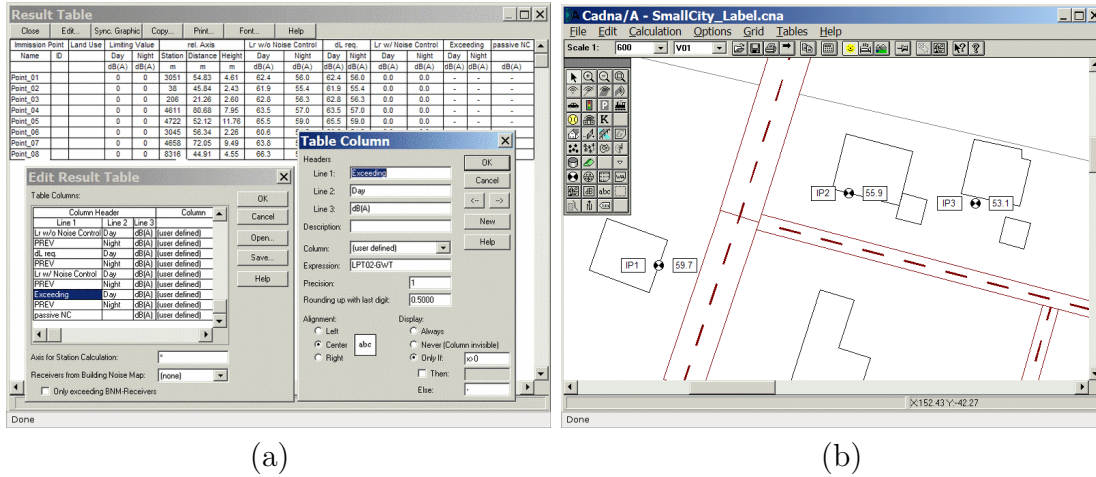


Figure 7.6: CadnaA: Spreadsheet and distinct receiver points

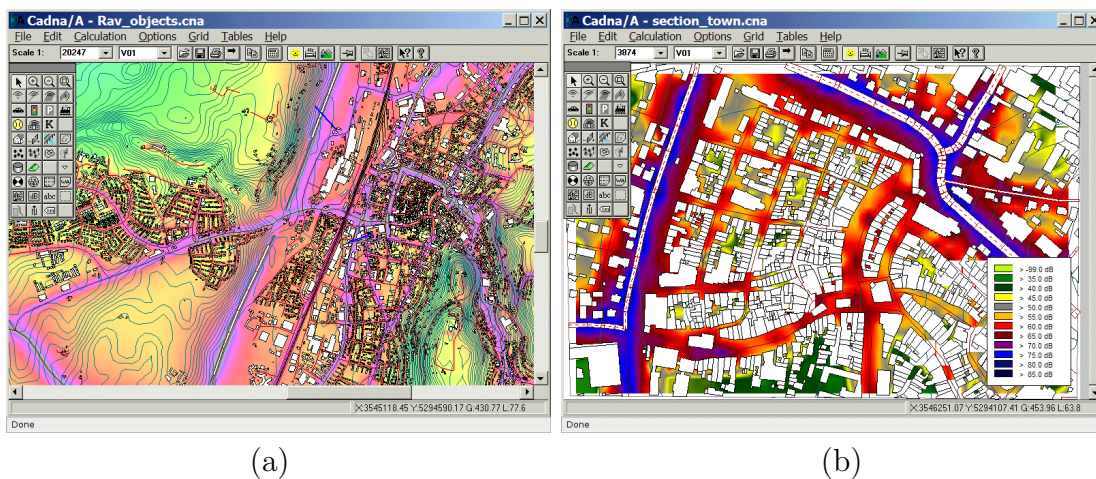


Figure 7.7: CadnaA: 2D noise maps with different coloring

heights. However, the height information is lost when the noise map is projected to the ground.

It is also possible to calculate the noise exposure at all building facades and either display the noise levels as icons at the calculation positions (figure 7.8 (c)) or use these values to generate textures for the buildings (figure 7.8 (d)).

SoundPlan from Braunstein + Bernd GmbH³ is a modularized noise calculation software. It consists of a main module which can be extended with additional

³<http://www.soundplan.de>

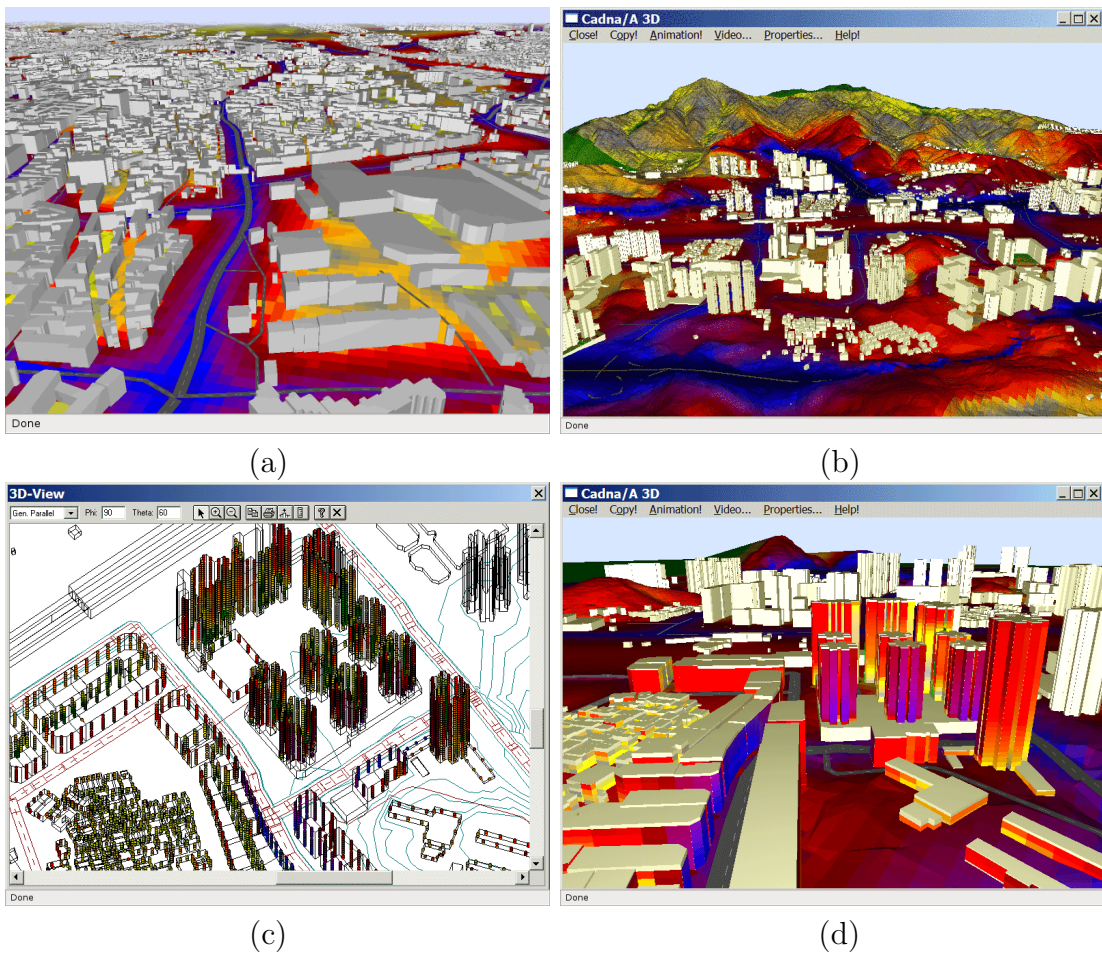


Figure 7.8: CadnaA: 3D + Facade

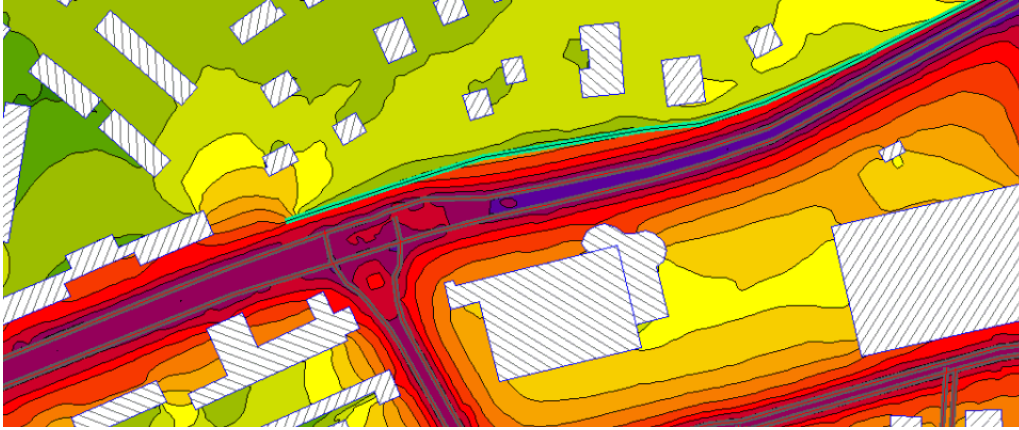


Figure 7.9: SoundPlan: Noise map

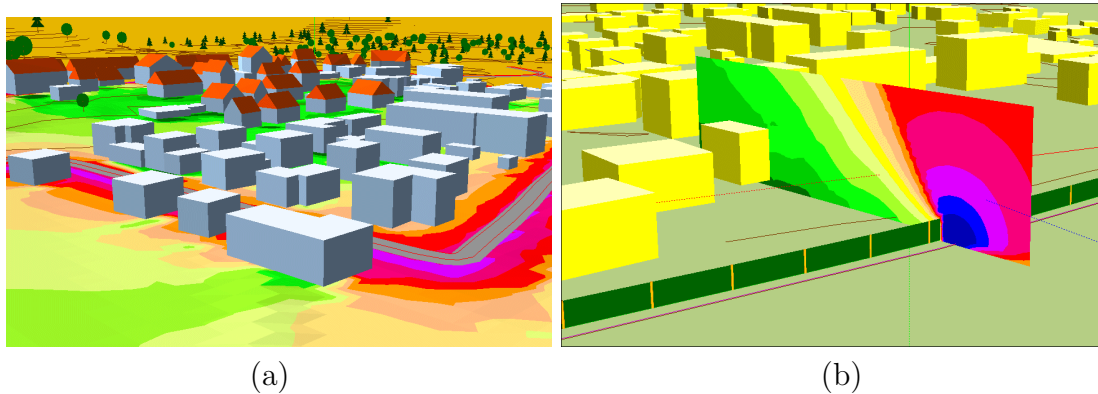


Figure 7.10: SoundPlan: 3D visualization and cross section

functionality, i.e. different calculation models or visualization techniques, depending on the field of application.

SoundPlans display capabilities range from simple spreadsheet to three dimensional visualizations dependant on the used modules. The noise can be displayed for distinct receiver points in a map or as noise map (figure 7.9) if the exposure levels are calculated on a grid. The noise maps can be used as ground texture in a three dimensional model of the calculation area (figure 7.10 (b)).

With SounPlan it is also possible to display noise on building facades either as distinct calculation points or as facade textures. Additionally vertical cross sections can be defined and visualized in the three dimensional model (figure 7.10 (b)).

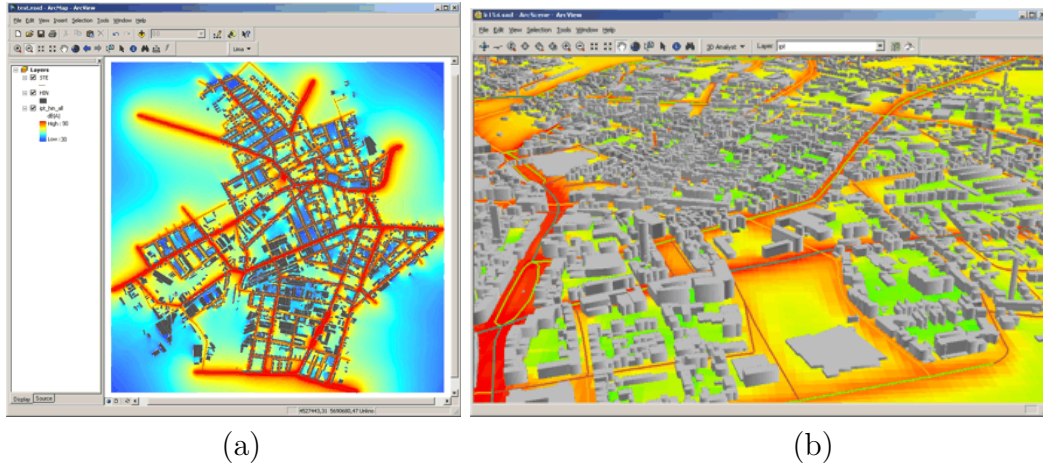


Figure 7.11: LimA: Noise map and 3D city model

LimA developed by Stapelfeldt Ingenieure GmbH⁴ is a noise calculation software which can be fully integrated into ArcGIS, a GIS software, using the extension *LimA^{arc}*. This enables the user to make noise calculations directly within ArcGIS which simplifies the use because the underlying data doesn't need to be converted. The results can then be visualized using the visualization tools which are integrated into ArcGIS.

LimA can also be used as a standalone application. The calculation model can be completely constructed and calculated within LimA. To visualize the noise levels, the results can then be imported into *LimA^{arc}*.

The techniques include two-dimensional noise maps which can be used inside a three-dimensional city model (figure 7.11 (a+b)) as well as the visualization of noise on building facades or vertical cross sections (figure 7.12 (a+b)).

7.2.2 Research

Due to the raised awareness and new regulations for noise exposure in recent years a lot of research has been done in the field of noise calculation and visualization. Especially the problem how to display noise within a three-dimensional digital city model with the goal to ease the information of the public and enable them to par-

⁴<http://www.stapelfeldt.de>

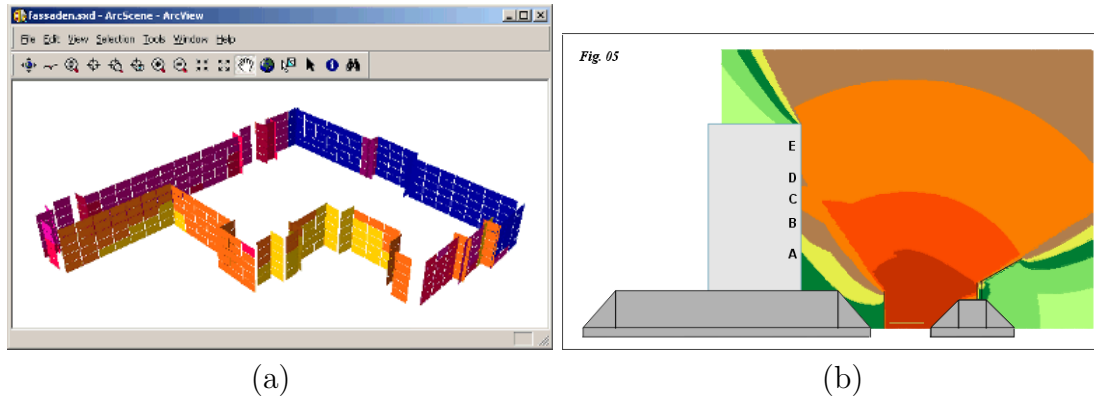


Figure 7.12: LimA: Building facades and cross section

ticipate in the city planning process as demanded by the EU directive. This section gives a brief overview of selected research projects.

Kurakula et al. [Kur07, KK08] introduced a GIS based approach for noise modeling where virtual microphones were laid out as a grid around buildings and streets. The noise is calculated with a standard software and two different visualization methods are used to display the noise, isolines and color interpolation (figure 7.13 (a)). There is no interaction with the city model possible, so only the buildings in front are displayed completely and the farther away buildings are obstructed. To see the model from another viewpoint a new image has to be rendered. The three dimensional visualization is also used to display the impact of different parameters (height, position) of a noise barrier on the noise field (figure 7.13 (b)).

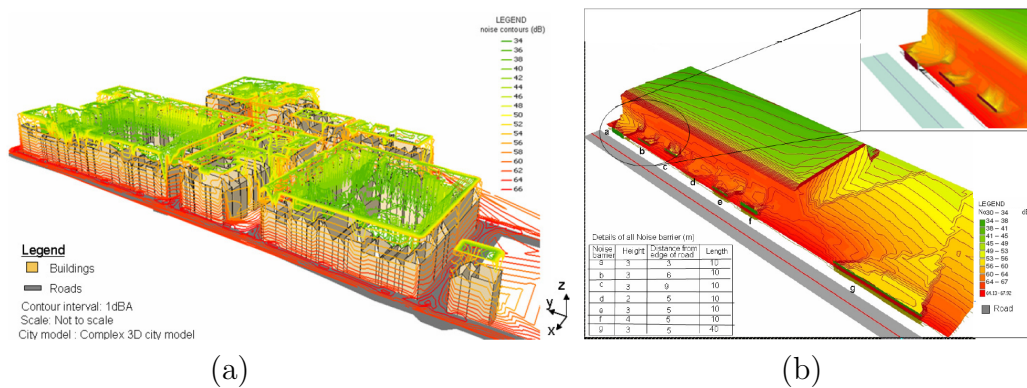


Figure 7.13: Kurakula [Kur07]: Visualizing noise levels on the building facade with isolines (a). Impact of different parameters of a noise barrier on the abatement (b).

It is also possible to only show the noise above a certain threshold or highlight the most affected buildings, but due to the lack of interaction with the model again a new image has to be rendered for every change. The author also proposed a method to visualize volumetric noise data, but the system is not able to display the volumetric data and the city model at the same time.

LAW et al [LLT06] used facade maps as textures on a photorealistic city model to show the impact of noise mitigation screens on the surrounding buildings (figure 7.14 (a+b)). The city model could be navigated in 3D and the noise textures of the buildings can be turned on and off to allow an easier identification of the current location.

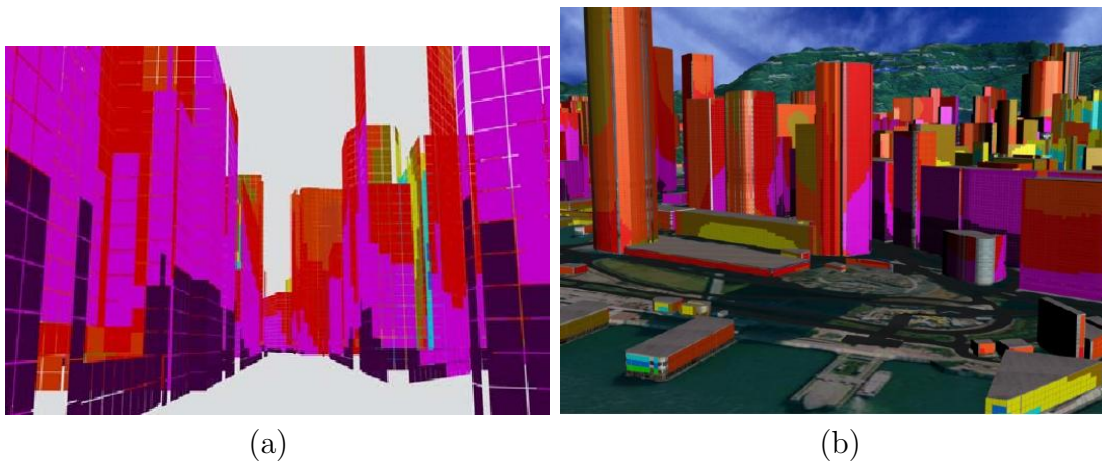


Figure 7.14: Law et al [LLT06]: Visualizing noise levels on the building facade as quads (a) and within a photorealistic 3D city model (b).

The visualization is suitable for the presentation of proposed noise abatement measures but cannot give insight into the noise propagation and thus one cannot identify which sources are the most important noise producers. Additionally there is no information on the noise in building free areas, e.g. parks or projected building areas.

VEPS⁵ (Virtual Environmental Planning system) project employs the visualization of noise in a 3D environment as part of its public participation system. Different noise maps for planning scenarios are calculated by external software either 4 m

⁵<http://www.veps3d.net>

above ground or at the building facades and are then integrated alongside a 3D city model into GoogleEarth or Acrobat3D (figure 7.15 (a+b)).

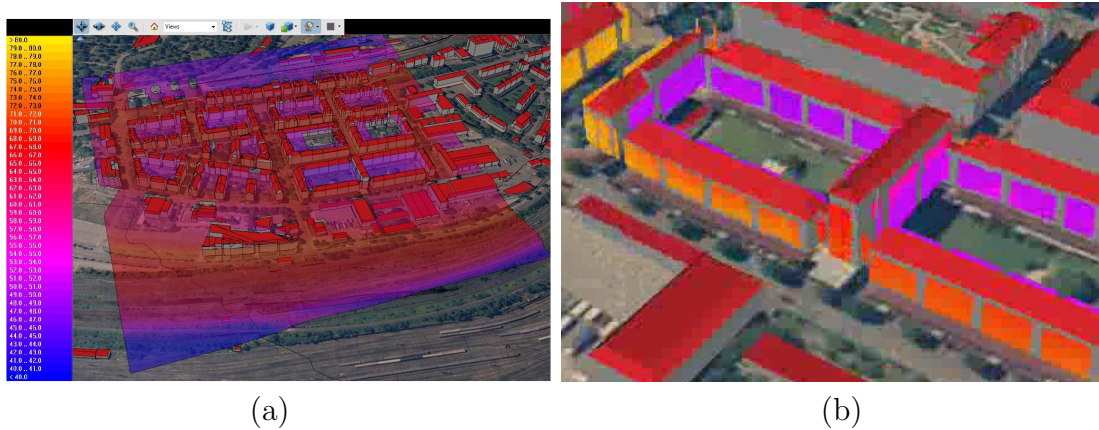
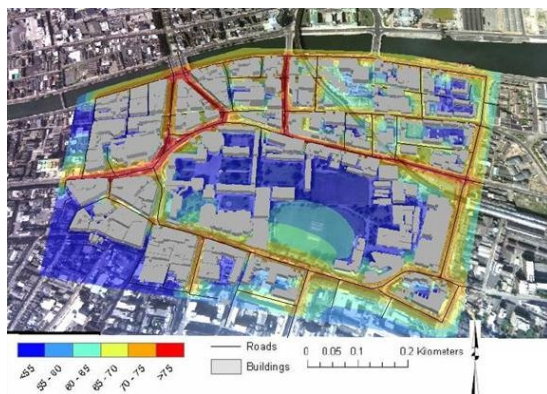


Figure 7.15: VEPS: Visualizing a noise map in a 3D city model (a) and as building facades (b).

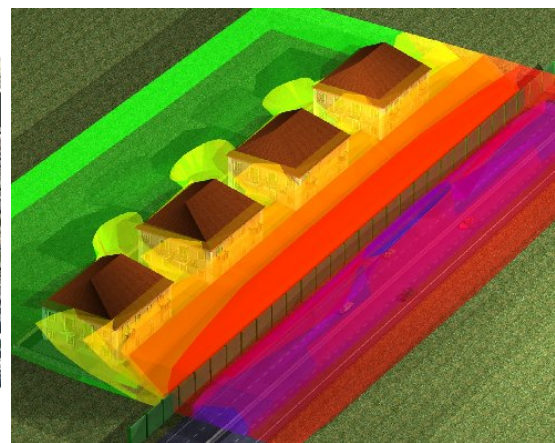
Therefore the possible interaction with the model is limited to the capabilities of GoogleEarth or Acrobat which can already give a better understanding of the noise situation by moving through the 3D model and switching between different noise scenarios. But again it is only a projection of the 2-dimensional maps into a 3D world and the spatial propagation and interaction of the noise with the environment cannot be seen.

Trinity College Dublin Besides researching new visualization techniques for 2D maps like animated uncertainty visualization the ETI Capability Development Project⁶ at the Trinity College in Dublin also integrates the 2D noise maps in a GoogleEarth like environment (figure 7.16 (a)) to display different noise scenarios [PR07]. They also work on the visualization of three dimensional noise data sets. First visualizations have been conducted using Cinema4D to construct isosurfaces (figure 7.16 (b)).

⁶<http://www.mecheng.tcd.ie/eoin>



(a)



(b)

Figure 7.16: Pilla [PR07]: Visualizing a noise map in a 3D city model (a). Volumetric noise visualization using Cinema4D (b).

Chapter 8

Simulation

In this chapter the method for the simulation of traffic noise is presented. The computation is based on the German implementation of Directive 2002/49/EU regulations published as part 6 (§47 a-f) of the 'Bundes-Immissionsschutzgesetz (BImSchG)' (Federal Immission Protection Law) concretized in the '34. Verordnung zur Durchführung des Bundes-Immissionsschutzgesetzes (34. BImSchV)'. The computation methods were published in the 'Interim methods for the calculation of environmental noise' (VBU) [VBU06a] chapter street traffic (VBUS) [VBU06d]. In section 8.1 the VBUS is presented including details on the different variables. Section 8.2 depicts the implemented algorithm. Section 8.2.1 describes the needed input data for the simulation. The verification of the implementation is discussed in section 8.2.2. Finally in section 8.3 the extension to calculate 3D noise volumes (8.3.1) and a variant to dynamically interact with the calculation (8.3.2) are presented. Further information about the implementation can be found in [Str08].

8.1 Calculation method - VBUS

For the assessment of traffic noise the two indicators L_{den} (day-evening-night) and L_{night} are used. As described in section 6.2.3 the day-evening-night level L_{den} is defined by the following formula:

$$L_{den} = 10 \lg \frac{1}{24} \left(12 \times 10^{\frac{L_{day}}{10}} + 4 \times 10^{\frac{L_{evening}+5}{10}} + 8 \times 10^{\frac{L_{night}+10}{10}} \right) \quad (8.1)$$

where L_{day} , $L_{evening}$ and L_{night} are the A-weighted long-term-average sound levels. For the evening and night times a penalty of 5 and 10 dB is added to the sound level, because of the heightened sensitivity of human hearing during quiet and night times.

The 'Interim method for the calculation of environmental noise caused by streets' (VBUS) prescribes how to calculate these indicators.

8.1.1 Street segments

For the calculation of emitted traffic noise the streets need to be split into segments which are nearly linear and the emission due to traffic as well as the propagation conditions are constant. For each segment a noise source is placed $0.5m$ above the surface. Depending on the scenario a maximum distance for the sound sources and thus the length of the segments is given. The difference in noise emission depending on the maximum distance between noise sources is depicted in figure 8.1. In (a) the $40m$ long segment is not split, thus represented by one sound source, whereas in (b) and (c) the maximum distance is set to $20m$ and $4m$ respectively.

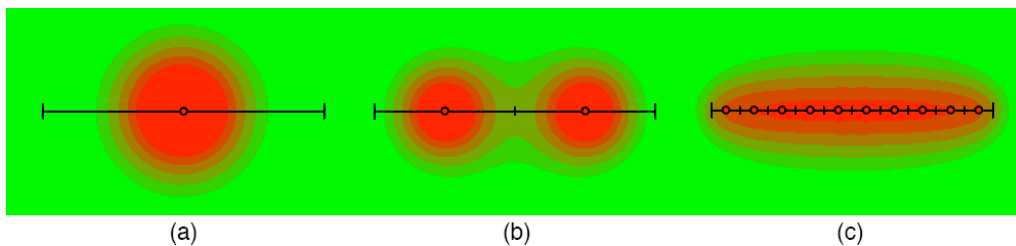


Figure 8.1: Effect of maximum distance between sound sources when splitting streets into segments. Street length = $40m$. maximum source distance = $40m$ (a), $20m$ (b) and $4m$ (c).

Because the noise emission of a segment depends on the length of the segment the emission levels are different in the three depicted cases.

The effects of linearity and constant emission and propagation conditions is shown in figure 8.2. The street length of $\sim 22m$ and a maximum source distance of $9m$ would suggest three segments but because of shorter segments due to the aforementioned conditions the splitting results in a total of nine segments.

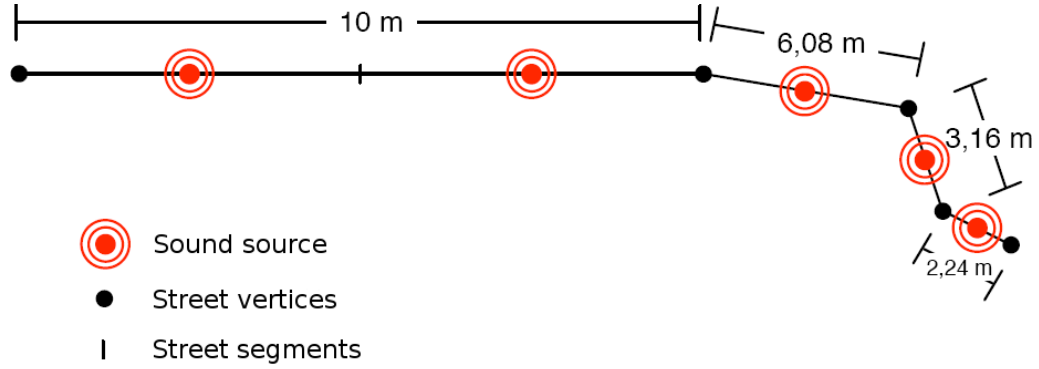


Figure 8.2: Segmentation of a $\sim 22m$ long street into nine instead of 3 segments due to the requirement of linear segments with constant emission and propagation conditions.

8.1.2 Noise levels

The noise level at a distinct position in the calculation area is the total average level L_m in $dB(A)$. It is defined as the sum of all average levels $L_{m,j}$ for all sound sources j which represent one street segment each (see section 8.1.1):

$$L_m = 10 \cdot \lg \sum_j 10^{\frac{L_{m,j}}{10}} \quad (8.2)$$

The received average noise level $L_{m,j}$ from source j is defined as follows:

$$L_{m,i} = L_{m,E} + D_l - D_s - \max(D_{BM}, D_z) + D_{met} + D_{refl} \quad (8.3)$$

with parameters

- $D_l = 10 \cdot \lg(l)$ the correction factor for the street segment length
- D_s the level change caused by distance and air absorption (8.1.4)
- D_z the level change caused by screening (8.1.5)
- D_{BM} the level change caused by ground and meteorological damping (8.1.6)
- D_{met} level change caused by other propagation conditions (8.1.7)
- D_{refl} level raise due to multi-reflections (8.1.9)

and the emission level $L_{m,E}$ of the sound source.

8.1.3 Emission level $L_{m,E}$

The emission level $L_{m,E}$ of a sound source is calculated as:

$$L_{m,E} = L_m^{(25)} + D_v + D_{StrO} + D_{Stg} + D_E \quad (8.4)$$

with parameters

- D_v the correction factor for different speed limits
- D_{StrO} the correction factor for the street surface
- D_{Stg} the correction factor for the longitudinal slope
- D_E the correction factor for mirror sources (8.1.8)

and the average level in 25m distance, assuming non corrugated mastic asphalt, a speed limit of 100km/h, slope of less than 5% and free sound propagation (no screening objects).

$$L_m^{(25)} = 37,3 + 10 \cdot \lg[M \cdot (1 + 0,082 \cdot p)] \quad (8.5)$$

At this point the distinction between different times of the day is made which results in the different noise indicators L_{day} , $L_{evening}$ and L_{night} which are needed to calculate the main indicator L_{den} . Figure 8.3 depicts the values for the parameters M and p in equation 8.5 depending on the time of day.

8.1.4 Distance and air absorption D_s

The correction factor for level decrease due to distance and air absorption D_s is calculated by equation 8.6. The equation only depends on the distance s between sound source and the immission point.

	Straßengattung	tags (6.00-18.00 Uhr)		abends (18.00-22.00 Uhr)		nachts (22.00-6.00 Uhr)	
		M [Kfz/h]	p [%]	M [Kfz/h]	p [%]	M [Kfz/h]	p [%]
	1	2	3	4	5	6	7
1	Bundesautobahnen	$0,062 \cdot DTV$	25	$0,042 \cdot DTV$	35	$0,014 \cdot DTV$	45
2	Bundesstraßen	$0,062 \cdot DTV$	20	$0,042 \cdot DTV$	20	$0,011 \cdot DTV$	20
3	Landes-, Kreis-, und Gemeindeverbindungsstraßen	$0,062 \cdot DTV$	20	$0,042 \cdot DTV$	15	$0,008 \cdot DTV$	10
4	Gemeindestraßen	$0,062 \cdot DTV$	10	$0,042 \cdot DTV$	6,5	$0,011 \cdot DTV$	3

Figure 8.3: Values for parameters M and p in equation 8.5 for different times of the day [VBU06d].

$$D_s = 20 \cdot \lg(s) + s/200 - 11,2 \quad (8.6)$$

Figure 8.4 depicts the damping factor in $dB(A)$ depending on the distance s . When calculating noise levels at the standard height of $4m$ above ground the minimum distance s is $3.5m$ (standard height for sound sources is $0.5m$ above ground). When the noise is calculated for arbitrary heights (i.e. below $4m$) the minimum value for D_s needs to be set to $0dB(A)$ to avoid infinite noise levels around sources.

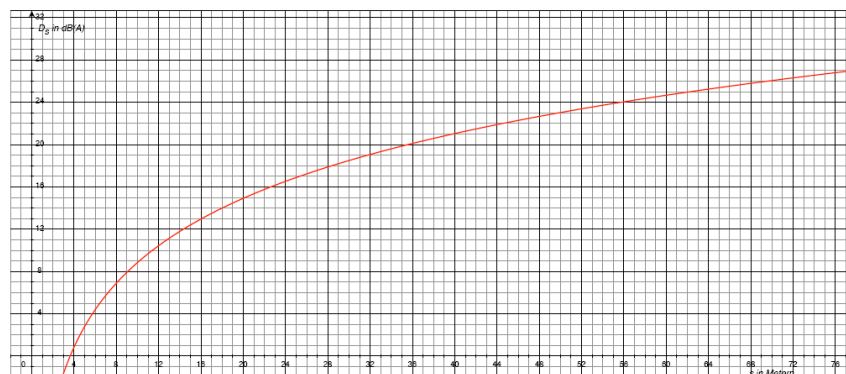


Figure 8.4: Depiction of parameter D_s in $db(A)$ depending on the distance s between source and receiver.

8.1.5 Screening D_z

The use of screening elements (i.e. noise abatement walls) is the most important tool for urban planners to reduce noise exposure. Screening has to be taken into

account when line of sight between source and receiver is obstructed by an obstacle. The extend of screening is expressed in the parameter D_z :

$$D_z = \begin{cases} 10 \cdot \lg[3 + 60 \cdot z] & \text{if } z > -\frac{1}{30} \\ 0 & \text{else} \end{cases} \quad (8.7)$$

where

$$z = \sum_i A_i + B - (\sum_i A'_i + B') \quad (8.8)$$

The calculation of the screening value z is depicted in figure 8.5.

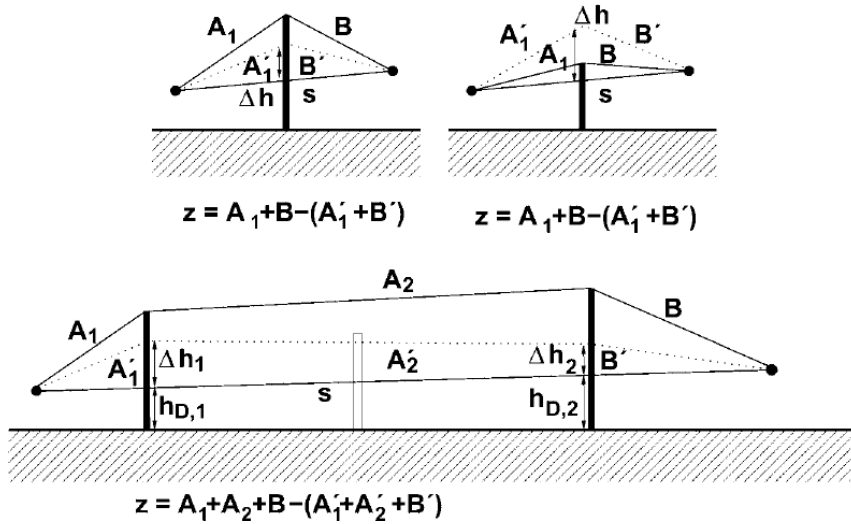


Figure 8.5: Sketch depicting the calculation of D_z [VBU06d].

The parameters $h_{D,i}$ and Δh_i in figure 8.5 are calculated as:

$$h_{D,i} = h_{GE} + \frac{a_i}{s_0} (h_{SI} - h_{GE}) \quad (8.9)$$

and

$$\Delta h_i = \frac{a_i \cdot b_i}{2 \cdot \gamma} \cdot \left(\frac{s}{s_0}\right)^2 \quad (8.10)$$

with

$$\gamma = \begin{cases} 1000 & \text{if } s \leq 125m \\ 8 \cdot s & \text{if } s > 125m \end{cases} \quad (8.11)$$

Δh_i raises the original piercing point $h_{D,i}$ of the direct connection between source and receiver and the screening objects and thus accounts for the parabolic flection of sound rays around edges.

Figure 8.6 depicts the difference in noise levels if screening is neglected in the calculation (a) and with screening taken into account (b).

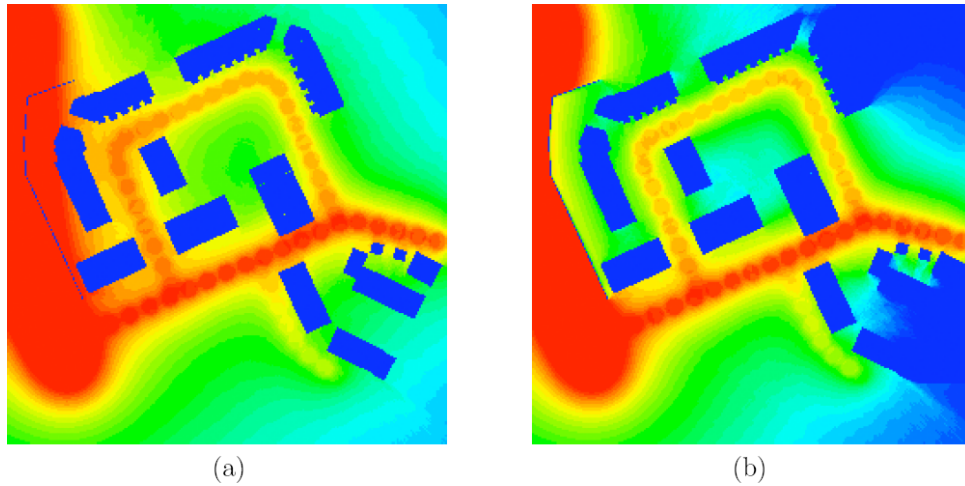


Figure 8.6: Impact of screening factor D_z . Same calculation scenario with $D_z = 0$ (a) and screening calculated according to equation 8.7.

8.1.6 Ground and meteorological damping D_{BM}

The parameter D_{BM} for ground and meteorological damping takes the difference in sound propagation for different heights above ground into account. D_{BM} is calculated as:

$$D_{BM} = 4,8 - (h_m/s) \cdot (34 + 600/s) \geq 0 \quad (8.12)$$

with the average distance h_m of s above ground

$$h_m = \frac{F}{s} \quad (8.13)$$

Here s is the path of the sound from source to receiver taking all obstacles into account, for example $A_1 + A_2 + B$ in figure 8.5. F is the resulting area between this path and the ground.

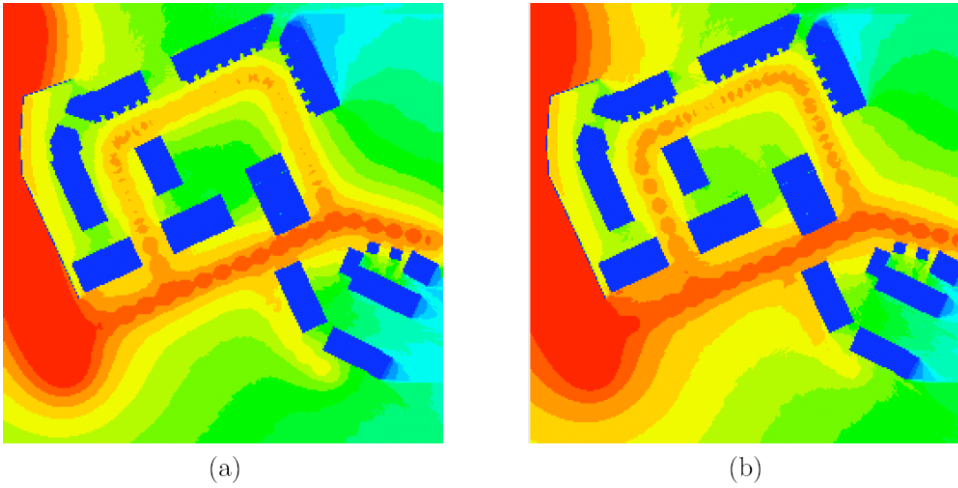


Figure 8.7: Impact of ground and meteorological damping D_{BM} . Calculated noise levels with (a) and without (b) taking D_{BM} into account.

Figure 8.7 shows the comparison of calculated noise levels when taking ground and meteorological damping into account (a) and neglecting it (b).

8.1.7 Time of day dependent sound propagation D_{met}

Additionally to the different emission levels $L_{m,E}$ for day, evening and night hours the parameter D_{met} takes the variable sound propagation conditions for different times of the day into account. During nighttimes the sound propagates better than during daytimes. D_{met} is calculated as:

$$D_{met} = \begin{cases} 0 & s_0 \leq 10 \cdot (h_{GE} + h_{GI}) \\ -C_0 \cdot [1 - 10 \cdot (h_{GE} + h_{GI})/s_0] & s_0 > 10 \cdot (h_{GE} + h_{GI}) \end{cases} \quad (8.14)$$

with h_{GE} and h_{GI} as height above ground for source (emission) and receiver (immission), respectively. s_0 is the distance of source and receiver in the x-y plane and C_0 the time of day dependent parameter as depicted in table 8.1.

daytime	C_0
day	$2.0dB(A)$
evening	$1.0dB(A)$
night	$0.0dB(A)$

Table 8.1: Values for parameter C_0 in equation 8.14

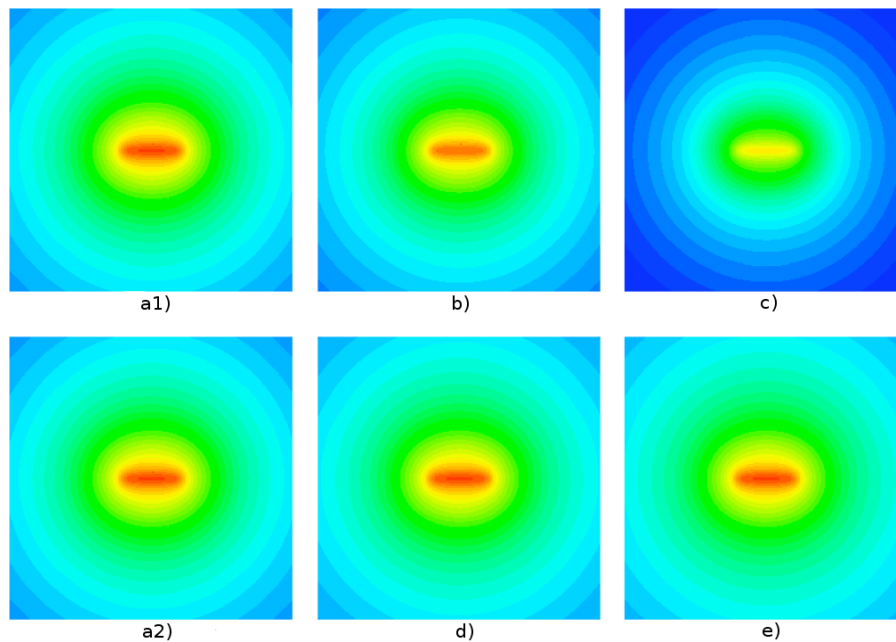


Figure 8.8: Impact of time of day on the sound propagation D_{met} .

Figure 8.8 depicts the calculated noise levels for different times of day and propagation conditions. The top row (a1-c) shows the noise propagation at day (a1), evening (b) and night (c) with corresponding values for D_{met} . Due to the decreased emission in the evening and night the resulting noise levels are lower than during the day despite the better sound propagation. In figure 8.8 (a2-e) the emission level is set to daytime but with propagation conditions for day (a2), evening (d) and night (e). The results have no practical relevance but depict the better propagation conditions in the evening and night resulting in higher noise levels.

8.1.8 First reflections

To account for reflected noise all sound sources are tested against the buildings or objects in the calculation area. If a possible reflector for a sound source is found and the reflector complies with equation 8.15, with h_R the height of the reflector and a_R the distance between source and reflector, an image source is generated.

$$h_R = 0,3 \cdot \sqrt{a_R} \quad (8.15)$$

The mirror sources are handled as normal noise sources with the following restrictions:

- the path between mirror source and receiver must intersect the reflector
- the emission level of the mirror source is $L_{m,E}$ decreased by D_E (table 8.2)
- the sound from the mirror source is not reflected again

reflector type	D_E in $dB(A)$
plain building facade or reflecting noise screen	-1
structured facade (i.e. balconies, etc.)	-2
absorbing noise screen	-4
highly absorbing noise screen	-8

Table 8.2: Correction factor D_E for mirror sources depending on the reflector type

Figure 8.9 depicts the same scenario with enabled (a) and disabled (b) mirror sources.

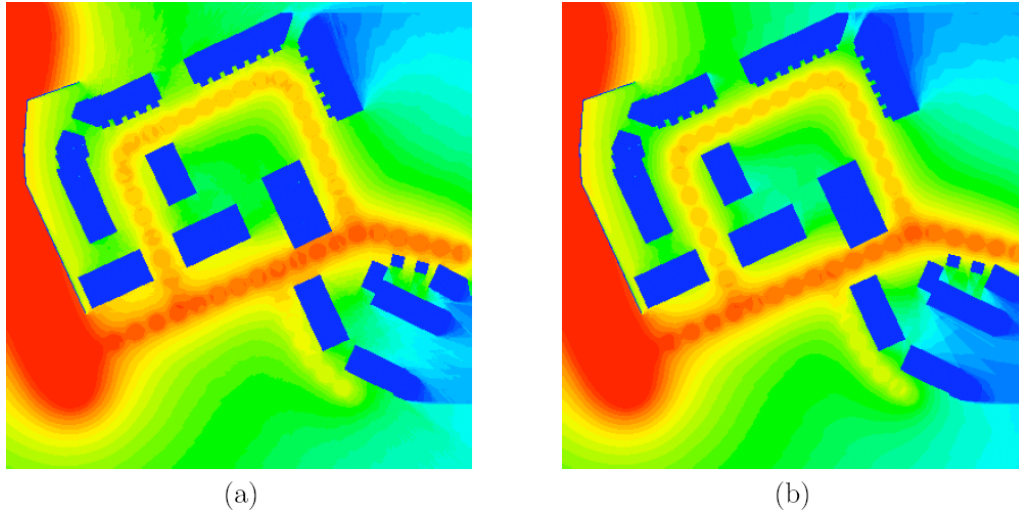


Figure 8.9: Impact of mirror sources. (a) enabled, (b) disabled

8.1.9 Multi-reflections D_{refl}

A sound source is only reflected once according to section 8.1.8. To account for multiple reflections, i.e. parallel buildings on both sides of a street, the average noise level of a sound source is increased. Therefore the parameter D_{refl} is calculated as follows:

$$D_{refl} = \begin{cases} 4 \cdot h_{Beb}/w \leq 3,2 & \text{if normal} \\ 2 \cdot h_{Beb}/w \leq 1,6 & \text{if absorbing} \\ 0 & \text{if highly absorbing} \end{cases} \quad (8.16)$$

with h_{Beb} the height of the parallel reflectors (buildings) and w the distance between them as depicted in figure 8.10.

A comparison of the calculated noise levels with (a) and without (b) taking D_{refl} into account is depicted in figure 8.11.

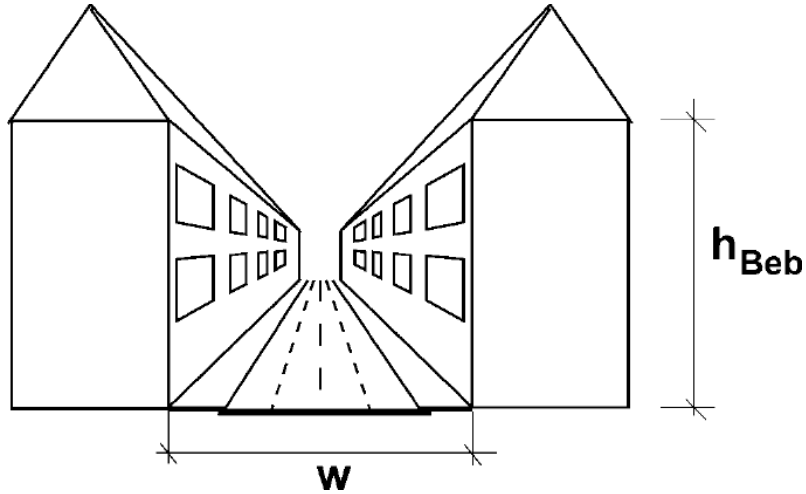


Figure 8.10: Depiction of parameters h_{Beb} and w in equation 8.16 [VBU06d].

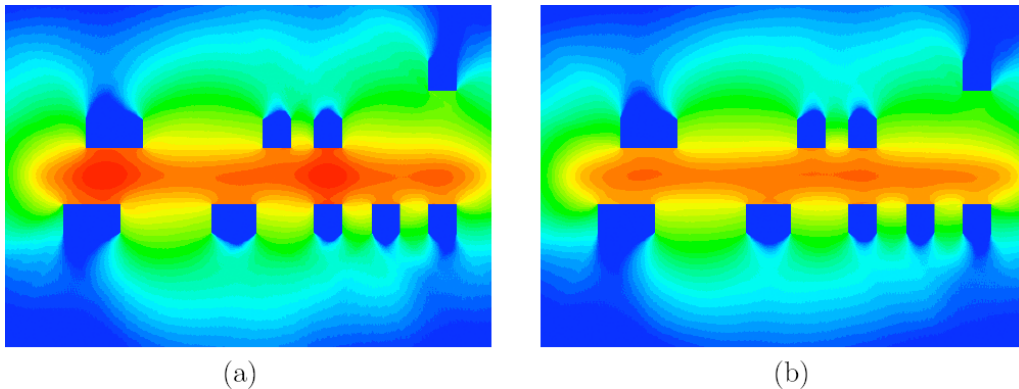


Figure 8.11: Impact of multi-reflections D_{refl} . (a) enabled and (b) disabled multi-reflections.

8.2 Implementation

The computation specification of the VBUS presented in detail in section 8.1 are implemented as a console based program in plain C++ to be as platform independent as possible. The only two prerequisites are libraries to provide POSIX multithreading and the Geospatial Data Abstraction Library (GDAL)¹ which should be both available for many operating systems.

The system uses a configuration file in which all settings for the input/output data and the actual noise calculation preferences are provided. This include paths to the

¹<http://www.gdal.org>

geodata files and settings like raster size, calculation height, number of threads to use etc. for the noise calculation as well as the output format and filenames for the calculated noise levels.

To be able to visualize the resulting noise levels independent of the visualization system in chapter 9 the system allows the results as Nearly Raw Raster Data (NRRD)². Unfortunately it is not possible to save multiple datasets, i.e. for indicators L_{den} and L_{night} , into one NRRD-file. Therefore an extended version of the NRRD-format has been implemented which is also used as input for the visualization system in chapter 9.

8.2.1 Input data

For the calculation according to the VBUS certain input data must be available to the algorithm to calculate correct noise levels.

The minimum required data are

- streets with additional attributes
- building geometries
- digital elevation model

The required attributes for the streets are needed to compute the correct parameters when calculating the average noises levels for the sound sources. These attributes are:

- speed limits for cars
- speed limits for trucks
- average daily traffic volume (DTV) in vehicles/24h
- longitudinal slope in %
- street surface type

²<http://teem.sourceforge.net/nrrd>

- street type (highway, federal highway, etc.)

Additional data, for example facade types of buildings, are optional but not necessary for the calculation. In most cases this information is not available and therefore the worst-case is assumed, i.e. in case of facade types plain facades or reflecting noise screens.

The current system allows the use of SHAPE files³ as input which is a common format in today's GIS tools for georeferenced spatial information. Additional information should be provided in the database (DBF) files belonging to the SHAPE files.

8.2.2 Verification Test-VBUS

Besides the computation methods for traffic noise in the VBUS, the 'Umweltbundesamt' (federal environmental agency) published the document 'Test cases for the verification of calculation tools using the VBUS' [BS06]. The document includes 14 scenarios with certified results and intermediate results to test different aspects of the implementation. The results are given as $dB(A)$ with two decimal places.

The current implementation passes all 14 test with a maximum deviation of 0.005 $dB(A)$ from the given noise levels and is thus verified to compute correct noise values based on the VBUS.

8.3 Extensions

With the system presented in the previous chapters it is possible to calculate noise maps according to the European directive 2002/49/EU [END02]. To get further insight into the noise propagation and noise exposure in areas not covered by the standard noise maps the system has been extended to calculate noise volumes (section 8.3.1).

The second extension, dynamic rendering (section 8.3.2), is a first step to enable interactive noise calculation for planning purposes.

³<http://www.esri.com>

8.3.1 Noise volumes

In order to visualize noise propagation in three dimensions it is necessary to compute noise levels not only at one distinct height above ground but also as noise volume. Therefore the system has been extended to allow the computation and output of three dimensional noise dataset. This feature can be enabled in the configuration file and needs the type of volume to compute and distance information for the layers as parameters.

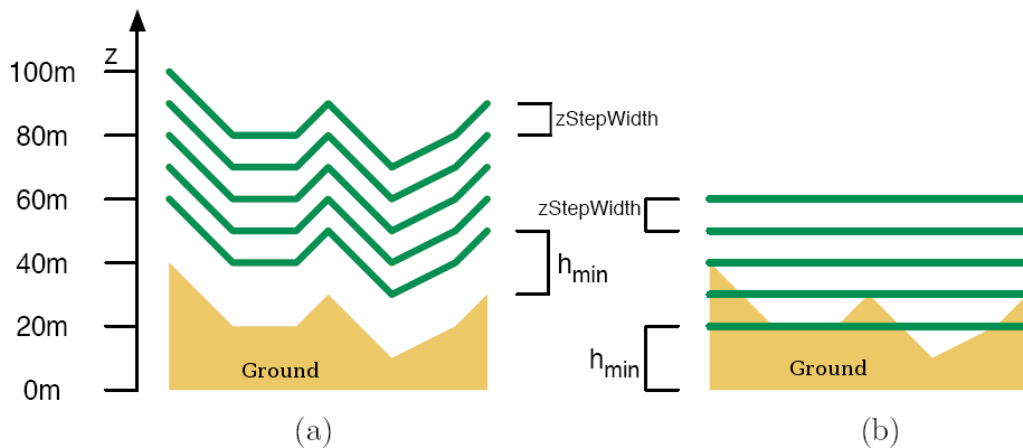


Figure 8.12: Different height options for multiple layers. (a) Height above ground (b) absolute height

It can be chosen from two different volume types. The first generates noise dataset of layers at a constant height above ground, like the standard noise maps. This can be used for the interactive visualization of noise maps at different heights, for example a noise map for the 5th story of an apartment building. The second volume type generates a noise dataset on a regular grid with layers at absolute heights. These datasets allow the visualization of noise with common volume visualization techniques to get a spatial insight into noise propagation and exposure. Figure 8.12 depicts the two options for the calculation of noise volumes.

The resulting three dimensional noise levels can be exported into the NRRD-format or the extended format used to store multiple dataset in one file as in the case of standard noise maps.

8.3.2 Dynamic rendering

When planning noise abatement measures, normally the calculation of noise maps is done for different preplanned scenarios, i.e. variants of noise screen size and position. This is mainly due to the computation time needed to calculate a complete noise map which is in no means interactive (depending on the size of the calculation area the computation takes tenth of minutes to hours). But for the planning process it is not essential to wait for the finished certified results. For example, in order to identify and reject a bad planning proposal it is sufficient to see the noise exposure due to the most important noise producer, i.e. main street. If the resulting noise levels are already above the threshold the proposed noise abatement measure can be rejected, because the incorporation of other noise sources can only increase the noise levels.

Therefore a dynamic and interactive calculation of noise levels can speed up the planning process by rejecting proposed measures at an early calculation speed. Another advantage of interactive noise level calculation is the possibility to change a proposed noise abatement measure, i.e. moving or modifying a noise screen, while calculating and visualizing the resulting noise exposures on the fly. This can lead to a huge speed up in the planning process by enabling the review and modification of proposed noise abatement measures in an interactive environment.

To enable the interactive dynamic noise level calculation the following extensions have been made to the original noise calculation system.

The first improvement is the incorporation of multithreading for the calculation of single noise layers. The number of threads can be adjusted to the available processors on the used computer. Therefor the calculation area is split into regions according to the number of processors and calculated independently. Figure 8.13 depicts the partitioning of a grid with 55×55 receiver points for a quad-core computer.

The next step is to change the order of computation for the grid points. The grid points are sorted into eight groups as depicted in figure 8.14. The noise levels are then computed in group order. To visualize the different stages of computation non calculated grid points are assigned the noise levels of the nearest calculated points.

The result is a level of detail computation. The results for the different calculation stages are shown in figure 8.15 for a noise grid with dimension 128×128 .

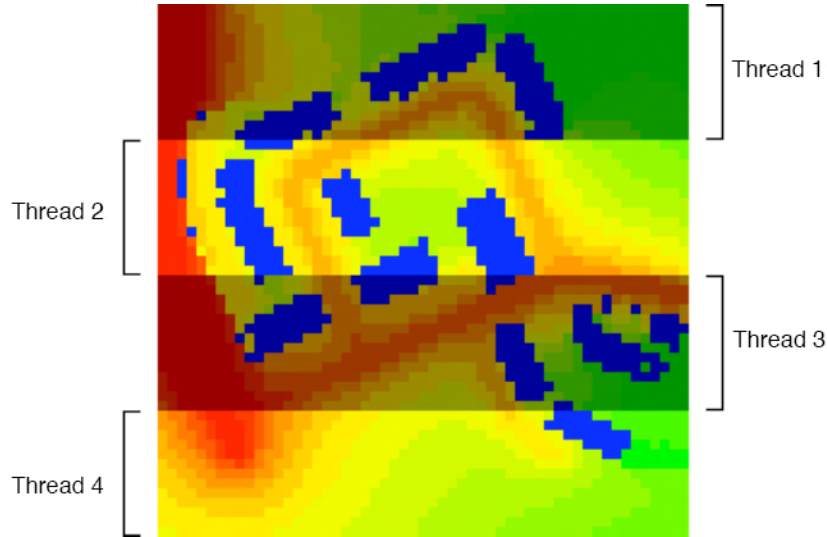


Figure 8.13: Partitioning of a receiver grid with dimensions 55×55 on a quad-core computer.

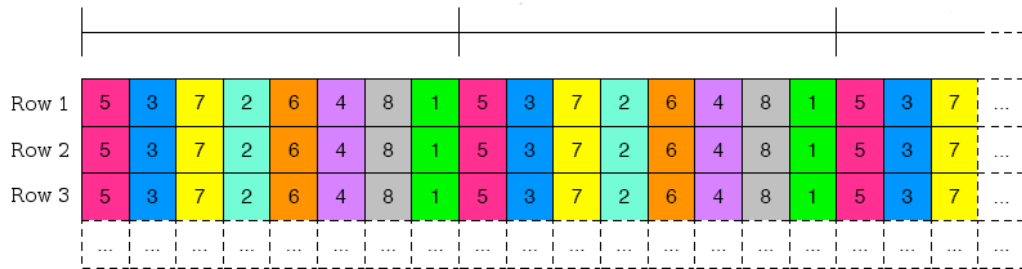


Figure 8.14: Order of computation for the level of detail noise calculation.

To enable the assignment of priorities for different noise sources the calculation has been split up on a per street basis. Each street is rendered separately and the noise levels are then combined into the final complete noise map. Figure 8.16 depicts the results for the single streets (top row) and the noise levels after combining the results (bottom)

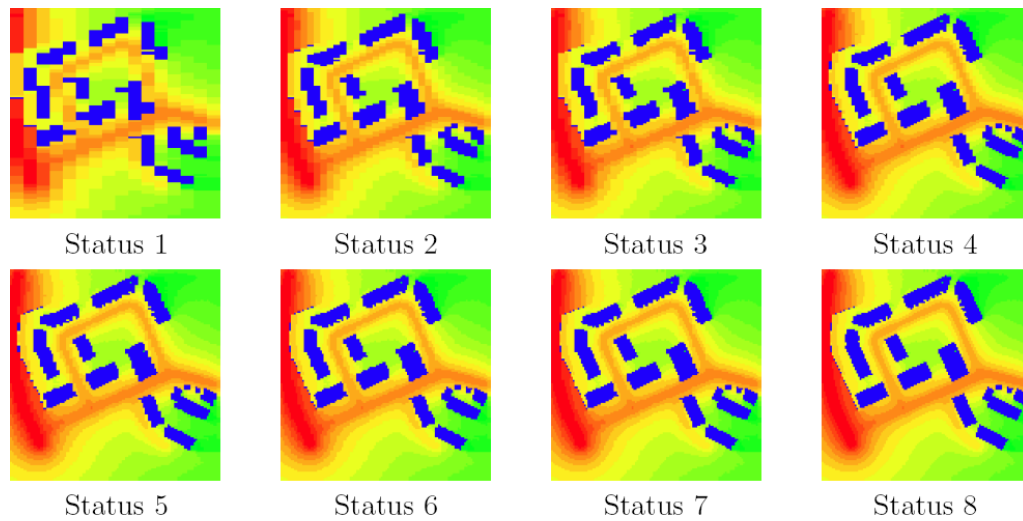


Figure 8.15: The different stages (level of detail) for a receiver grid with dimensions 128×128 .

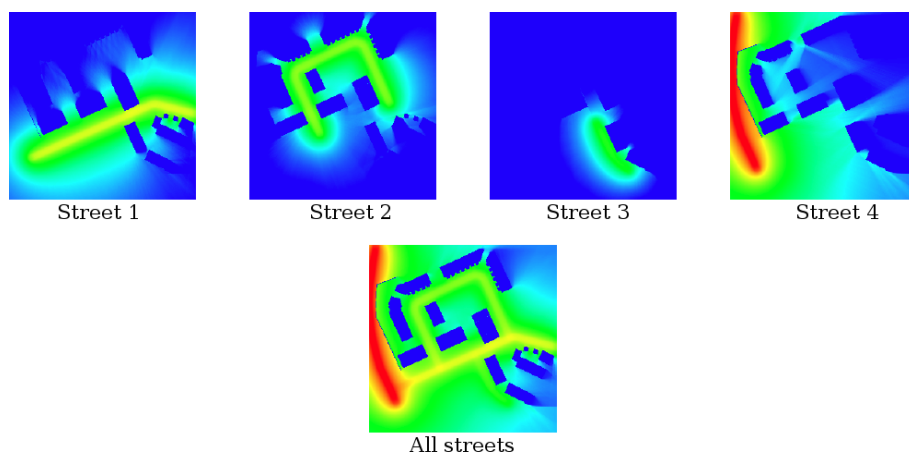


Figure 8.16: Noise levels for the independently calculated streets (top row) and the resulting levels after combining them.

With the option to render single streets independently it is now possible to assign priorities to different noise sources. For example, the street with the highest average emission level gets a priority of 100 and the one with the lowest level 0. In addition to that the calculation areas are also split into the eight groups mentioned before. To ensure the correct order of computation the priority of group 1 is increased by 8, group 2 by 7, and so on. An exemplary priority list based on this assignment is shown in figure 8.18.

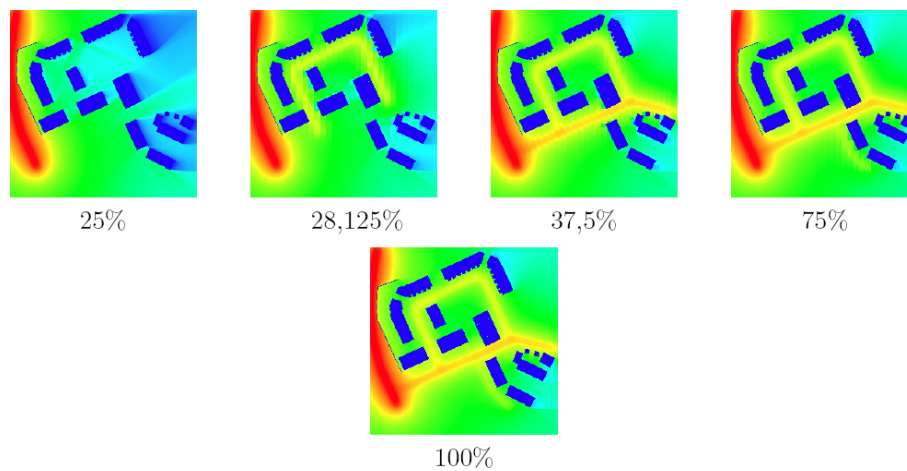


Figure 8.17: Intermediate results of the calculation for the priority list in figure 8.18.

The intermediate results of the calculation for the priority list in figure 8.18 are shown in figure 8.17.

The aforementioned assignment of priorities is only a simple example which can be extended to the needs of the user. For example, when interactively changing the geometry/position of streets or buildings/obstacles it is desirable to first recalculate the areas which are affected most by the change. Therefore the priorities should be adjusted depending on the distance to the location of the change in combination to the emitted noise levels of the streets.

Reidernr.	Straßenr.	Gruppe	Priorität
1	4	1	108
2	4	2	107
3	4	3	106
4	4	4	105
5	4	5	104
6	4	6	103
7	4	7	102
8	4	8	101
9	2	1	61,44811
10	2	2	60,44811
11	2	3	59,44811
12	1	1	58,93851
13	2	4	58,44811
14	1	2	57,93851
15	2	5	57,44811
16	1	3	56,93851
17	2	6	56,44811
18	1	4	55,93851
19	2	7	55,44811
20	1	5	54,93851
21	2	8	54,44811
22	1	6	53,93851
23	1	7	52,93851
24	1	8	51,93851
25	3	1	8
26	3	2	7
27	3	3	6
28	3	4	5
29	3	5	4
30	3	6	3
31	3	7	2
32	3	8	1

Figure 8.18: Priority list for the order of computation based on the average noise level of a street.

Chapter 9

Visualization

As presented in chapter 7 the visualization techniques used by standard noise prediction software are mostly the display of two dimensional noise maps. In addition to that some commercial tools allow the use of the noise map as ground texture within a three dimensional city model or calculated noise levels as facade textures of buildings. The same holds, with some exceptions, for the discussed research projects.

Due to the shortcomings of two dimensional maps, e.g. readability by laymen, missing interactivity, etc., a three dimensional visualization framework was implemented. This chapter presents the visualization framework that was developed to display noise maps in an interactive three dimensional environment [MWSH08]. The framework incorporates a three dimensional city and digital elevation model, two and three dimensional noise data as well as additional information related to buildings and streets which can be explored interactively. Further information about the implementation can be found in [Wac08].

In section 9.1 an overview of the framework is given. The implemented visualization techniques are discussed in section 9.2 and results are presented in section 9.3

9.1 General overview

The framework is intended for the interactive visualization of 3D traffic noise. A schematic overview of the system is given in figure 9.1. The system is based on

the Coin3D visualization toolkit¹ with the volume extension SimVoleon² and the Geospatial Data Abstraction Library³ for the handling of shapefiles.

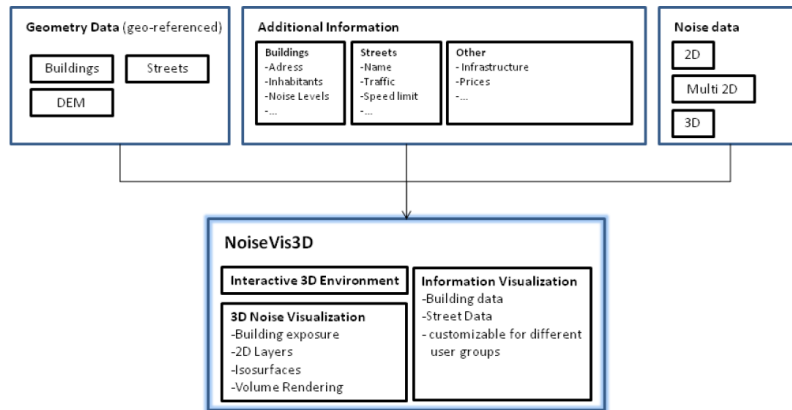


Figure 9.1: Schematic overview of the visualization framework.

The noise data is displayed in a three dimensional environment which consists of a digital elevation model (DEM), streets and a 3D city model. NoiseVis3D uses geo-referenced SHAPE files⁴, which is the common format for the most GIS applications, for the DEM, streets and the city model. In addition to the geometry (city model / streets) there exist various building (e.g.. address, inhabitants, and stories) and street (e.g. daily traffic, speed limits and percentage of trucks) information. These can be easily extended with arbitrary data to incorporate in the visualization for different user groups.

The noise data itself can be a standard 2D noise map or a 3D data set either as multiple 2D noise maps with distinct heights above ground (like the standard noise map) or a 3D volume grid. Supported file format for the 2D noise map is an ASCII raster file, e.g. the CadnaA output format. The different 3D data sets can be imported from NRRD⁵ (NearlyRawRasterData) or extended format calculated with the system presented in 8.

The framework consists of a viewer and settings windows (figure 9.3). The city model is displayed in the viewer window (figure 9.2). A color key is placed in the

¹<http://www.coin3d.org>

²<http://www.coin3d.org/lib/simvoleon>

³<http://www.gdal.org>

⁴<http://www.esri.com>

⁵<http://teem.sourceforge.net/nrrd>



Figure 9.2: Three dimensional city model and digital elevation model.

lower right corner of the screen to depict the noise levels associated with the colors depending on the chosen coloring scheme (figure 9.3). The mouse is used to navigate freely within the 3D environment and interact with the city model. This includes zooming, panning and rotating.

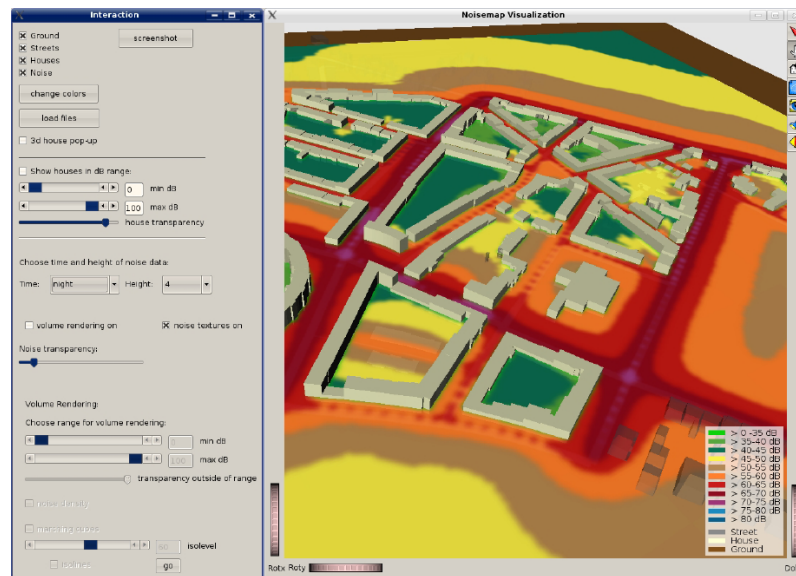


Figure 9.3: Settings and viewer window.

The settings window allows the user to adjust the visualization options. For all data sets the noise indicators L_{day} , $L_{evening}$, L_{night} or L_{den} can be interactively chosen. For multilayer 2D noise maps the height to display can be set. If instead of multiple heights different scenarios have been loaded the user can switch between the dif-

ferent data sets. The controls for noise transparency, noise thresholds and general environment options are also accessible from the settings window.

9.2 Noise visualization

This section covers the different kinds of visualization techniques which are implemented into the framework. First the visualization of additional information is presented in section 9.2.1 followed by the visualization of noise exposure for single buildings (section 9.2.2). Sections 9.2.3 and 9.2.4 cover the visualization of two and three dimensional noise data sets.

9.2.1 Information visualization

Additional information for buildings and streets is displayed in the top right corner of the screen if an object is selected (figure 9.4). This information includes for example name, DTV (vehicles per day), vmax (speed limit), etc., for streets and address, number of inhabitants, noise levels (day/night), etc., for the buildings and can be easily extended if other data like apartment rents, distances to points of interest, etc., is available.

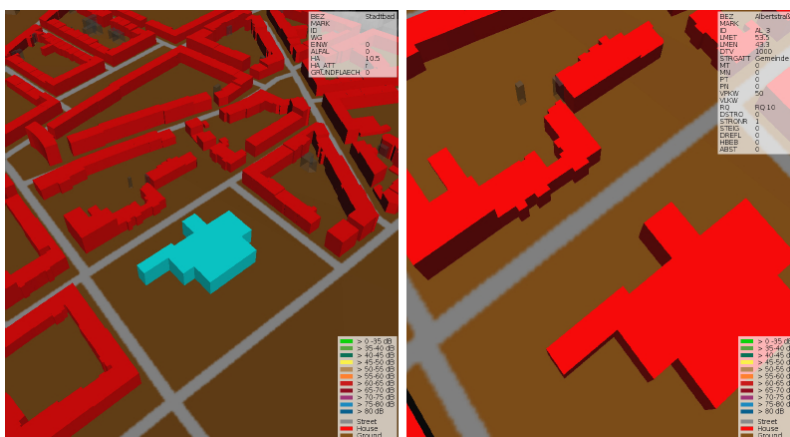


Figure 9.4: Display of additional information for (a) buildings and (b) streets.

Which data is displayed can be easily configured to only show important/interesting information for a certain user group or the splitting into standard and extended

information to reduce information overflow (figure 9.5). This makes the framework not only a tool which can be used by urban planners, but allows the adaption to other tasks, for example presenting planning proposals to a wider range of people which can include decision makers, local residents or investors.

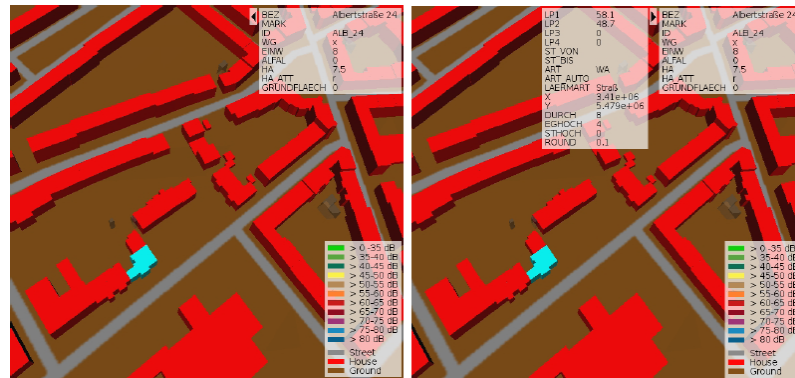


Figure 9.5: Display of (a) standard and (b) extended information for a building.

9.2.2 Building exposure

If calculated noise levels for each building are provided, the buildings can be colored according to their respective noise exposures as depicted in figure 9.6.

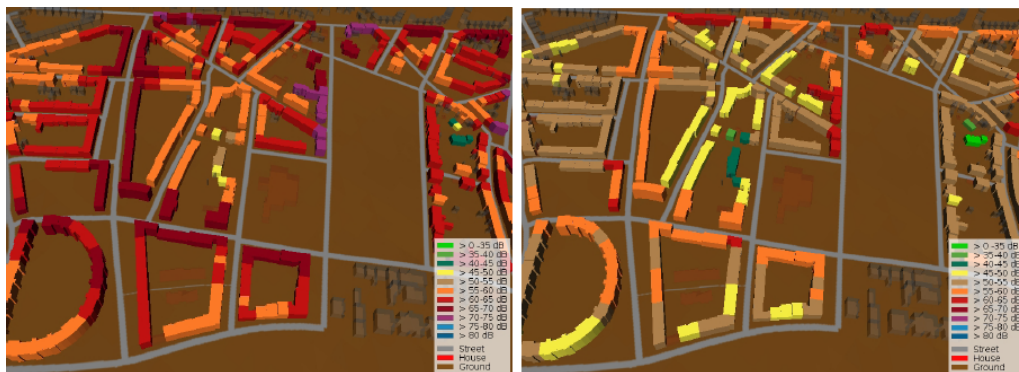


Figure 9.6: Buildings colored according to their noise exposure. Left: daytime L_{day} , right: nighttime L_{night} .

The user can also specify noise thresholds to display only buildings with a certain exposure, i.e. buildings with noise levels above 65dB. Buildings outside the chosen interval are displayed transparent to preserve the overall context (figure 9.7). This

allows a fast and easy identification of areas where noise abatement measures need to be installed.

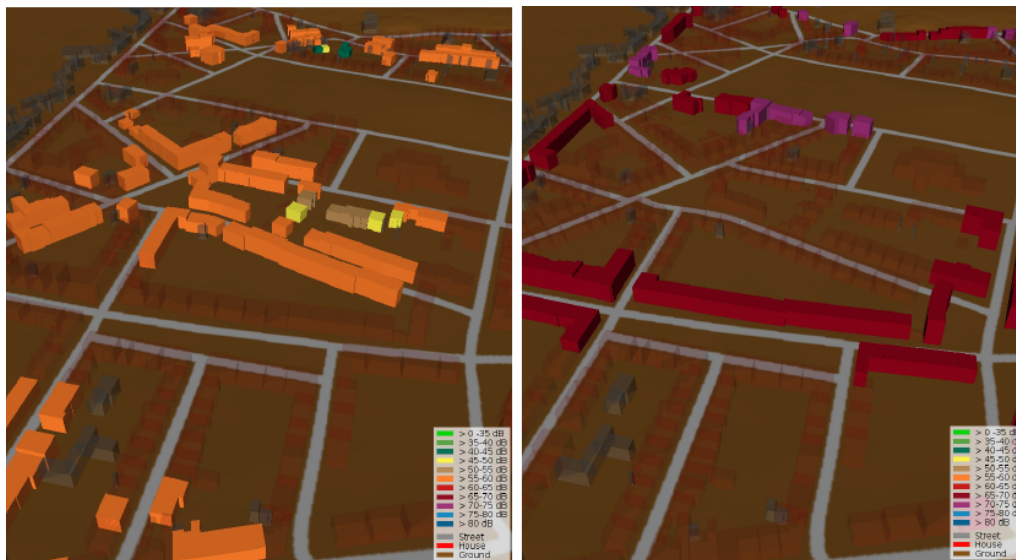


Figure 9.7: Visualization of buildings according to thresholds. Left: Noise level below 60 dB, right: above 65 dB for daytime noise L_{day}

9.2.3 Noise maps

The Visualization of the 2D noise maps takes place at the correct height above ground, so that it eliminates the possibility of misinterpretation caused by the projection to the digital elevation model.

9.2.3.1 2D maps

The standard transfer function for noise, using the same color for 5dB intervals, is used for the visualization of the noise layer. For the display of different aspects the user can also generate arbitrary transfer functions (e.g. areas above 65dB in red) or use other standard color schemes (i.e. blue-red, green-red or rainbow gradients). Figure 9.8 shows two different transfer functions used on the same data set.

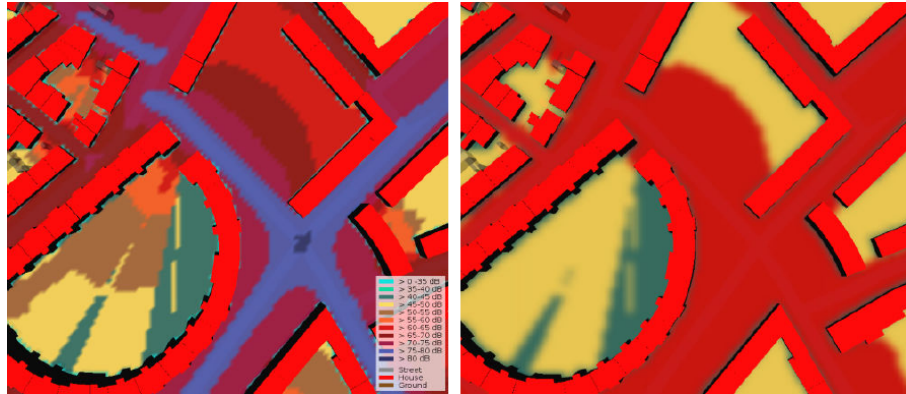


Figure 9.8: Visualization of 2D noise maps 4 meters above ground using different coloring schemes. Left: Standard colors for 5dB ranges. Right: Using only three different colors to depict quiet and noisy areas. Noise below 45dB = green, between 45 and 65 dB = yellow, above 65dB = red.

9.2.3.2 Multilayer 2D maps

If multilayer 2D noise maps are used, e.g. a set of noise maps ranging from 1m to 15m above ground with spacing of 1m, the user can interactively browse through the different noise layers which are displayed at their respective height above ground. This allows the inspection of the noise situation for example on the balcony of a fourth floor apartment instead of the second floor with standard noise maps. The coloring schemes and possibilities are the same as for the single 2D noise maps.

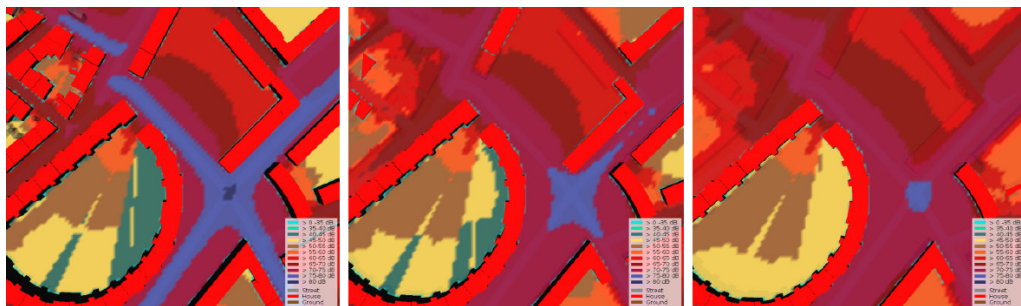


Figure 9.9: Visualization of multilayer 2D noise maps using the standard coloring scheme with colors for 5dB intervals. Left to right: Noise indicator L_{den} in 4, 8 and 12 m above ground respectively.

Browsing through the different heights also gives a first insight in the spatial propagation and interaction of the sound with the environment. An example is given in figure 9.9.

9.2.4 Noise volumes

3D data sets resulting from the noise calculation in chapter 8 are given on a regular grid instead of distinct heights above the actual ground. Therefore standard visualization techniques are easily applied to the noise data. The framework incorporates volume rendering and isosurface extraction. For both techniques the transfer functions are customizable like in the 2D case. In addition the transparency can be adjusted for different values to fit the users needs.

9.2.4.1 Isosurfaces

For isosurfaces the framework allows two options. The first is to choose a specific noise value which is then displayed in the city model. This allows, as in the volume rendering case, the identification of areas which are exposed to a certain degree of noise. The second option is to compute isosurfaces for every 5dB which is directly related to the isobands or lines in the 2D maps transferred into three dimensions. The surfaces are colored according to the chosen transfer function. Figure 9.10 gives an example for the 5dB isosurfaces.

9.2.4.2 Volume rendering

The volume rendering can be interactively influenced by setting different thresholds for the noise displayed. The user can set minimum and maximum values which should be visualized in the rendering interactively. With this thresholding it is possible to display only certain areas of interest in the data set. For example only the spatial regions with a noise level above 65dB can be chosen to detect regions where noise mitigation measures are most urgent or the maximum value can be set to 45dB to identify quiet areas. Figure 9.11 depicts a volume rendering colored according to the standard noise map coloring.



Figure 9.10: Visualization of isosurfaces every 5 dB analog to the isobands in standard noise maps.

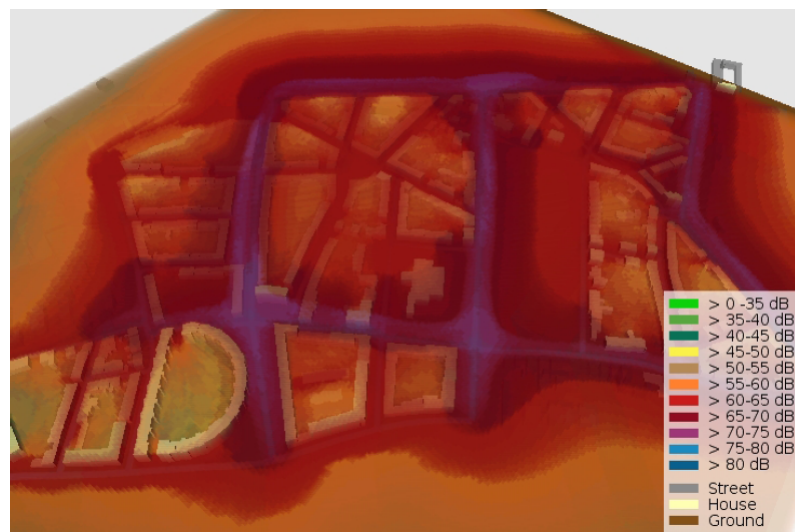


Figure 9.11: Volume rendering of the three dimensional data set colored according to the standard scheme.

To enhance certain aspects of noise, for example to illustrate regions with high noise exposure the transfer functions for the volume rendering can be adjusted to the users need. Two different transfer functions for the same data set are shown in figure 9.12. The same holds for isosurfaces. Figure 9.13 depicts the isosurfaces for 71 dB and 61 dB respectively.

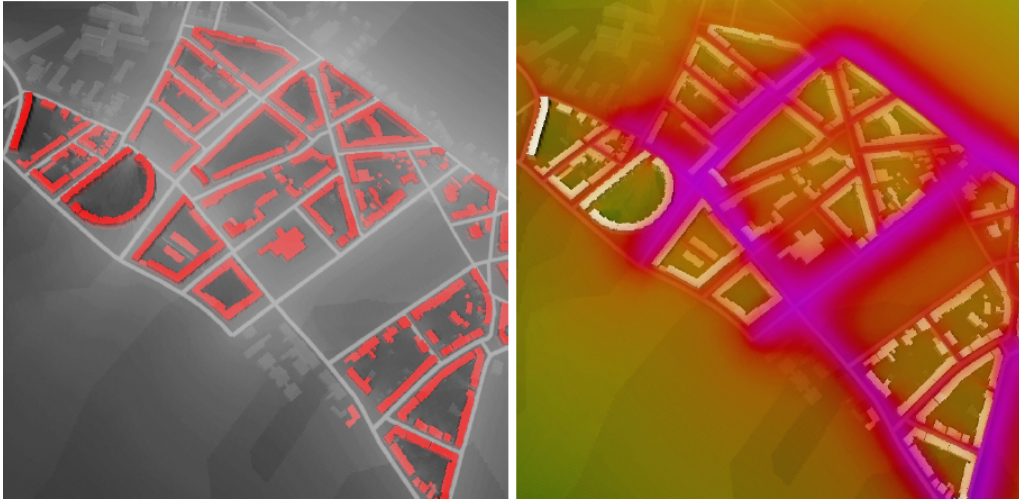


Figure 9.12: Different transfer functions for the same data set to enhance certain aspects of noise exposure.

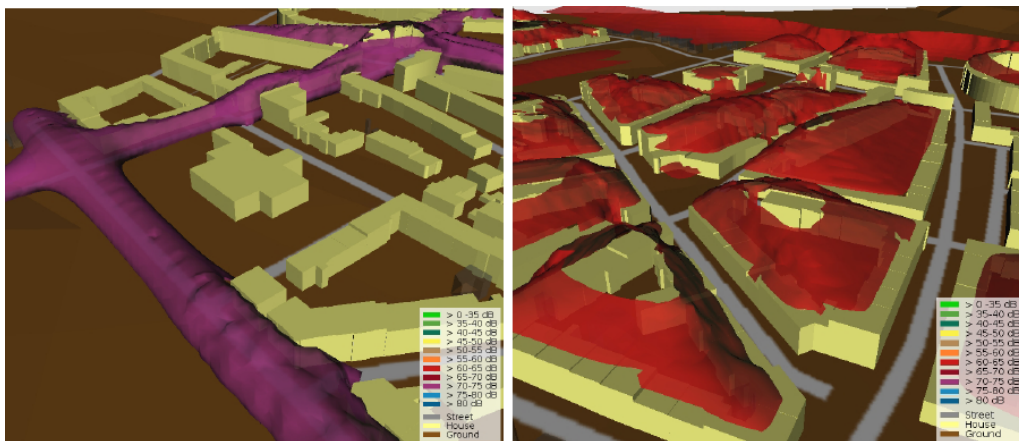


Figure 9.13: Different isosurfaces for the same data set to enhance certain aspects of noise exposure. Left 71 dB, right 61 dB for L_{day}

9.3 Results

If the underlying noise data is also calculated for single streets the user can view the noise emanating from these and compare it to the overall noise levels. This enables the easy identification of sources causing high noise levels and can speed up the development of noise abatement measures. Examples of the implemented visualization techniques are given in figures 9.14 to 9.16.

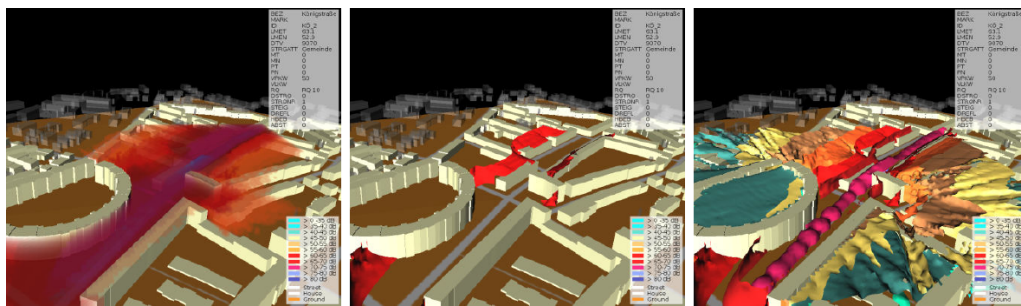


Figure 9.14: Volume rendering and isosurfaces for a 3D data set of a single street giving insight into the influence of this street to the overall noise. Left: Volume rendering of noise above 55dB Middle: Isosurface for 55 dB Right: Isosurfaces for every 5 dB. All images for noise indicator L_{den} .

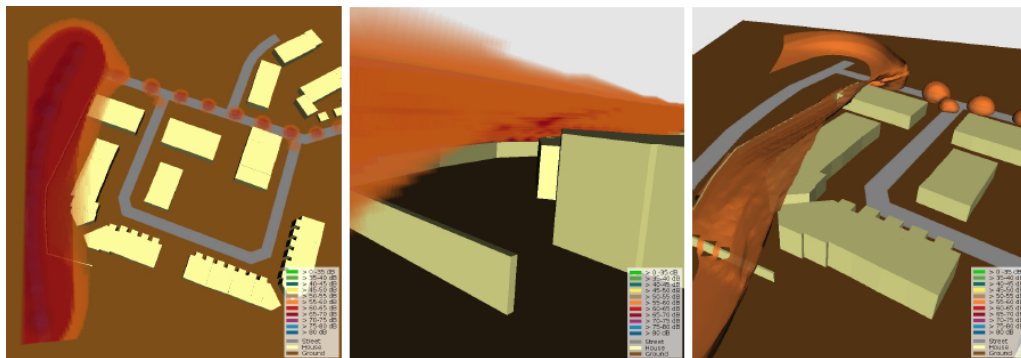


Figure 9.15: Noise deflection at a noise screen. Left and middle: Volume rendering of noise above 58 dB from different perspectives. Right: Isosurface for 58 dB. Noise indicator L_{day}



Figure 9.16: Visualization of noise emitted from a single street as volume rendering, isosurfaces and 2D noise map.

Chapter 10

Conclusion and future work

In this part of the thesis, concerned with environmental noise, new approaches for the simulation and visualization of traffic noise were presented. For the simulation of noise levels the computation instructions regulated by national law were discussed, and the effects of the different parameters on the resulting noise levels were analysed in detail. An extension to calculate noise volumes in addition to the requested noise layers has been presented. This extension allowed the development of new visualization approaches for traffic noise. Furthermore acceleration techniques to allow the interactive calculation and visualization of noise levels were introduced. These techniques enable the preview of intermediate calculation results and the manipulation of noise related objects in the calculation scenario interactively.

The presented simulation techniques were used to develop new approaches for the visualization of traffic noise. An interactive framework using this data was presented which integrates the simulated noise data, layers and volumes, into a three dimensional environment incorporating the georeferenced data, city and digital elevation model, used for the simulation. Furthermore additional information to enhance the comprehensibility of the data or to present other aspects interesting for different user groups can be integrated into the visualization. To the noise data itself visualization techniques like isosurfaces or volume rendering were applied to allow the easy identification of noise polluted areas and assess noise abatement measures not only at a given height but in three dimensional space. The presented approaches eases the understanding of noise effects for laymen and overcomes problems like lo-

calization or orientation inherent in two dimensional maps and give an insight into the three dimensional propagation and effects of traffic noise which is not possible with standard noise maps.

There are still challenging tasks left in the field of simulation and visualization of environmental sound. The presented enhancements to the simulation of noise immissions were only the first step to enable interactive noise calculations. A great opportunity would be the integration of these methods into a planning system to facilitate the interactive development of noise abatement measures or new building areas which would speed up the whole planning process. Equally interesting is the further advancement of the visualization of environmental noise. Additional techniques could be developed, on the one hand for the noise data itself, on the other hand for the additional information, which would further improve the comprehensibility of noise pollution and its causes, as well as allowing the use of the system for other purposes.

Appendix A

Room Acoustics

A.1 Wave Equation

In the field of the wave-based room acoustics the main intention is the solution of the wave equation A.1. Assuming a periodical behaviour of the pressure (harmonic wave) the wave equation then reads [Kut00]:

$$\Delta p + k^2 p = 0 \tag{A.1}$$

where $k = \frac{\omega}{c}$ is the wave number, with the angular frequency $\omega = 2\pi f$, and Δ is the Laplacian operator. This equation is known as the *Helmholtz equation*. Locally reacting room surfaces (surfaces with impedances independent on the incident sound [Kut00]) imply the following boundary condition:

$$\zeta \frac{\partial p}{\partial n} + ikp \tag{A.2}$$

where ζ is the specific impedance of the surface, and $\frac{\partial}{\partial n}$ denotes the partial differentiation in the direction of the surface normal n . Given the boundary condition the wave equation has non-zero solutions only for particular values k_n of k , the *eigenvalues* (see [Kut00]). Each *eigenvalue* k_n is assigned to a solution, the *eigenfunction* $p_n(r), r \in \mathbb{R}^3$, which is a three dimensional standing wave, a so-called *normal mode* or *eigenmode* of the room.

A.2 Room acoustic parameters

In room acoustics numerous studies have been done in order to measure the subjective assessment criteria of acoustical behavior of a room with objective characterization quantities [Rei68, Ber04, Thi53, LB61, Yam72, Kür69]. Some of these metrics, which can be derived from the measured or simulated room impulse response, are incorporated into the ISO 3382 norm [ISO97]. In the following several objective metrics are discussed. More criteria can be found in [FKS84].

Sound strength G

The *sound strength* G describes the perceived loudness of a sound source inside a room. G is defined as the energy covered by the room impulse response:

$$G = 10 \lg \frac{\int_0^\infty p^2(t) dt}{\int_0^\infty p_{10}^2(t) dt} \quad (\text{A.3})$$

where $p(t)$ is the room impulse response at a given listener position and $p_{10}(t)$ is the impulse response at a distance of 10 meters from the source in free field.

Early and late sound energy relation

The following parameters base on the experiences that the early arrived sound (direct from the source as well as reflected wave fronts) enhances the auditory event. It facilitates e.g. the intelligibility of speech. The time limit lies approximately between 50ms and 100ms [Kut00]. Mostly, the ratio between the energy of the early sound ("useful" energy)

$$E_e = \int_0^{t_l} p^2(t) dt \quad (\text{A.4})$$

and the residual energy ("disturbing" energy)

$$E_r = \int_{t_l}^\infty p^2(t) dt \quad (\text{A.5})$$

is build with limit time t_l .

Thiele [Thi53] assigned the time limit of useful energy t_l to 50ms and defined the *definition* (original *Deutlichkeit*) as:

$$D_{50} = \frac{\int_0^{50ms} p^2(t) dt}{\int_0^{\infty} p^2(t) dt} \quad (\text{A.6})$$

Definition is primary a metric for measuring the intelligibility of speech inside the room, but it can be applied to determine the quality of the recognizability of music instruments. A value of 0.5 denotes a 90 percent syllable intelligibility [MM04].

Ahnert [FKS84] proposed a logarithmic metric for the definition of the *definition index* (original *Deutlichkeitsmaß*) which is the tenfold of the base 10 logarithm of the ratio between early and residual energy with $t_l = 50$ ms:

$$C_{50} = 10 \lg \left(\frac{D_{50}}{1 - D_{50}} \right) = 10 \lg \left(\frac{\int_0^{50ms} p^2(t) dt}{\int_{50ms}^{\infty} p^2(t) dt} \right) \quad (\text{A.7})$$

$C_{50} > 0$ dB indicates good speech intelligibility [FKS84].

Beranek and Schulz [BS65] used the reciprocal term of the definition to classify different concert halls in North America, the ratio of reverberant to early energy:

$$R = 10 \lg \left(\frac{\int_{50ms}^{\infty} p^2(t) dt}{\int_0^{50ms} p^2(t) dt} \right) = -C_{50} \quad (\text{A.8})$$

If R is too high the sound is muddy, though full and well-blended. If R is small, the sound is clear and well-defined, but dry. Good values are in the range between 3 dB and 8 dB [FKS84]. Reichardt et. al. [RAAS74] have detected that the limit time t_l can (or should) be determined higher than that for speech. Therefore they set $t_l = 80ms$ and defined the *clarity index* (original *Klarheitsmaß*) to characterize the transparency of music presentations:

$$C_{80} = 10 \lg \left(\frac{\int_0^{80ms} p^2(t) dt}{\int_{80ms}^{\infty} p^2(t) dt} \right) \quad (\text{A.9})$$

Convenient values of C_{80} depend on the music style. For baroque music, Mozart for example, values of $C_{80} = 0$ dB may be acceptable, whereas music of romantic period (Tchaikovsky) may require a clarity index between -3 dB and 0 dB [RAAS74].

The so far described metrics assume a strict limiting value where the late arriving sound has a negative effect to speech or music. A continuous shift of a strong reflection beyond this limit will cause a jump in the value of these criteria, which is not natural. Therefore, Lochner and Burger [LB58, LB61] defined a metric where the early energy is weighted by a function $a(t)$ depending on the delay time (and also the relative echo level). This function decreases gradually from 1 at the starting time (arrival of direct sound) to 0 at $t_l = 95$ ms. This quantity was named the *signal-to-noise ratio* by the authors and is calculated as follows:

$$SNR = \frac{\int_0^{95ms} p^2(t)a^2(t)dt}{\int_{95ms}^{\infty} p^2(t)dt} \quad (\text{A.10})$$

The running time limit is also used for the next criterion, the *center time* (original *Schwerpunktszeit*), proposed by Kürer [Kür69]:

$$t_s = \frac{\int_0^{\infty} tp^2(t)dt}{\int_0^{\infty} p^2(t)dt} \quad (\text{A.11})$$

Low values of t_s indicate high intelligibility of speech or high transparency of music [MM04]. Speech intelligibility can also be characterized by the *speech transmission index* (STI), or the simplified version the *rapid speech transmission index* (RASTI) proposed by Houtgast and Steeneken [HS73, HS84]. STI and RASTI can be calculated by use of the modulation transfer function (see [Sch81]) which, when white noise is used as a source signal, can be derived from the impulse response [MM04]. The interested reader is referred to the original work of the authors for more details concerning this metric and the calculation algorithm.

Bibliography

- [AB79] J.B. Allen and A. Berkeley. Image method for efficiently simulating small-room acoustics. *J. Acoust. So. Amer.*, 65(4):943–950, Apr. 1979.
- [AFST04] F. Antonacci, M. Foco, A. Sarti, and S. Tubaro. Real time modeling of acoustic propagation in complex environments. In *Proceedings of the 12th European Signal Processing Conference (EUSIPCO '04)*, pages 1773–1776, Vienna, Austria, September 2004.
- [Ama84] J. Amanatides. Ray tracing with cones. *Computer Graphics*, 18(3):129–135, July 1984.
- [AS01] A.C. Antoulas and D.C. Sorensen. Approximation of large-scale dynamical systems: An overview. Technical report, Rice University, 2001.
- [Bab02] W. Babisch. The noise/stress concept, risk assessment and research needs. *Noise Health*, 4(16):1–11, 2002.
- [BDM⁺05] M. Bertram, E. Deines, J. Mohring, J. Jegorovs, and H. Hagen. Phonon tracing for auralization and visualization of sound. In *IEEE Visualization 2005*, pages 151–158, Minneapolis, MN, USA, October 23–28 2005.
- [Ber04] L.L. Beranek. *Concert halls and opera houses : music, acoustics, and architecture*. Springer, New York, 2004. 2. ed., rev. ed.
- [BLSG99] B. Berglund, T. Lindvall, D. Schwela, and K.T. Goh. World health organization: Guidelines for community noise. *World Health Organization*, 1999.
- [BMD⁺08] J. Bellmann, F. Michel, E. Deines, M. Hering-Bertram, J. Mohring, and H. Hagen. Sound tracing: Rendering listener specific acoustic room properties. In *Proceedings of EuroVis 2008*, Eindhoven, Netherlands, May 2008.
- [Bor84] J. Borish. Extension of the image model to arbitrary polyhedra. *Journal of the Acoustical Society of America*, 75(6):1827–1836, 1984.

- [Bot95] D. Botteldooren. Finite-difference time-domain simulation of low-frequency room acoustic problems. *Journal of the Acoustical Society of America*, 98(6):3302–3308, December 1995.
- [Bra03] D. Braess. *Finite Elemente: Theorie, schnelle Löser und Anwendungen in der Elastizitätstheorie*. Springer, Berlin, 2003. 3., korrigierte und ergänzte Auflage.
- [Brü01] Brüel&Kjaer. Environmental noise, 2001.
- [BS65] L.L. Beranek and Th.J. Schultz. Some recent experiences in the design and testing of concert halls with suspended panel arrays. *Acustica*, 15:307–316, 1965.
- [BS06] W. Bartolomaeus and L. Schade. Testaufgaben für die überprüfung von rechenprogrammen nach der 'vorläufigen berechnungsmethode für den umgebungslärm an straßen (vbus)'. *Umweltbundesamt*, 2006.
- [CM78] L. Cremer and H.A. Müller. *Die wissenschaftlichen Grundlagen der Raumakustik, Band I*. S. Hirzel Verlag Stuttgart, 1978. 2. völlig neubearbeitete Auflage.
- [CR05] C. L. Christensen and J. H. Rindel. A new scattering method that combines roughness and diffraction effects. In *Proceedings of Forum Acusticum*, pages 1173–1179, Budapest, Hungary, August 29 – September 2 2005.
- [CSF05] P. T. Calamia, U. P. Svensson, and T. A. Funkhouser. Integration of edge-diffraction calculations and geometrical-acoustics modeling. In *Proceedings of Forum Acusticum*, Budapest, Hungary, August 29 – September 2 2005.
- [Dal96] B.-I. Dalenbäck. Room acoustic prediction based on a unified treatment of diffuse and specular reflection. *Journal of the Acoustical Society of America*, 100(2):899–909, 1996.
- [DBM⁺06] E. Deines, M. Bertram, J. Mohring, J. Jegorovs, F. Michel, H. Hagen, and G. M. Nielson. Comparative visualization for wave-based and geometric acoustics. *IEEE Transactions on Visualization and Computer Graphics*, 12(5):1173–1180, Sep. 2006.
- [Dei07] E. Deines. *Acoustic Simulation and Visualization Algorithms*. PhD thesis, University of Kaiserslautern, 2007.

- [DIN91] Deutsches Institut für Normung e.V. DIN. Schallschutz im städtebau "Lärmkarten - kartenmäßige darstellung von schallimmissionen". *DIN EN ISO 18005-2:1991*, 1991.
- [DIN00] Deutsches Institut für Normung e.V. DIN. Messung der nachhallzeit von räumen mit hinweis auf andere akustische parameter. *DIN EN ISO 3382:2000*, 2000.
- [DMB⁺06] E. Deines, F. Michel, M. Bertram, H. Hagen, and G. M. Nielson. Visualizing the phonon map. In *Eurographics / IEEE-VGTC Symposium on Visualization Eurovis2006*, pages 291–298, Lisbon, Portugal, May 2006.
- [EAS01] J. J. Embrechts, D. Archambeau, and G.B. Stan. Determination of the scattering coefficient of random rough diffusing surfaces from room acoustics applications. *Acusica*, 87:482–494, 2001.
- [END02] END. Directive 2002/49/ec of the european parliament and of the council of 25 june 2002 relating to the assessment and management of environmental noise. *Official Journal of the European Community*, 189:12–25, June 2002.
- [Far95] A. Farina. Ramsete - a new pyramid tracer for medium and large scale acoustic problems. In *Proceedings of EURO-NOISE 95 Conference*, March 1995.
- [FCE⁺98] T.A. Funkhouser, I. Carlbom, G. Elko, G.P.M. Sondhi, and J. West. A beam tracing approach to acoustic modeling for interactive virtual environments. In *Computer Graphics (SIGGRAPH 98)*, pages 21–32, Orlando, FL, July 1998.
- [FKS84] W. Fasold, W. Kraak, and W. Schirmer, editors. *Taschenbuch Akustik. Teil 2*. VEB Verlag Technik, Berlin, 1984.
- [FMC99] T.A. Funkhouser, P. Min, and I. Carlbom. Real-time acoustic modeling for distributed virtual environments. In *Computer Graphics (SIGGRAPH 99)*, pages 365–374, Los Angeles, August 1999.
- [FSO06] Y. Fukushima, H. Suzuki, and A. Omoto. Visualization of reflected sound in enclosed space by sound intensity measurement. *Acoust. Sci. & Tech.*, 27(3):187–189, 2006.
- [FTC⁺04] T. Funkhouser, N. Tsingos, I. Carlbom, G. Elko, M. Sondhi, J. E. West, G. Pingali, P. Min, and A. Ngan. A beam tracing method for interactive architectural acoustics. *Journal of the Acoustical Society of America*, 115(2):739–756, February 2004.

- [Gel] S.A. Gelfand. *Essentials of Audiology*. New York.
- [Glü73] K. Glück. *Möglichkeiten zur Erstellung und Verwendung von Lärmkarten als Hilfsmittel für die Stadtplanung*. Bonn-Bad Godesberg, Schriftenreihe "Städtebauliche Forschung" edition, 1973.
- [Hei93] R. Heinz. Binaural room simulation based on an image source model with addition of statistical methods to include the diffuse sound scattering of walls and to predict the reverberant tail. *Applied Acoustics*, 38:145–159, 1993.
- [HS73] T. Houtgast and H.J.M. Steeneken. The modulation transfer function in room acoustics as a predictor of speech intelligibility. *Acustica*, 28:66–73, 1973.
- [HS84] T. Houtgast and H.J.M. Steeneken. A multi-language evaluation of the rasti-method for estimation speech intelligibility in auditoria. *Acustica*, 54:185–199, 1984.
- [Ihl98] F. Ihlenburg. *Finite element analysis of acoustic scattering*. Springer, New York, 1998.
- [ISO87] International Organisation of Standardization ISO. Acoustics - description and measurement of environmental noise - part 2: Acquisition of data pertinent to land use. *ISO 1996-2:1987*, 1987.
- [ISO97] International Organisation of Standardization ISO. Acoustics – measurement of the reverberation time of rooms with reference to other acoustical parameters. *ISO 3382:1997*, 1997.
- [JC98] H.W. Jensen and P.H. Christensen. Efficient simulation of light transport in scene with participating media using photon maps. In *Computer Graphics (SIGGRAPH 98)*, pages 311–320, July 1998.
- [Jen96] H.W. Jensen. Global illumination using photon maps. In *Rendering Techniques '96 (Proceedings of the 7th Eurographics Workshop on Rendering)*, pages 21–30, 1996.
- [JK04] M. Jedrzejewski and M. Krzysztof. Computation of room acoustics using programable video hardware. In *International Conference on Computer Vision and Graphics ICCVG'2004*, Warsaw, Poland, September 22-24 2004.
- [KFW98] S. Khoury, A. Freed, and D. Wessel. Volumetric visualization of acoustic fields in cnmat's sound spatialization theatre. In *Visualization '98*, pages 439–442 & 562. IEEE, 1998.

- [KJM04] B. Kapralos, M. Jenkin, and E. Millios. Sonel mapping: Acoustic modeling utilizing an acoustic version of photon mapping. In *IEEE International Workshop on Haptics Audio Visual Environments and their Applications (HAVE)*, pages 1–6, 2004.
- [KJM05a] B. Kapralos, M. Jenkin, and E. Millios. Acoustical diffraction modeling utilizing the Huygens-Fresnel principle. In *IEEE International Workshop on Haptics Audio Visual Environments and their Applications (HAVE 2005)*, Ottawa, Canada, October 1–2 2005.
- [KJM05b] B. Kapralos, M. Jenkin, and E. Millios. Acoustical modeling using a Russian roulette strategy. In *118th Convention of Audio Engineering Society*, Barcelona, Spain, May 28–31 2005.
- [KK08] V.K. Kurakula and M. Kuffer. 3d noise modeling for urban environmental planning and management. In *REAL CORP 08*, Vienna, Austria, May 2008.
- [KP07] R. Kempiak and M. Petz. Lärmkartierung Hessen 2007. Technical report, Hessisches Landesamt für Umwelt und Geologie, 2007.
- [Kro68] U. Krockstadt. Calculating the acoustical room response by the use of a ray tracing technique. *Journal of Sound and Vibrations*, 8(18):118–125, 1968.
- [Kul84] U. Kulowski. Algorithmic representation of the ray tracing technique. *Applied Acoustics*, 18:449–469, 1984.
- [Kür69] R. Kürer. Zur Gewinnung von Einzelkriterien bei Impulsantworten in der Raumakustik. *Acustica*, 21:370–372, 1969.
- [Kur07] V. Kurakula. A GIS-based approach for 3d noise modelling using 3d city models. Master’s thesis, ITC Enschede, The Netherlands, 2007.
- [Kut71] H. Kuttruff. Simulierte Nachhallkurven in Rechtecksräumen mit diffusen Schallfeld. *Acustica*, 25:333–342, 1971.
- [Kut00] H. Kuttruff. *Room acoustics*. Spon Press, London, 2000. 4th. edition.
- [LB58] J.P.A. Lochner and J.F. Burger. The subjective masking of short time delayed echoes by their primary sounds and their contribution to the intelligibility of speech. *Acustica*, 8:1–10, 1958.
- [LB61] J.P.A. Lochner and J.F. Burger. The intelligibility of speech under reverberant conditions. *Acustica*, 11:195–200, 1961.

- [LCM07a] C. Lauterbach, A. Chandak, and D. Manocha. Adaptive sampling for frustum-based sound propagation in complex and dynamic environments. In *19th International Congress on Acoustics (ICA2007)*, Madrid, Spain, Sep. 2007.
- [LCM07b] C. Lauterbach, A. Chandak, and D. Manocha. Interactive sound propagation in dynamic scenes using frustum tracing. In *In Proceeding of IEEE Visualization 2007*, pages 1672–1679, Sacramento, CA, USA, Nov. 2007.
- [Lev98] D. Levin. The approximation power of moving least-squares. *Mathematics of Computation*, 67(224):1517–1531, October 1998.
- [Lew93] T. Lewers. A combined beam tracing and radiant exchange computer model of room acoustics. *Applied Acoustics*, 38:161–178, 1993.
- [LLT06] Chi-Wing Law, Chee Kwan Lee, and Moon Kwong Tai. Visualization of complex noise environment by virtual reality technologies. Environment Protection Department (EPD), Hong Kong, 2006.
- [LN06] T. Lokki and V. Nenonen. Immersive visualization of room acoustics. In *Joint Baltic-Nordic Acoustics Meeting*, Gothenburg, Sweden, November 8–10 2006.
- [Lok02] T. Lokki. *Physically-based Auralization*. PhD thesis, Helsinki University of Technology, 2002.
- [LSS02] T. Lokki, P. Svensson, and L. Savioja. An efficient auralization of edge diffraction. In *Audio Engineering Society, 21th International Conference*, pages 166–172, St. Petersburg, Russia, June 2002.
- [Mas03] C. Maschke. Stress hormone changes in persons exposed to simulated night noise. *Noise Health*, 5(17):35–45, 2003.
- [MDHB⁺07] F. Michel, E. Deines, M. Hering-Bertram, C. Garth, and H. Hagen. Listener-based analysis of surface importance for acoustic metrics. *IEEE Transactions on Visualization and Computer Graphics*, 13(6):1680–1687, Nov. 2007.
- [MLPK01] J. Merimaa, T. Lokki, T. Peltonen, and M. Karjalainen. Measurements, analysis, and visualization of directional room responses. In *Proceedings of the 111th Audio Engineering Society (AES) Convention*, New York, NY, USA, September 21–24 2001.

- [MM93] D. van Maercke and J. Martin. The prediction of echograms and impulse responses within the epidaure software. *Applied Acoustics*, 38:93–114, 1993.
- [MM04] G. Müller and M. Möser, editors. *Taschenbuch der Technischen Akustik*. Springer, 2004. 3., erweiterte und überarbeitete Auflage.
- [MOD00] M. Monks, B.M. Oh, and J. Dorsey. Audiooptimization: Goal-based acoustic design. *IEEE Computer Graphics and Applications*, 20(3):76–91, 2000.
- [Moh08] J. Mohring. Modal reduction of non-symmetric systems. Technical report, Fraunhofer ITWM Kaiserslautern, Germany, Mar. 2008.
- [MWSH08] F. Michel, P. Wacker, S. Strupp, and H. Hagen. Noisevis3d. In *Proceedings of Computer Graphics and Visualization (CGV) 2008*, Amsterdam, July 2008.
- [Nay93] G. M. Naylor. Odeon – another hybrid room acoustical model. *Applied Acoustics*, 38:131–143, 1993.
- [NHA04] E.M. Nosal, M. Hodgson, and I. Ashdown. Improved algorithms and methods for room sound-field prediction by acoustical radiosity in arbitrary polyhedral rooms. *Journal of the Acoustical Society of America*, 116(2):970–980, 2004.
- [Ols02] K.H.A. Olsson. Model order reduction in FEMLAB by dual rational Arnoldi, 2002.
- [OU04] A. Omoto and H. Uchida. Evaluation method of artificial acoustical environment: Visualization of sound intensity. *Journal of Physiological Anthropology and Applied Human Science*, 23:249–253, 2004.
- [PB04] T. Prenzel and M. Barnat. Aktiv gegen lärm - handlungsstrategien gegen straßenlärm. Bund für Umwelt- und Naturschutz (BUND), 2004.
- [PL03] V. Pulkki and T. Lokki. Visualization of edge diffraction. *Acoustics Research Letters Online (ARLO)*, 4(4):118–123, 2003.
- [PLS02] V. Pulkki, T. Lokki, and L. Savioja. Implementation and visualization of edge diffraction with image-source method. In *Proceedings of the 112th Audio Engineering Society (AES) Convention*, Munich, Germany, May 2002.

- [PR05] S. Petrausch and R. Rabenstein. Highly efficient simulation and visualization of acoustic wave fields with the functional transformation method. In *Simulation and Visualization*, pages 279–290, Otto von Guericke Universität, Magdeburg, March 2005.
- [PR07] F. Pilla and H. Rice. Exploring environmental noise in a virtual 3d world. In *19th International Congress on Acoustics (ICA2007)*, Madrid, Spain, Sep. 2007.
- [RAAS74] W. Reichardt, O. Abdel Alim, and W. Schmidt. Abhängigkeit der grenzen zwischen brauchbarer und unbrauchbarer durchsichtigkeit von der art des musikmotives, der nachhallzeit und der nachhalleinsatzzeit. *Applied Acoustics*, 7:243–264, 1974.
- [Rei68] W. Reichardt. *Grundlagen der technischen Akustik*. Akademische Verlagsgesellschaft Geest & Portig K.-G., Leipzig, 1968.
- [RHC03] S. Rivas, R. Hernandez, and J.L. Cueto. Evaluation and prediction of noise pollution levels in urban areas of cdiz (spain). *Journal of the Acoustical Society of America*, 114(4):2439–2439, Oct. 2003.
- [Rum06] M. Rumberg. *Modellierung und Management kombinierter Umgebungslärmmissionen - Ansätze für die risiko- und qualitätsorientierte Lärminderung in der Stadtplanung*. PhD thesis, University of Kaiserslautern, 2006.
- [Sch81] M.R. Schroeder. Modulation transfer functions: Definition and measurement. *Acustica*, 49:179–182, 1981.
- [Sch02] H. Scharlach. *Lärmkarten - Kartographische Grundlagen und audiovisuelle Realisierung*. PhD thesis, Ruhr-University Bochum, 2002.
- [SG89] A. Stettner and D.P. Greenberg. Computer graphics visualization for acoustic simulation. In *International Conference on Computer Graphics and Interactive Techniques*, pages 195–206. ACM, 1989.
- [SLH02] L. Savioja, T. Lokki, and J. Huopaniemi. Auralization applying the parametric room acoustic modeling technique - the diva auralization system. In *International Conference on Computer Auditory Display*, pages 219–224, Kyoto, Japan, July 2-5 2002.
- [SLS07a] S. Siltanen, T. Lokki, and L. Savioja. Acoustic radiance transfer method. In *19th International Congress on Acoustics (ICA2007)*, Madrid, Spain, Sep. 2007.

- [SLS07b] S. Siltanen, T. Lokki, and L. Savioja. The room acoustic rendering equation. *Journal of the Acoustical Society of America*, 2007. Accepted for publication.
- [Str08] S. Strupp. Simulation von schallimmissionsdaten. Master's thesis, University of Kaiserslautern, 2008.
- [SZ93] Jiaoying Shi and Aidong Zhang. A Modified Rayosity Algorithm for Integrated Visual and Auditory Rendering. *Comput. and Graphics*, 17(6):633 – 641, 1993.
- [TFNC01] N. Tsingos, T. Funkhouser, A. Ngan, and I. Carlbom. Modeling acoustics in virtual environments using the uniform theory of diffraction. In *28th Annual Conference on Computer Graphics nad Interactive Techniques (SIGGRAPH 01)*, pages 545–552, Los Angeles, August 2001.
- [TG97] N. Tsingos and J.-D. Gascuel. Soundtracks for computer animation: Sound rendering in dynamic environments with occlusions. In *Proceedings of the Conference on Graphics Interface*, pages 9–16, Kelowa, British Columbia, Canada, May 1997.
- [TG98] N. Tsingos and J.-D. Gascuel. Fast rendering of sound occlusion and diffraction effects for virtual acoustic environment. In *Proceedings of the Audio Engineering Society (AES) 104th Convention*, Amsterdam, Netherlands, May 1998. preprint no. 4699.
- [Thi53] R. Thiele. Richtungsverteilung und zeitfolge der schallrückwürfe in räumen. *Acustica*, 3:291–302, 1953.
- [TLDD07a] N. Tsingos, S. Lefebvre, C. Dachsbacher, and M. Dellepiane. Extending geometrical acoustics to highly detailed architectural environments. In *19th International Congress on Acoustics (ICA2007)*, Madrid, Spain, Sep. 2007.
- [TLDD07b] N. Tsingos, S. Lefebvre, C. Dachsbacher, and M. Dellepiane. Instant sound scattering. In *Proceedings of the 18th Eurographics Symposium on Rendering (EGSR)*, Juli 2007.
- [TSK01] R. R. Torres, U. P. Svensson, and M. Kleiner. Computation of edge diffraction for more accurate room acoustics auralization. *Journal of the Acoustical Society of America*, 109(2):600–610, February 2001.
- [TY05] Y. Tokita and Y. Yamasaki. Visualization of 3-dimensional sound fields by numerical solutions of particle displacement. *Acoust. Sci. & Tech.*, 26(2):215–217, 2005.

- [Umw07] Umweltbundesamt. Lärm - das unterschätzte Risiko!, 2007.
- [VBE07] VBEB. "Vorläufige Berechnungsmethode zur Ermittlung der Belastetenzahlen durch Umgebungslärm". *Bundesanzeiger Nr. 75*, Apr. 2007.
- [VBU06a] VBU. "Vorläufige Berechnungsmethode für den Umgebungslärm" nach §5 Abs. 1 der Verordnung über die Lärmkartierung (34. BImSchV). *Bundesanzeiger Nr. 154a*, Aug. 2006.
- [VBU06b] VBUF. "Vorläufige Berechnungsmethode für den Umgebungslärm an Flugplätzen". *Bundesanzeiger Nr. 154a*, Aug. 2006.
- [VBU06c] VBUI. "Vorläufige Berechnungsmethode für den Umgebungslärm durch Industrie und Gewerbe". *Bundesanzeiger Nr. 154a*, Aug. 2006.
- [VBU06d] VBUS. "Vorläufige Berechnungsmethode für den Umgebungslärm an Straßen". *Bundesanzeiger Nr. 154a*, Aug. 2006.
- [VBU06e] VBUSch. "Vorläufige Berechnungsmethode für den Umgebungslärm an Schienenwegen". *Bundesanzeiger Nr. 154a*, Aug. 2006.
- [Vor88] M. Vorländer. Ein strahlenverfolgungs-verfahren zur berechnung von schallfeldern in räumen. *Acustica*, 65:138–148, 1988.
- [Vor89] M. Vorländer. Simulation of the transient and steady-state sound propagation in rooms using a new combined ray-tracing/image-source algorithm. *J. Acoust. So. Amer.*, 86(1):172–178, 1989.
- [Wac08] P. Wacker. Visualisierung von lärm-daten. Master's thesis, University of Kaiserslautern, 2008.
- [Wey05a] S. Weyna. Application of "microflow" probe to visualization of acoustic power flow. In *Polish-Scandinavian Structured Conference on Acoustic*, Poznan-Wagrowiec, Poland, September 11–15 2005.
- [Wey05b] S. Weyna. Microflow based identification of vortex shading in the space of real acoustic flow fields. In *Twelfth International Congress on Sound and Vibration*, Lisbon, Portugal, July 11–14 2005.
- [WF98] J.R. Walker and F. Fahy. *Fundamentals of noise and vibration*. London, 1998.
- [WH05] A. Wareing and M. Hodgson. Beam-tracing model for predicting sound fields in rooms with multilayer bounding surfaces. *Journal of the Acoustical Society of America*, 118(4):2321–2331, October 2005.

- [Wu00] T. W. Wu, editor. *Boundary element acoustics: Fundamentals and computer codes*. WIT Press, Southhampton, 2000.
- [Yam72] K. Yamagushi. Multivariate analysis of subjective and physical measures of hall acoustics. *Journal of the Acoustical Society of America*, 52(5):1271–1279, 1972.
- [Yee66] K. S. Yee. Numerical solution of initial boundary value problems involving maxwell’s equations in isotropic media. *IEEE transactions on Antennas and Propagation*, 14(3):302–307, May 1966.
- [YST02] T. Yokota, S. Sakamoto, and H. Tachibana. Visualization of sound propagation and scattering in rooms. *Acoust. Sci. & Tech.*, 23(1):40–46, 2002.

List of Figures

2.1	Flow chart diagram of the phonon emission step.	27
2.2	Flow chart diagram of the phonon emission step including diffuse reflections.	29
2.3	Geometry of the room (a) and simulated scenario (b).	33
2.4	Visualization of particle (phonon) propagation from the sound source in three consecutive time steps.	34
2.5	Interference pattern. FEM simulation (a, c) and phonon tracing (b, d) for the wave number $k=6$ (a, b) and $k=12$ (c, d).	36
2.6	Visualization of wave propagation. FEM simulation (a, c) and phonon tracing (b, d) for the wave number $k=6$ (a, b) and $k=12$ (c, d).	37
2.7	Sound strength visualization (values in dB). (a, d, g) FEM simulation, (b, e, h) phonon tracing, and (c, f, i) the relative error by wave number $k=3, 6$ and 12 . (top to bottom)	39
3.1	Phonon map representation with increasing number of phonons	43
3.2	Particle paths represented by line segments	44
3.3	Visualization of particular phonons. First (a) and fourth (b) reflection using all frequencies for coloring (RGB). First (c, e) and fourth (d, f) reflection colored using single frequencies (HSV). 160 Hz and at 10240 Hz.	47
3.4	<i>Selecting wave fronts by material reflection.</i> (a) Phonons reflected at least once by a wall (b) phonons reflected from floor (c) phonons reflected from canvas (behind viewpoint). <i>Changing material of the floor.</i> (d) all phonons at $d = 1.5m$ (e) phonons at $d = 4.5m$ (f) same as (e) with old material.	49
3.5	Wave front traversed from the sound source (a), separated after reflections (b).	51

3.6	Clustered wave fronts. (a) first reflection color coded using the overall frequency spectrum. (b) Traversed distance represented by use of cones. (c) first reflection color coded using the frequency band at 10240 Hz.	53
3.7	Clustered wave fronts. First (a) and second (b) reflections at the bottom. (c) Second reflections at the bottom reflected before at the wall and canvas, respectively.	53
3.8	Deformed spheres representation at four listener positions. (a) color coded using the overall frequency spectrum (b) by 80 Hz and (c) by 1280 Hz.	57
3.9	Deformed spheres representation at 80 Hz collected before (a) and after (b) 50 msec at one listener position. Deformed spheres representation at 5120 Hz at three position in a room with a separating wall with total absorption (c).	57
3.10	(a) Calculation of the contribution con_{ph} for phonons sharing the same path. (b) Illustration of one phonon path.	59
3.11	Surface subdivision. (a) initial triangulated surface. (b) triangulation after first subdivision step. (c) triangulation after second subdivision step.	62
3.12	Example for clarity (C_{50}) visualization using glyphs. Left: C_{50} above given threshold (green lower semicircle). Right: C_{50} below given threshold (red lower semicircle).	65
3.13	Lecture Room setup. Green: speaker, blue: audience	65
3.14	C_{50} Glyphs at listener positions in the lecture hall. (a) Actual materials/absorption coefficients. (b) Glyphs at listener positions for changed ceiling (above speaker) material with highly absorbing material (sound absorbing foam). (c) Glyphs at listener positions for changed backwall material with sound absorbing foam.	66
3.15	Importance values whole audience and 1kHz mapped to the room surfaces (topview). (a) Importance for early reflections ($< 50ms$), (b) Importance for late reflections ($> 50ms$) red: highest importance, blue: unimportant. (c) Difference (importance for late reflections - importance for early reflections) red: only important for late reflections blue: only important for early reflections.	67
3.16	Same as figure 3.15 from side view.	67
3.17	Importance values for listener position A and 1kHz mapped to the room surfaces (a) Importance for early reflections. (b) Importance for late reflections. (c) Difference. (Same as figure 3.15 for single listener).	68

3.18	Same as figure 3.17 for listener position B	69
3.19	The pressure at the point L can be calculated by the pressure on the surface of an infinitesimal sphere S around L with diameter $d = 2\rho$ (a). In analogy, the pressure at the surface point E can be calculated by the pressure on an infinitely small hemisphere H around E with diameter d (b).	72
3.20	Huygens' principle: A reflected sound wave corresponds to an infinite set of point sources. When adding the individual pressure fields, shape and direction of the wave front are preserved.	72
3.21	The same setup traced with recursion depth $rd=1$, $rd=3$ and $rd=20$ @640Hz. The floor has 1% and the other surfaces 90% scattering. The impact of the recursion depth can be clearly observed.	75
3.22	(a) Phonon map of simple wall with point source in front of it. The left half is interpolated with Shepard, the right half with gauss interpolation. (b) Legend for $min_{ampl} = 10^{-4}$	76
3.23	Configuration of the simulation scenario in two different lecture rooms. Orange spheres mark the sources and blue sphere marks the listener position.	77
3.24	The visualization of the phonon map using the described approach (a,b) and the phonon visualization described in section 3.1.2 (c,d) for the second reflection showing the global (a,b) and local (c,d) influence of scattering. Pictures (a,c) are traced with a scattering coefficient of 1% and (b,d) with a scattering coefficient of 50%	79
3.25	Phase visualization of sound received at one listener position for the frequencies 452Hz (a,d), 640Hz (b,e), and 1280Hz (c,f) for the first reflection and after six reflections (d-f) for the scenario shown in Figure 3.23 (a).	80
3.26	Room HS46-110 at the university @452Hz	80
3.27	Visualization methods implemented to visualize the pressure field. Isosurfaces (left) and streamlines(right). The streamlines make use of the additionally computed gradient field.	83
3.28	Geometry and FEM mesh of the simulated room.	84
3.29	Visualization of Isosurfaces for real and imaginary part as well as the amplitude of the complex pressure value spanning over the eigenfrequency of 137 Hz. The values for the isosurfaces are fixed and colored between red (positive) and blue (negative) values. The grey isosurface denotes the zero isosurface. The topological changes of the pressure field can be observed.	85

3.30	Phase of the complex pressure for 137Hz. Red = π , green = 0, Blue = $-\pi$. The phase is nearly a binary function and undefined at the zero crossings and therefore difficult to visualize.	86
3.31	Gradient (top) and streamline (middle, bottom) visualization for 137 Hz (left) and 276 Hz (right). The gradient vectors and streamlines are colored according to the value of the underlying scalar field (red/blue = maximum/minimum value). The grey isosurface depicts isovalue = 0. In the middle row the streamlines are started on a sphere around the saddle points of the gradient field.	88
3.32	Isosurface visualization for 169 Hz using two different reflection coefficients for the radiator (3.28 on front left wall). Left column high, right column low absorption. Top to bottom amplitude, imaginary and real part of the complex pressure. The isovalues are fixed (red/blue = positive/negative). The phase shift is clearly recognizable by the greater imaginary part for the high absorption (left).	89
6.1	(a) Curves of equal loudness. (b) A-weighting filter curve.	101
6.2	Equivalent sound level for car (top) and train (bottom) [Rum06]. . .	102
6.3	Attenuation of sound regarding distance and sound frequency [Brü01].	105
6.4	Change of sound paths due to wind speeds [Brü01].	105
6.5	Change of sound paths due to temperature gradient [Brü01].	106
6.6	Ground attenuation for different frequencies and ground types. Source-receiver distance = 100m, height 2m [Brü01].	106
6.7	Depiction of attenuation on a barrier for different frequencies [Brü01].	107
6.8	Attenuation of a typical noise screen as function of barrier height [Brü01].	107
6.9	Noise effects reaction scheme [Bab02]	110
6.10	Noise map of a Berlin city district (1938) [Glü73]	113
7.1	Measured air traffic noise in Berlin as colored dots on a map (1968/69) [Glü73].	118
7.2	Visualizing noise using smiley faces to depict noise 'quality' [Sch02]. .	118
7.3	Ribbonlike visualization of traffic noise in Munich with varying width and color depicting different noise levels (1990) [Sch02].	119
7.4	2002/49/EC compliant noise map [KP07].	120
7.5	Default coloring for noise maps [DIN91].	120

7.6	CadnaA: Spreadsheet and distinct receiver points	122
7.7	CadnaA: 2D noise maps with different coloring	122
7.8	CadnaA: 3D + Facade	123
7.9	SoundPlan: Noise map	124
7.10	SoundPlan: 3D visualization and cross section	124
7.11	LimA: Noise map and 3D city model	125
7.12	LimA: Building facades and cross section	126
7.13	Kurakula [Kur07]: Visualizing noise levels on the building facade with isolines (a). Impact of different parameters of a noise barrier on the abatement (b).	126
7.14	Law et al [LLT06]: Visualizing noise levels on the building facade as quads (a) and within a photorealistic 3D city model (b).	127
7.15	VEPS: Visualizing a noise map in a 3D city model (a) and as building facades (b).	128
7.16	Pilla [PR07]: Visualizing a noise map in a 3D city model (a). Volumetric noise visualization using Cinema4D (b).	129
8.1	Effect of maximum distance between sound sources when splitting streets into segments. Street length = 40m. maximum source distance = 40m (a), 20m (b) and 4m (c).	132
8.2	Segmentation of a $\sim 22m$ long street into nine instead of 3 segments due to the requirement of linear segments with constant emission and propagation conditions.	133
8.3	Values for parameters M and p in equation 8.5 for different times of the day [VBU06d].	135
8.4	Depiction of parameter D_s in $db(A)$ depending on the distance s between source and receiver.	135
8.5	Sketch depicting the calculation of D_z [VBU06d].	136
8.6	Impact of screening factor D_z . Same calculation scenario with $D_z = 0$ (a) and screening calculated according to equation 8.7.	137
8.7	Impact of ground and meteorological damping D_{BM} . Calculated noise levels with (a) and without (b) taking D_{BM} into account.	138
8.8	Impact of time of day on the sound propagation D_{met}	139
8.9	Impact of mirror sources. (a) enabled, (b) disabled	141
8.10	Depiction of parameters h_{Beb} and w in equation 8.16 [VBU06d].	142

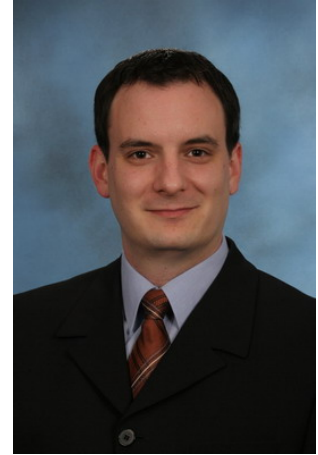
8.11	Impact of multi-reflections D_{refl} . (a) enabled and (b) disabled multi-reflections.	142
8.12	Different height options for multiple layers. (a) Height above ground (b) absolut height	145
8.13	Partitioning of a receiver grid with dimensions 55×55 on a quad-core computer.	147
8.14	Order of computation for the level of detail noise calculation.	147
8.15	The different stages (level of detail) for a receiver grid with dimensions 128×128	148
8.16	Noise levels for the independently calculated streets (top row) and the resulting levels after combining them.	148
8.17	Intermediate results of the calculation for the priority list in figure 8.18.149	
8.18	Priority list for the order of computation based on the average noise level of a street.	150
9.1	Schematic overview of the visualization framework.	152
9.2	Three dimensional city model and digital elevation model.	153
9.3	Settings and viewer window.	153
9.4	Display of additional information for (a) buildings and (b) streets. . .	154
9.5	Display of (a) standard and (b) extended information for a building. .	155
9.6	Buildings colored according to their noise exposure. Left: daytime L_{day} , right: nighttime L_{night}	155
9.7	Visualization of buildings according to thresholds. Left: Noise level below 60 dB, right: above 65 dB for daytime noise L_{day}	156
9.8	Visualization of 2D noise maps 4 meters above ground using different coloring schemes. Left: Standard colors for 5dB ranges. Right: Using only three different colors to depict quiet and noisy areas. Noise below 45dB = green, between 45 and 65 dB = yellow, above 65dB = red. .	157
9.9	Visualization of multilayer 2D noise maps using the standard coloring scheme with colors for 5dB intervals. Left to right: Noise indicator L_{den} in 4, 8 and 12 m above ground respectively.	157
9.10	Visualization of isosurfaces every 5 dB analog to the isobands in standard noise maps.	159
9.11	Volume rendering of the three dimensional data set colored according to the standard scheme.	159

-
- 9.12 Different transfer functions for the same data set to enhance certain aspects of noise exposure. 160
- 9.13 Different isosurfaces for the same data set to enhance certain aspects of noise exposure. Left 71 dB, right 61 dB for L_{day} 160
- 9.14 Volume rendering and isosurfaces for a 3D data set of a single street giving insight into the influence of this street to the overall noise. Left: Volume rendering of noise above 55dB Middle: Isosurface for 55 dB Right: Isosurfaces for every 5 dB. All images for noise indicator L_{den} 161
- 9.15 Noise deflection at a noise screen. Left and middle: Volume rendering of noise above 58 dB from different perspectives. Right: Isosurface for 58 dB. Noise indicator L_{day} 161
- 9.16 Visualization of noise emitted from a single street as volume rendering, isosurfaces and 2D noise map. 162

List of Tables

2.1	Absolute and relative error in dB between FEM and phonon tracing.	38
8.1	Values for parameter C_0 in equation 8.14	139
8.2	Correction factor D_E for mirror sources depending on the reflector type	140

Curriculum Vitae



Frank Michel
Marital status: single
Born: 06.05.1976 in Boppard

Education

1982–1986	Elementary school Bad Salzig
1986–1995	Staatl. Kant Gymnasium Boppard Certificate: General Qualification for University Entrance (Abitur)
10/1996–09/1998	Study of Technical Mathematics at the University of Kaiserslautern
10/1998–02/2005	Study of Computer Science at the University of Kaiserslautern Degree: Diplom-Informatiker (Dipl.-Inf.) Master Thesis: Interactive Reconstruction of 3D Models
06/2005–04/2008	Graduate student at the International Research Training Group (IRTG) "Visualization of Large and Unstructured Data Sets - Applications in Geospatial Planning, Modeling, and Engineering"
01/2006–04/2006 & 11/2006–05/2007	Research visits at the PRISM Lab at Arizona State University

Work Experience

05/2008 to date	Researcher at the German Research Center for Artificial Intelligence (DFKI GmbH) in Kaiserslautern, Germany
-----------------	---

Publications

Interactive Reconstruction of 3D Models for Virtual Walkthroughs

Hagen, H., Münchhofen, M., and Michel, F., in Proceedings of CEMVRC05, pp. 101-105, Prag, Czech Republic, 2005

DaMaViS - Data Management and Visualization System

Hagen, H., Münchhofen, M., Ruby, M., Scheler, I., Wadle, M., and Michel, F., WSCG 2005, Plzen, Czech Republic.

Interaktive Rekonstruktion von Gebäudemodellen für virtuelle Rundgänge

Hagen, H., Münchhofen, M., Ruby, M., Scheler, I., and Michel, F., AGIT 2005, Salzburg, Österreich

Datenmanagementsystem für die Stadtplanung

Hagen, H., Steinebach, G., Münchhofen, M., Ruby, M., Scheler, I., Wadle, M., and Michel, F., CORP2005, Wien, Österreich.

Visualizing the Phonon Map

Deines, E., Michel, F., Bertram, M., Hagen, H., and Nielson, G.M. in Proceedings of Eurovis 2006, pp. 291-298, Lisbon, Portugal, May 2006

RAVis: Room Acoustics Visualization Using Phonon Tracing

Michel, F., Deines, E. in Workshop Proceedings Visualization of Large and Unstructured Data Sets 2006

Comparative Visualization for Wave-based and Geometric Acoustics

Deines, E., Bertram, M., Mohring, J., Jegorovs, J., Michel, F., Hagen, H., and Nielson, G.M. in IEEE Transactions on Visualization and Computer Graphics, 12(5), pp. 1173-1180, September 2006

Room Acoustic Visualization and Auralization

Deines, E., Michel, F., Bertram, M., Hagen, H., Kuester, F. in Scientific Animation Theatre of IEEE Visualization 2006

Simulation, Visualization and Virtual Reality based Modeling of Room Acoustics

Deines, E., Michel, F., Hering-Bertram, M., Mohring, J., Hagen, H. in Proceedings of 19th International Congress on Acoustics, Madrid, Spain, September 2007

Listener-based Analysis of Surface Importance for Acoustic Metrics

Michel, F., Deines, E., Hering-Bertram, M., Garth, C., Hagen, H. in IEEE Transactions on Visualization and Computer Graphics, 13(6), November 2007 pp. 1680-1687.

Continuous improvement process in virtual reality

G. Wagner, P. Keller, F. Michel, M. Bertram, D. Ostermayer, and H. Hagen in Proceedings of Spring Conference on Computer Graphics (SCCG) 2007, pp. 158-164.

On the modification of phonon tracing

Deines, E., Michel, F. to appear in Workshop Proceedings IRTG 1131 2007

Sound Tracing: Rendering Listener Specific Acoustic Room Properties

Jens Bellmann, Frank Michel, Eduard Deines, Martin Hering-Bertram, Jan Mohring, and Hans Hagen in Proceedings of Eurovis 2008 , Eindhoven, Netherlands, May 2008

NoiseVis3D: A Framework for Interactive 3D Traffic Noise Visualization

Michel, F., Wacker, P., Strupp, S., and Hagen, H. to appear in Proceedings of IADIS International Conference on Computer Graphics and Visualization CGV2008, Amsterdam, Netherlands, July 2008